

BIOMECHANICAL TOOLS FOR ASSESSING FOOT AND ANKLE INJURY RISK IN
FRONTAL AUTOMOTIVE COLLISIONS

BIOMECHANICAL TOOLS FOR ASSESSING FOOT AND ANKLE INJURY RISK IN
FRONTAL AUTOMOTIVE COLLISIONS

By JULIA DE LANGE, B.Eng.

A Thesis Submitted to the School of Graduate Studies in Partial Fulfilment of the Requirements
for the Degree Master of Applied Science

McMaster University © Copyright by Julia de Lange, November 2019

McMaster University MASTER OF APPLIED SCIENCE (2019) Hamilton, Ontario
(Biomedical Engineering)

TITLE: Biomechanical tools for assessing foot and ankle injury risk in
frontal automotive collisions

AUTHOR: Julia de Lange, B.Eng. (University of Guelph)

SUPERVISOR: Cheryl E. Quenneville, B.Sc., M.E.Sc., Ph.D.

NUMBER OF PAGES: xv, 119

Lay Abstract

Foot and ankle injuries are common in automotive collisions and often lead to pain and long-term impairment. Experimental work on these types of injuries is traditionally conducted with the foot and ankle positioned in a neutral ankle posture, which does not reflect the range of ankle postures individuals may assume in a car crash.

The purpose of this work was to use biomechanical tools to assess foot/ankle injury risk. Impact testing was performed on two commonly used crash test dummy lower legs in conditions relevant to those experienced in car crashes. A technique was developed to mount cadaveric feet to crash test dummy tibias to gather injury information of the foot, while also collecting load data in the tibia shaft – relevant metrics for industry crash testing.

The results of this work outline the shortcomings of traditional injury assessment methods and may be used to improve future practices.

Abstract

Injuries to the lower extremity are frequent and severe in frontal automotive collisions, often leading to pain and long-term impairment. Most injury criteria developed for the lower extremity are conducted with the foot and ankle in a neutral posture, do not take into account footwear, and assess injury risk to the entire lower extremity at the tibia. An instrumented boot, designed to address some of these challenges, was calibrated over a range of impact energies expected in frontal automotive collisions. A dynamic calibration method was developed to convert changes in voltage across a piezoresistive polymer to the applied axial force.

The instrumented boot was then used to examine the axial impact response of two commonly used Anthropomorphic Test Device (ATD) lower legs, under altered ankle postures. Both posture and ATD model were found to affect the load distribution on the foot, highlighting the need to establish injury limits for non-neutral postures as well as selecting the appropriate ATD model. The instrumented boot provided regional loading information that was not reflected in standard industry metrics, emphasizing the importance of increased instrumentation in this area.

A technique was developed for mounting cadaveric feet to ATD tibia shafts, in order to gather industry-relevant load data while examining the impact characteristics of the foot. Load data were collected at the plantar surface of the foot using the instrumented boot, as well as the tibia load cells in the ATD shaft, that highlighted differences in load transmission through cadaveric and ATD feet.

Understanding the impact characteristics of ATDs under non-standard ankle postures as well as examining the load transmission through cadaveric feet highlighted some shortcomings

with current injury assessment techniques. The results of this work can be used to improve future collision testing practices, in order to reduce the incidence of lower extremity injuries.

Acknowledgements

Thank you to my supervisor, Dr. Cheryl Quenneville, for your mentorship and support throughout this process. Your optimism in the face of challenges is admirable, preventing me from ever shying away from new “learning opportunities.” I truly appreciate your guidance and feedback, and the opportunity to pursue graduate studies. I am excited for what’s to come!

Thank you to everyone who contributed to the success of this project: Dr. Bashar Alolobi for teaching me how to suture and dissect the cadavers, providing sutures and reading x-rays; Jackie Pacheco for taking the x-rays; Chris Purves and Tribe Medical Group for providing FibreWire sutures for this project; Lindsey Wong for her help with dissections and suturing; and Marisa Kohut for her help with dissections. I’d also like to thank the machine shop guys for your guidance and assistance in instrumentation troubleshooting and the designing and generating of parts: Dan, John, Justin, Mark, Michael, and Rob. A special thanks to my group members in the Injury Biomechanics Lab: Cooper, Fatemeh, Marisa and Noah. Thank you to all of my friends and family for your support and the laughs. I’d also like to thank McMaster University for providing me with the funding to conduct this work.

Finally, to my father, who inspired my curiosity and love for research and through demonstration, instilled in me the importance of hard work; and my mother for the support and encouragement throughout this process. Thank you – this work would not have been possible without either of you.

Table of Contents

Chapter 1 – Introduction	1
1.1 Motivation.....	1
1.2 Anatomy of the Foot	5
1.3 Surrogate Options	8
1.3.1 Post-Mortem Human Subjects (PMHS).....	8
1.3.2 Anthropomorphic Test Devices (ATDs).....	8
1.4 The Generation of Injury Limits Through High-Speed Impact Testing	12
1.4.1 Lower Leg ATD Injury Criteria in Impact Testing	13
1.4.2 PMHS Injury Testing.....	15
1.5 Mechanisms of Injury to the Lower Extremity in Frontal Collisions.....	17
1.6 Review of Previous Experimental Axial Foot Impact Literature	18
1.6.1 Neutral Ankle Posture.....	19
1.6.2 Altered Ankle Postures	19
1.7 Effects of Muscle Tension on Axial Impact Response.....	21
1.8 Effects of Postural Changes in ATD Impact Studies.....	22
1.9 A Novel Instrumented Boot.....	23
1.10 Study Rationale and Overview	25
1.11 Objectives and Hypothesis.....	26
Chapter 2 – Instrumented Boot Sensor Calibration.....	28
2.1 Introduction.....	28
2.1.1 Instrumented Boot Design	30
2.1.2 Prior Boot Testing.....	31
2.1.3 Improved Sensor Calibration	32
2.2 Methods.....	33
2.1.4 Dynamic Sensor Calibration Impact Procedure.....	36
2.2.1 Data Analysis	37
2.3 Results.....	38
2.4 Discussion	41

Chapter 3 - ATD Impact Testing in Altered Ankle Postures.....	44
3.1 Introduction.....	44
3.2 Methodology	47
3.2.1 Experimental Testing Protocol	47
3.2.2 Data Analysis	48
3.3 Results.....	49
3.4 Discussion	58
3.4.1 Study Limitations.....	63
3.5 Conclusions.....	64
Chapter 4 – A Technique to Assess the Impact Response of the Human Foot/Ankle Using an ATD Tibia.....	66
4.1 Introduction.....	66
4.2 Methodology	69
4.2.1 General Testing Approach	69
4.1.2 MIL-Lx Testing	71
4.1.3 Intact PMHS Testing.....	71
4.1.4 Adapted Legform Testing	72
4.1.5 Data Analysis	77
4.3 Results.....	77
4.4 Discussion	80
4.1.6 Study Limitations.....	82
4.5 Conclusions.....	84
Chapter 5 – General Discussion and Conclusions	85
5.1 Summary	85
5.2 Limitations and Strengths	87
5.3 Future Directions	89
5.4 Significance.....	90
References	92
Appendix A – Glossary of Anatomical Terms.....	102
Appendix B – Variations in Sensor Voltage Responses.....	104
Appendix C – Technical Drawings.....	105
Appendix D – Settling Impact Effects.....	107
Appendix E – LabVIEW® Program.....	108
Appendix F – Matlab® Sensor Calibration Program	109

Appendix G – Sensor Calibration Repeated Impacts.....	112
Appendix H – Sensor Calibration Curves	113
Appendix I – X-ray Images	117

List of Figures

Figure 1.1: Distribution of Injuries to the Lower Extremity by Region	2
Figure 1.2: Lower Leg Injury Criteria Development.....	4
Figure 1.3: Foot Anatomy.....	5
Figure 1.4: Anatomy of the Lower Leg	6
Figure 1.5: Rotations of the Foot	7
Figure 1.6: Lower Leg Anthropomorphic Test Devices.....	11
Figure 1.7: Injury Risk Curve, Yogananden <i>et al.</i> (1996)	16
Figure 1.8: Pictorial Representation of Lower Leg Loading in a Frontal Collision	17
Figure 1.9: Instrumented Boot Insole	24
Figure 2.1: MIL-Lx in the Pneumatic Impacting Apparatus	35
Figure 2.2: Sensor Calibration Impact Setup.....	36
Figure 2.3: Repeated Trials of Sensor 1 Impacts.....	39
Figure 2.4: Sensor 1 Calibration Curve	41
Figure 3.1: Regional Sensor Groupings.....	48
Figure 3.2: Average Force-Time Traces.....	51
Figure 3.3: Peak Axial Forces.....	52
Figure 3.4: Tibia Indices	53
Figure 3.5: Peak ATD Tibia Forces in Comparison to Net Insole Sensor Forces	54
Figure 3.6: Regional Boot Loading	57
Figure 4.1: Three Lower Leg Representations Tested.....	68
Figure 4.2: Test Setup with Cadaveric Leg in Place.....	72
Figure 4.3: Suturing Technique	74
Figure 4.4: 3D Printed Distal Tibia and Fibula.....	75
Figure 4.5: Newly Formed Ankle Joint	76
Figure 4.6: Net Insole Sensor Forces	79
Figure 4.7: Comparison of Regional Loading Responses	79
Figure 4.8: Comparison of Proximal and Distal Load Cell Forces.....	80
Figure C.1: Fixture for Securing Load Cell to Impact Plate.....	105
Figure C.2: Component to Facilitate Attaching ATD to PMHS.....	106
Figure D.1: Repeatability Testing.....	107
Figure E.1: Sensor Calibration Back Panel.....	108
Figure H.1: Sensor 1 Calibration Curve	113
Figure H.2: Sensor 2 Calibration Curve	113
Figure H.3: Sensor 3 Calibration Curve	114
Figure H.4: Sensor 4 Calibration Curve	114
Figure H.5: Sensor 5 Calibration Curve	115

Figure H.6: Sensor 6 Calibration Curve	115
Figure H.7: Sensor 7 Calibration Curve	116
Figure H.8: Sensor 8 Calibration Curve	116
Figure I.1: Specimen C171338-L (Specimen 1) Before Dissection	117
Figure I.2: Specimen C171338-L (Specimen 1) X-rays After Impact.....	118
Figure I.3: Specimen F171528-L (Specimen 2) Before Dissection.....	119
Figure I.4: Specimen F171528-L (Specimen 2) X-rays After Impact	120
Figure I.5: Specimen F180193-L (Specimen 3) Before Dissecting.....	121
Figure I.6: Specimen F1890193-L (Specimen 3) X-rays After Impact.....	122

List of Tables

Table 1.1: Injury Criteria	15
Table 2.1: Impact Parameters for Sensor Calibration.....	37
Table 2.2: Repeated Trials of Sensor Impacts	39
Table 2.3: Calibration Curve Coefficients	40
Table 4.1: Lower Leg Characteristics	70
Table 4.2: Specimen Impact Information	78
Table G.1: Detailed Sensor Calibration Results	112

List of Abbreviations and Symbols

°	Degree
%	Percent
±	Plus/minus
ABS	Acrylonitrile Butadiene Styrene
AIS	Abbreviated Injury Scale
ATD	Anthropomorphic Test Device
CAD	Computer-Aided Design
DAQ	Data Acquisition Device
F_c	Critical force value used in the Tibia Index
F_x	Force in the x-direction
F_y	Force in the y-direction
F_z	Force in the z-direction (axial force)
HIH	Hybrid III 50 th Male
IARV	Injury Assessment Reference Values
IRC	Injury Risk Curve
IIHS	Insurance Institute for Highway Safety
M_c	Critical moment value used in the Tibia Index
M_x	Moment about the x-axis
M_y	Moment about the y-axis
MIL-Lx	Military Lower Extremity
NATO	North Atlantic Treaty Organization

NHTSA	National Highway Traffic Safety Administration
NI	National Instruments
PMHS	Post Mortem Human Subjects
PMMA	Polymethyl Methacrylate
PVC	Polyvinyl Chloride
STL	Stereolithography File Format
TI	Tibia Index
TI_{Adj}	Adjusted Tibia Index
UBB	Underbody Blasts

Declaration of Academic Achievement

The following is a declaration that I, Julia de Lange, completed the research outlined in this thesis and recognizes the contributions of Dr. Cheryl Quenneville, Dr. Bashar Alolobi, Jackie Pacheco, Lindsey Wong, and Marisa Kohut. I contributed to the study design and was responsible for the experimental testing protocols, data collection, data analysis and writing of the manuscript. Dr. Cheryl Quenneville assisted with the study design and review of the manuscript. Jackie Pacheco took the x-rays of the specimens, and Dr. Bashar Alolobi assessed the scans. Dr. Alolobi and Lindsey Wong also assisted with suturing the specimens, and Marisa Kohut assisted with dissections.

Chapter 1 – Introduction

***Overview:** Fractures to the foot during frontal automotive collisions are common and can be very debilitating. Most research conducted by the automotive field to develop injury criteria involves the positioning of surrogates in a neutral ankle posture, and it is not well understood how changing this posture may affect injury mechanism and severity. This chapter outlines the anatomy of the foot, surrogates that are often used in impact testing, methods of developing injury tolerance limits, previous research that has been conducted in this area, and an instrumented boot that was employed for the present research. It concludes with the study rationale, objectives, and hypotheses for this work.¹*

1.1 Motivation

With advancements in seatbelt and airbag technology providing better protection for the head, neck, and torso, lower extremities are now the most frequent site for “non-minor” (Abbreviated Injury Scale, AIS, 2+) injuries to occur in a frontal collision, of which trauma to the foot and ankle make up 30% (Salzar *et al.*, 2015; Schmitt *et al.*, 2010, Figure 1.1). Injuries to the foot are most common in frontal impacts, occurring in approximately 3.2% of all car crashes (Richter *et al.*, 2001). Axial loading of the lower extremity is responsible for injuries with the most significant long-term impairment and causes an estimated 40% of all injuries to this region in frontal collisions (Funk *et al.*, 2002; Yoganandan *et al.*, 1996). Significant advancements in

¹ Due to the interdisciplinary nature of this work, a glossary of frequently used anatomical terms is included in Appendix A.

research to quantify and prevent lower limb injuries have occurred in the past 20 years due to the frequency and severity of these types of injuries.

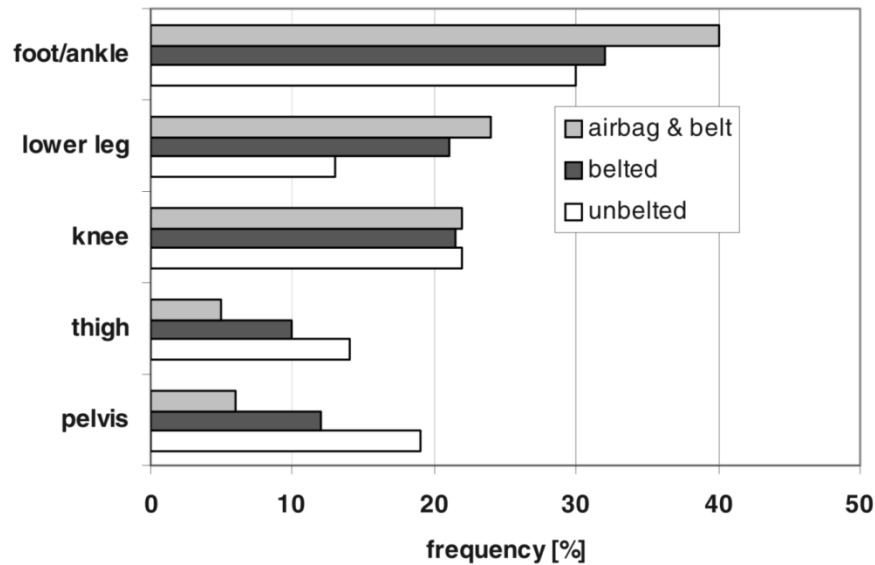


Figure 1.1: Distribution of Injuries to the Lower Extremity by Region

The frequency of AIS 2+ (non-minor) injuries in frontal impacts by region in unbelted, belted, and airbag and belted occupants (Schmitt *et al.*, 2010).

The human body can withstand a certain amount of load, whether that be compressive force, torsion, *etc.* before tissue failure or dysfunction occurs. The magnitude of load that induces failure is known as the mechanical injury tolerance (Forman *et al.*, 2015). Injury tolerance information informs the automotive industry on how much load the body can safely withstand. These injury tolerances also serve as metrics for developing regulations and assessment procedures for vehicle safety (Forman *et al.*, 2015).

To develop bone injury limits, fracture tolerance must be determined, so impact studies are conducted. For ethical reasons, researchers are generally currently unable to conduct impact

studies *in vivo*, so human surrogates are used. These surrogates are in the form of post-mortem human subjects (PMHS, or cadavers), Anthropomorphic Test Devices (ATDs, or ‘crash test dummies’), and computational models (for example, Finite Element Models). Injury limits are developed in laboratory settings, while ATDs are used to evaluate risk in industry. Each of these surrogates has advantages and disadvantages.

Lower leg injury assessment is generally conducted while the foot-ankle complex is positioned in a neutral posture (Figure 1.2, Funk *et al.*, 2002; Seipel *et al.*, 2001; Yoganandan *et al.*, 1996). However, in real-world collision scenarios, the human body can assume a variety of postures that may lead to different injury outcomes (Behr *et al.*, 2010). A limited number of PMHS studies have investigated the axial impact tolerance of the lower leg in a non-standard ankle posture, making it challenging to discern which ankle postures are most vulnerable, and the resulting or associated injury outcome (Crandall *et al.*, 1998; Funk *et al.*, 2002; Grigoriadis *et al.*, 2019; Smolen & Quenneville, 2016). Some results have suggested that dorsiflexed ankle postures are more resistant to injury (Crandall *et al.*, 1998) and that plantarflexed ankle postures are more likely to result in distal tibial fractures (Grigoriadis *et al.*, 2019; Smolen & Quenneville, 2016). However, ATD models have been shown to be relatively insensitive to postural changes (Grigoriadis *et al.*, 2019; Van Tuyl *et al.*, 2016). Therefore, ankle posture and its effect on injury risk have not been reflected in injury risk curves currently employed in the automotive industry.

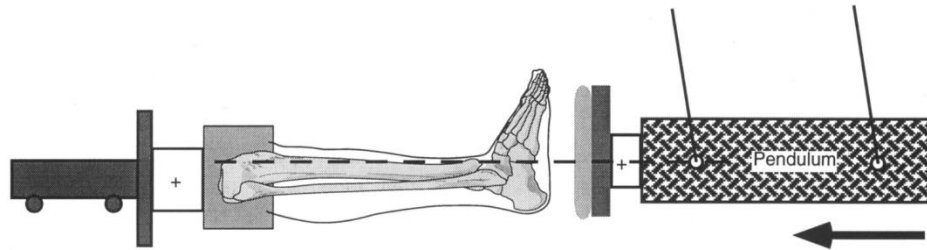


Figure 1.2: Lower Leg Injury Criteria Development

The lower leg is often positioned in a neutral ankle posture when injury criteria are developed for this region, as shown (Yoganandan *et al.*, 1996).

As foot fractures are disabling and associated with a high cost of injury, this thesis endeavours to improve the understanding of the axial response of the lower leg, critical in order to reduce the incidence of lower leg injuries. Improving this understanding involves evaluating the axial impact response under nonstandard ankle postures that are frequently assumed while driving. During these impacts, regional loading such as the midfoot and forefoot loads will be examined, which have historically been ignored. This will lead to the development of devices and models with increased sensitivity to accurately detect injury risk to this vulnerable region in collisions. Without accurate representation, it is challenging to implement effective modifications in vehicles to reduce the incidence of lower extremity injuries.

The overall purpose of the research conducted herein was to investigate the effect of combined ankle postures during axial impacts representative of an automotive collision. Force magnitude and distribution across the plantar surface of the foot, as well as the tibia forces and moments, were comparatively investigated under axial impact loads between two frequently used ATDs, the Hybrid III Lower Leg and the MIL-Lx, under combined ankle postures. These factors were also investigated using cadaveric feet to compare the peak axial force and load distribution

of the foot for three lower leg representations: the intact PMHS lower leg, the MIL-Lx, and cadaveric feet mounted to the MIL-Lx tibia.

1.2 Anatomy of the Foot

The foot is an extremely complex anatomical region, consisting of 26 bones, 33 joints and over 100 ligaments (Figure 1.3). The foot consists of three regions; the hindfoot, midfoot and forefoot. The hindfoot consists of two large bones, the calcaneus, and talus, the forefoot consists of the phalanges and five metatarsal bones that are located between the phalanges and midfoot, and the midfoot consists of the remainder of the bones in the foot (Salzar *et al.*, 2015). The calcaneus is the heel bone, which is the most frequent site of injury in axial impacts, and also serves as the insertion point for the Achilles tendon.

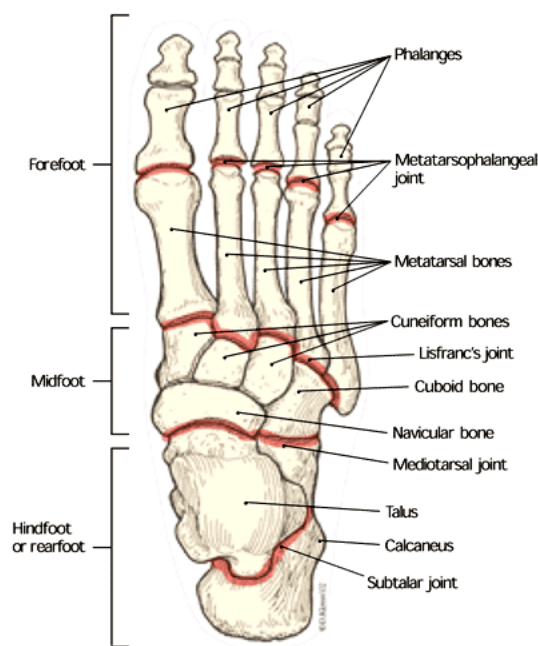


Figure 1.3: Foot Anatomy

Illustration of the bone structure and regional divisions of the foot (Gore & Spencer, 2004).

The ankle consists of two joints: the talocrural, or tibiotalar joint (between the tibia/fibula and talus, Figure 1.4), and the subtalar, or talocalcaneal, joint (between the talus and calcaneus, Figure 1.5). These joints permit motion about three anatomical axes. In the sagittal plane, the foot rotates in plantarflexion or dorsiflexion; the frontal plane, inversion or eversion; and in the transverse plane, internal and external rotation (Figure 1.5). The Society of Automotive Engineering (SAE) has proposed sign conventions intended to keep results consistent among studies in this field, in which the z-axis points inferiorly (Funk *et al.*, 2010).

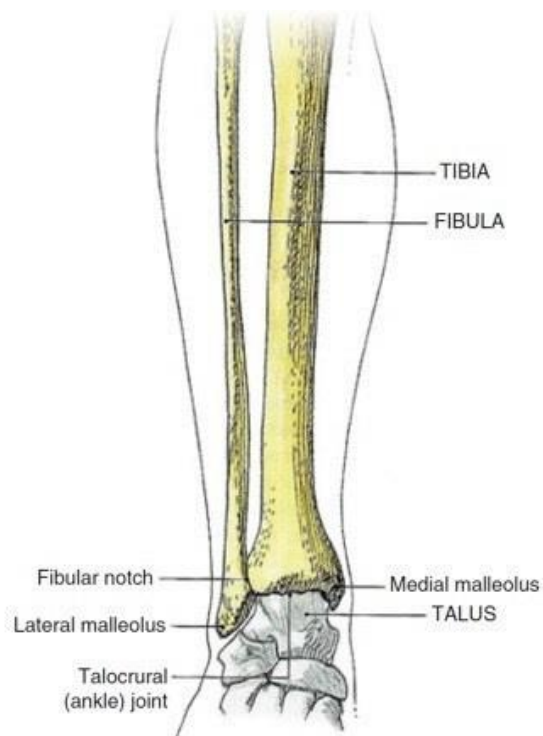


Figure 1.4: Anatomy of the Lower Leg

Frontal view of the bones distal to the knee and proximal to the midfoot of the right-sided lower leg. Adapted from King, 2018.

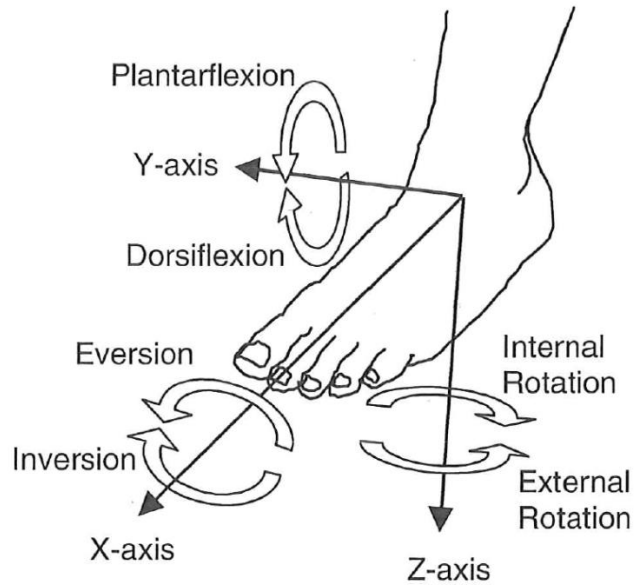


Figure 1.5: Rotations of the Foot

This research used SAE sign conventions and ankle rotations, where the arrow denotes a positive direction (Funk *et al.*, 2010).

Ligaments are fibrous connective tissues that attach bone to bone and serve to stabilize joints and guide motion (King, 2018). The ligaments around the ankle can be divided into three main groups: the medial deltoid ligaments, the lateral ligaments, and the ligaments of the tibiofibular syndesmosis (Golano *et al.* 2010). Tendons are also fibrous connective tissues, attaching muscle to bone and are capable of withstanding tension. They assist in the control of foot motion, including rotating the foot about the ankle (Salzar *et al.*, 2015). The Achilles tendon is the largest tendon in the body, inserting into the posterior aspect of the calcaneus and attaching to the triceps surae muscles (King, 2018). This muscle group is activated in a number of scenarios, including when occupants are generating braking forces in impending collisions (Funk *et al.* 2002). Pedal forces have been measured in a number of volunteer driver simulation studies (Owen *et al.*, 1998; Palmertz *et al.*, 1998) and provide an estimated tension through the Achilles tendon of 1.5 to 2 kN.

1.3 Surrogate Options

1.3.1 Post-Mortem Human Subjects (PMHS)

Post-Mortem Human Subjects are used to establish injury limits, as it is ethically irresponsible to conduct these tests on live subjects. Human cadaveric testing is advantageous as it provides realistic tissue response, allows for the insertion of instrumentation to measure forces and moments, and can actually undergo injuries (Funk, 2011). They also represent a range of populations, allowing for the development of criteria specific to a subset of individuals. It is also necessary to reproduce an injury in a cadaver so the cause of injury mechanism as a result of the applied load can be identified. Although PMHS lack the properties of a physiologically active human being, in particular, active muscle tensioning, they are considered to be the most accurate representation of the response of the natural human body (Funk, 2011). Challenges associated with PMHS testing include the lack of repeatability of the specimens, the expensive nature of testing, preparation and storage disposal and ethical considerations. Cadaveric specimens are also generally obtained from an older demographic, making it challenging to develop injury criteria for other age groups. Varying age, sex, and anthropomorphic sizes have been shown to alter the mechanical behaviour of cadaveric specimens (Yoganandan *et al.*, 1996).

1.3.2 Anthropomorphic Test Devices (ATDs)

Due to the limitations associated with cadaveric testing, ATDs are designed to act as a representation of the human body in impact loading. While PMHS are used to establish injury limits, they are not practical for industry use, so ATDs have been developed for measuring injury risk. Anthropomorphic Test Devices are instrumented to collect data including load, acceleration, and deformation at strategic places throughout the body during automotive crash

tests, and Injury Assessment Reference Values (IARV's) or Injury Risk Curves (IRC's) are developed that relate these measures to injury potential (Salzar *et al.*, 2015). Classified according to size, sex, age, and impact direction, ATDs attempt to account for population variation and directional impact responses (Salzar *et al.*, 2015). There are many limitations associated with ATD testing, as due to the complexities of the human body, it is challenging to have a device that is biofidelic (*i.e.* accurately represents the human body), instrumented with data-collection devices, and behaves in a repeatable and reproducible manner. Human tissue is also very challenging to replicate in an engineered surrogate due to its nonhomogeneous, anisotropic and viscoelastic properties (Iyo *et al.*, 2004).

Anthropomorphic Test Devices are used in a number of industries, but in the automotive industry, they are designed to be biofidelic in order to simulate the mechanical responses of humans. This means they attempt to mimic the geometry, mass, kinematics and kinetics of the human body, and are instrumented with load cells, accelerometers, and displacement transducers to collect data during impact testing. These devices can be repeatedly impacted, acting as a consistent tool for predicting injury. Injury limits are determined from PMHS testing and translated to ATD measures through identical impacts. When safety evaluations (*i.e.* crash tests) are performed in the automotive industry, ATD measures are recorded, and corresponding injury risk is evaluated. This method of using ATD-produced peak forces and PMHS-produced injury outcomes requires the use of a transformation function or ratio to account for the differences in stiffness, geometry, and responses between ATD models and PMHS (Yoganandan *et al.*, 2015). Several surrogates have been developed for safety testing of the lower leg, including the Hybrid III, THOR-Lx, and MIL-Lx. The present study assessed two commonly used ATD models: the Hybrid III lower leg and the Military Lower Extremity (MIL-Lx).

1.3.2.1 Hybrid III Lower Leg

The Hybrid III 50th Male (HIII, Humanetics Innovative Solutions, Plymouth, MI, USA), is the most widely used ATD in frontal automotive collision testing (Humanetics Innovative Solutions, 2019), and was designed based on the size and mass distribution of a 50th percentile American male between 1970 and 1980 (Carpanen *et al.*, 2016). The ankle of the HIII ATD is represented by a ball joint, in which the stiffness of the joint can be adjusted with a screw (Figure 1.6a). The tibia is represented by a simple steel shaft that is mounted on an angle between the ankle joint and knee clevis, causing the Hybrid III leg shaft to be angled when positioned in a neutral position, and inducing bending moments under axial loading. A number of studies have shown that the Hybrid III ATD leg is stiffer than the human leg (Grigoriadis *et al.*, 2019; Pandelani *et al.*, 2010; Quenneville & Dunning, 2012). The leg is instrumented with two 5-axis tibial load cells, located at the upper and lower tibia. When using the HIII leg form, load measurement is typically assessed at the lower tibia load cell (Carpanen *et al.*, 2016). The threshold for injury to the entire lower leg of the HIII, corresponding to a 10% probability of injury, has been established as 5.4 kN of axial compressive force measured at the lower tibia load cell (Yoganandan *et al.*, 1996).

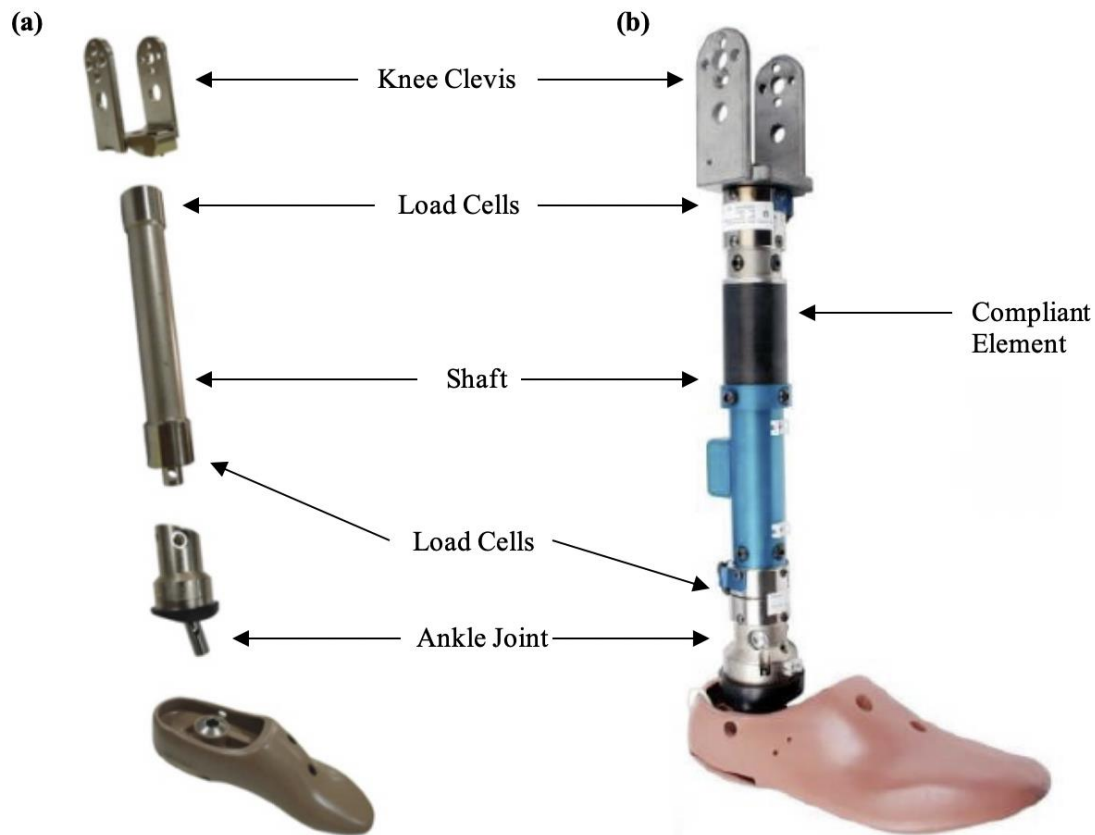


Figure 1.6: Lower Leg Anthropomorphic Test Devices.

(a) The Hybrid III Lower leg (Humanetics Innovative Solutions, 2015), and (b) the Military Lower Extremity (MIL-Lx) (Adapted from Humanetics Innovative Solutions, 2013), showing key components of the two models.

1.3.2.2 Military Lower Extremity (MIL-Lx)

Concerns over the Hybrid III's response to high-rate loading led to the development of the Military Lower Extremity (MIL-Lx, Humanetics Innovative Solutions, Plymouth, MI, USA), designed specifically for analyzing high-rate loading, typical of anti-vehicular land mine blasts (McKay, 2010). This leg form incorporated a compliant element and included a straight shaft, knee clevis and ankle (Humanetics Innovative Solutions, 2013, Figure 1.6b). This leg form was also instrumented with upper and lower tibia load cells; however, typically the measurements

obtained at the upper tibia load cell are used to evaluate injury risk due to the location of the compliant element (Carpanen *et al.*, 2016). The threshold for injury to the entire lower leg, corresponding to a 10% risk of injury, has been established as 2.6 kN at this location on this surrogate (North Atlantic Treaty Organization, 2007).

1.3.2.3 Test Device for Human Occupant Restraint Lower Extremity (THOR-Lx)

The THOR-Lx was designed to be retrofitted to the distal femur of the Hybrid III 50th percentile adult male ATD. Its design was based upon updated biomechanical data, including basic geometric dimensions of the lower extremity, the static and dynamic response characteristics to axial loading, and torque-angle characteristics at the ankle joint (Crandall *et al.*, 1996; Kuppa *et al.*, 1998). It included a compliant element in the leg, a straight leg shaft, and an Achilles tendon. It also contained rotational potentiometers to measure rotation about the ankle (Longhitano & Turley, 2001).

1.4 The Generation of Injury Limits Through High-Speed Impact Testing

To determine injury thresholds for ATD measures, researchers conduct injurious testing on PMHS, attempting to reproduce injuries that are observed in real-world scenarios in a laboratory. This is done in order to identify the cause of injury, referred to as the injury mechanism, and obtain metrics for quantification. From this point, Injury Risk Curves (IRCs) are derived using statistical techniques, such as Weibull analyses (Yoganandan *et al.*, 2015).

Injury severity is numerically classified according to the widely used Abbreviated Injury Scale (AIS) (North Atlantic Treaty Organization, 2007). The AIS coding system scores from 1 to 6, where 1 indicates a minor injury and 6 indicates a maximum (*i.e.* currently untreatable) injury. It has been determined that a 10% risk of AIS 2+ injuries (indicating moderate injury or greater)

is accepted as pass/fail criterion for military blast testing, and this criterion has also been translated into the automotive industry (Mertz *et al.*, 2003; North Atlantic Treaty Organization, 2007).

To create injuries at energy levels representative of automotive collisions, a variety of experimental apparatuses have been used. Common mechanisms include drop towers, linear pistons, pendulums, and projectiles. A pneumatic impacting apparatus in the McMaster Injury Biomechanics Laboratory has been developed to apply impact forces by accelerating a projectile down a tube into a testing chamber containing specimens.

1.4.1 Lower Leg ATD Injury Criteria in Impact Testing

Injury risk to the lower leg is assessed using data collected from the upper and lower tibia load cells of ATDs. The Peak Axial Force (F_z) and the Tibia Index (TI) are calculated from values obtained from these measures and are the basis of safe limits in the lower leg in the automotive industry (Mertz, 1994). Limits that are placed on these ATD metrics are called Injury Assessment Reference Values (IARVs), with the goal of the ATD response in collision tests to be below its corresponding IARV for all conditions being evaluated (Salzar *et al.*, 2015). A probabilistic approach is taken to determine an individual's risk of injury, and this is typically only defined for the 50th percentile male.

The TI , proposed by Mertz in 1993, takes into account the bending moments as well as the axial impact force when assessing injury risk (Salzar *et al.*, 2015). A Tibia Index less than 1.0 indicates a passing test, whereas a value greater than or equal to 1.0 is a failing test.

$$\frac{F}{F_c} + \frac{M}{M_c} \leq 1, \quad \text{Equation 1.1}$$

In this equation, F is the axial force measured in the tibia load cell, M is the bending moment in the tibia load cell, and F_c and M_c are the critical axial force and bending moments, respectively. The critical values vary for different anthropometries and for the midsized male have been established as 35.9 kN and 225 Nm for the F_c and M_c , respectively (Salzar *et al.*, 2015).

As it was observed that the HIII, having an angled tibia, induced bending moments under axial compression, an Adjusted Tibia Index (TI_{Adj}) was developed (Insurance Institute for Highway Safety, 2014). The TI_{Adj} has been widely adopted for use in crash testing and uses adjusted moments about the y-axis (Figure 1.5).

$$\frac{\sqrt{M_x^2 + (M_y - 0.02832 * F_z)^2}}{M_c} + \frac{F_z}{F_c} \leq 1, \quad \text{Equation 1.2}$$

In this equation, F_z is the axial force measured in the tibia load cells in the z-direction, which is positive in compression of the leg (Figure 1.5). M_x is the bending moment in the x-direction, acting parallel to the long axis of the foot (anterior-posterior direction), and M_y is the bending moment in the y-direction, following the right-hand rule (Figure 1.5). F_c and M_c are the critical axial force and bending moments, respectively.

Many different limits to injury criteria have been proposed, but the crash testing limits used by the Insurance Institute for Highway Safety (IIHS) are shown in Table 1.1 (2014). Acceptable safety ratings correspond to values below the proposed IARV, whereas good ratings occur to values well below the proposed IARV. The proposed IARV of 8.0 kN corresponds to a 50% risk of foot/ankle injury in a 45-year-old male, as found by Yogananden *et al.* (1996).

Table 1.1: Injury Criteria

These lower leg injury criteria are proposed by the Insurance Institute for Highway Safety (2014) and are associated with possible injury protection ratings assigned to vehicles.

Parameter	IARV	Good – Acceptable	Acceptable – Marginal	Marginal – Poor
Tibia Index (TI)	1.00	0.80	1.00	1.20
Tibia axial force (kN)	8.0	4.0	6.0	8.0

This method of assessing injury risk, which is globally accepted, groups all injuries to the lower limb together, and provides no indication of the location or severity of the injury. Foot acceleration has also been proposed as a safety limit, with a limit of 150 g based on tests with volunteers and dummies (Zeidler, 1984). Although ankle and toe load cells exist, they are not often used and no known injury limits have been developed for them.

1.4.2 PMHS Injury Testing

Injury Risk Curves (IRCs) are generally derived from cadaveric studies as a probabilistic approach to assessing injury risk. Data assessed during impact studies are either classified as “injurious,” with a probability of injury at 1.0 (*i.e.* specimen fractured) or “non-injurious,” with a probability of injury at 0 (Figure 1.7). Statistical techniques are then employed to develop an equation with input variables, such as force (Salzar *et al.*, 2015).

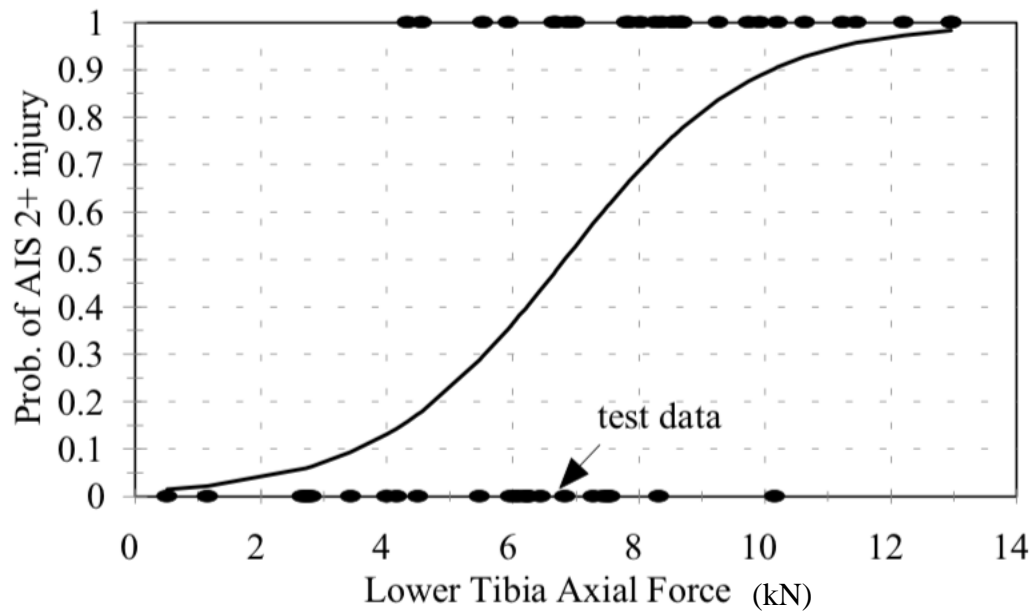


Figure 1.7: Injury Risk Curve, Yogananden *et al.* (1996)

The probability of sustaining an AIS 2+ calcaneal, talar, midfoot or ankle fracture as a function of lower tibia axial force (kN). This analysis indicated lower tibia axial force of 5.2 kN and 6.8 kN correspond to a 25 and 50% probability of AIS 2+ calcaneal/talar/ankle and midfoot fractures, respectively.

Lower leg injury risk is currently grouped together to evaluate the risk of the foot, ankle and lower leg at the tibia (Insurance Institute for Highway Safety, 2014). Tolerance is variable among subjects and is dependent on a number of factors, such as age and sex. While injury tolerance of the isolated tibia has been examined (Chakravarty *et al.*, 2017; Martinez *et al.*, 2018; Quenneville *et al.*, 2011), no studies to date have focused on injury specifically in the foot. It has not been determined how these criteria relate to injury specifically in the ankle and foot, as these existing criteria are based on lower limb impact testing where all injuries to the lower leg are grouped together.

1.5 Mechanisms of Injury to the Lower Extremity in Frontal Collisions

Axial loading applied to the plantar surface of the foot (Figure 1.8) is an important lower extremity injury mechanism due to the frequency and severity of injuries this loading type causes in frontal collisions. Axial compression to this region is likely to cause fractures along the axial load path of the lower leg, particularly calcaneal, talar and tibial pilon fractures (Funk, 2002). These fractures can lead to malunion, infection, and osteoarthritis (Funk, 2002; Morris *et al.*, 1997). Belted front seat occupants in frontal and offset impacts sustain injuries primarily in the calcaneus and tibia complex, both with and without the involvement of their articular surfaces (Yoganandan *et al.*, 2015). Several studies have been conducted to assess the axial injury response of the lower leg under impact loading. The majority of these studies considered the entirety of the lower leg, disarticulated either at the mid-femur or distal to the knee.



Figure 1.8: Pictorial Representation of Lower Leg Loading in a Frontal Collision

The red arrow represents axial force applied to the lower leg, and θ represents the angle between the foot and tibia. Figure adapted from Behr *et al.*, 2010.

Frontal automotive collisions result in a number of different injuries to the lower leg. When forces are concentrated in the hindfoot, the calcaneus, talus and malleoli are at the highest risk of fracture (Crandall *et al.*, 1998). A Lisfranc fracture is a common midfoot fracture and occurs when the metatarsal bones are displaced relative to the tarsals. This fracture type is often caused by high contact forces between the midfoot and pedals of a vehicle (Morris *et al.*, 1997). Forefoot injuries may also occur in automotive collisions, typically to the metatarsals and phalanges, but are generally less severe in comparison to hindfoot injuries (Taylor *et al.*, 1997).

Retrospective studies of real-world collisions have provided data about the causes and locations of lower leg injuries. Richter *et al.* conducted a retrospective analysis of the incidence and mechanism of foot and ankle fractures in restrained front seat car occupants over 23 years (2001). This study found 51% of fractures occurred to the hindfoot or ankle, 20% to the midfoot, and 29% to the forefoot. Foot fractures were found to primarily be caused by foot compartment deformation, in both drivers and front-seat passengers, and moderate foot injury severity (AIS 2) predominated, accounting for 75% of cases. Morgan *et al.* examined frontal impact National Automotive Sampling System (NASS) files and found 45% of foot-ankle injuries were caused by contact with foot controls, while 24% were a result of contact with the floor pan (1991).

1.6 Review of Previous Experimental Axial Foot Impact Literature

Cadaveric testing is an essential component of developing the aforementioned limits, so many researchers have conducted studies to determine the injury tolerance of the cadaveric foot-ankle complex during axial impact loading scenarios representative of those observed in a motor vehicle collision (Crandall *et al.*, 1998; Gallenberger, 2013; Klopp *et al.*, 1997; Kuppa *et al.*, 1997; Manning *et al.*, 1993; Morgan *et al.*, 1991; Rudd, 2009; Shin & Untaroiu, 2013;

Yoganandan *et al.*, 2016, 1996). Individuals may assume different postures while driving, so it is important to understand how these postures may translate to injury risk and mechanism.

1.6.1 Neutral Ankle Posture

Two primary previous studies have been conducted in this area. Yoganandan *et al.* analyzed the impact response of 43 specimens, aged 27 to 78 years positioned in a neutral ankle posture (1996). Specimens were impacted by a pendulum at velocities ranging from 2.2 to 7.6 m/s, with corresponding kinetic energies ranging from 58 to 693 J. Probability of injury with respect to axial force for specific ages was developed from this data set and serves as the basis for the evaluation of protective measures. This study found, for a 45-year-old, 10% injury risk corresponds to 5.4 kN of force and this metric has since been adopted as a standard threshold for injury by a variety of industries (North Atlantic Treaty Organization, 2007).

Seipel *et al.* impacted 22 lower extremity specimens, aged 27 to 74 years, axially at similar impact velocities, ranging from 2.2 to 6.7 m/s and kinetic energies ranging from 58 to 540 J (2001). The focus of this study was the fracture tolerance of the calcaneus and calcaneal fractures were generated in just over half of the specimens. The peak forces ranged from 3.6 to 11.4 kN in the fracture tests, and a 10% risk of calcaneal fracture was identified using logistic regression analysis to be 2.5 kN (Seipel *et al.*, 2001).

1.6.2 Altered Ankle Postures

Although individuals assume a range of postures while in vehicles, there has been limited testing of specimens positioned in non-standard initial ankle posture under axial loading. Lestina *et al.* (1992) reviewed accident data and postulated that inversion or eversion played a role in 65% of foot and ankle injuries and 92% of malleolar injuries; however, to date, there have been

few impact studies to support these findings. Dynamic ankle rotations have been tested, where the impacting device forces the foot to rotate about isolated anatomical axes, in which the specimens were initially positioned in a neutral posture, and experienced rotation upon impact. However, injuries generated as a result of dynamic ankle rotations may have different injury mechanisms in comparison to those that occur as a result of changes to initial ankle posture.

One of the largest studies to date on the effect of initial ankle posture was conducted by Klopp *et al.* (1997). In this study, 50 specimens were separated at the midshaft of the femur, and a load cell was implanted into the diaphysis of each tibia (1997). These tests were conducted in an effort to simulate frontal automotive collisions, and fractures of the calcaneus, talus, and malleoli were observed in 11 specimens. The initial position of the foot was found to influence injury outcome, as the dorsiflexed ankle posture was more resistant to injury (50% probability at 11kN) than the neutral or plantarflexed foot (50% probability at 2 kN). The initial eversion angle had no effect on injury outcome. Results from this study indicated an overall 10% risk of injury correlating to 3 kN of footplate contact forces (Klopp *et al.*, 1997).

The increased resistance to load in a dorsiflexed posture was confirmed in another study by Gallenberger *et al.* (2013). In this study, ankles positioned in 20° dorsiflexion were compared to ones in the neutral posture in 15 lower limbs. Fourteen of the 15 specimens tested sustained a calcaneal injury, while two also sustained tibia fractures. This study noted that the 50% risk of injury increased from 6.8 kN in the neutral posture to 7.9 kN in the dorsiflexed posture, supporting findings that increased contact area at the subtalar joint resulted in a lower risk of injury (Gallenberger *et al.*, 2013).

In recent years the focus in this field has shifted to blast injury, from which some findings may be applicable to the automotive industry. A recent study by Grigoriadis *et al.* investigated

the effects of plantarflexion on the mechanism of injury in response to underbody blasts (UBB) in ten PMHS (2019). Specimens were 49 to 57 years old and exposed to axial impacts at 12.7 m/s. These neutral and 30°-plantarflexed postures revealed differences in measured plantar forces, the type and location of fractures, and the loading mechanism of the tibia. Grigoriadis *et al.* found different fractures depending on initial ankle posture, with impacts conducted in a neutral posture generating only calcaneal fractures, while the 30° plantarflexed posture generated exclusively distal tibia pilon fractures (2019). The plantarflexed postures experienced fractures of higher severity, based on the type of fracture endured, than the neutral posture. Peak forces resulting in fracture collected from the plantar surface ranged from 4.1 to 13.8 kN.

1.7 Effects of Muscle Tension on Axial Impact Response

A significant limitation in PMHS testing is the lack of muscle activation that may occur in a living human prior to impact. In most impact studies, the justification of this is that impacts occur over a very short period of time (20 ms), and reflex contractions take more than 100 ms for muscles to respond (Kitagawa *et al.*, 1998). However, if an individual is bracing for an impending collision, braking forces may act through the Achilles tendon that could alter the fracture location and severity. An estimated 1.5 to 2 kN of Achilles tension is generated during emergency braking (Manning *et al.*, 2010).

Funk *et al.* hypothesized that active muscle tension during pre-impact bracing may predispose the distal tibia to fracture rather than the calcaneus (2002). Forty-three specimens were axially impacted on the plantar surface of the foot at approximately 5 m/s using a pneumatic impactor. The specimens were positioned in a neutral ankle posture and implanted with a 5-axis load cell at the tibia. A survival analysis was used to analyze the force to fracture,

and results showed that age, sex, body mass, and peak Achilles force were predictor variables of the probability of injury. With active muscle tension through the Achilles tendon, the axial tibial force associated with a 10% risk of fracture for a 45-year-old 50th percentile male increased by up to 2 kN, in comparison to the 5.8 kN without Achilles tension.

Kitagawa *et al.* impacted sixteen lower leg specimens, ranging from 59 to 83 years old, in a neutral posture while 1.8 kN axial force was applied to the Achilles tendon (1998). The application of this force remained constant during impact through the use of an energy absorber. A six-axis load cell measured force at the proximal end of the tibia and the impacting pendulum. Impacts delivered at 3 m/s produced five tibia pilon fractures, ten calcaneal fractures and one uninjured specimen. The average peak impactor force was 5.1 kN and peak tibial force was 7.7 kN in the fractured specimens.

1.8 Effects of Postural Changes in ATD Impact Studies

While both fracture force and location have been shown to be affected by ankle posture in PMHS, ATDs have been shown to be relatively insensitive to postural changes based on traditional methods of assessing injury risk, using peak axial force (F_z) and TI . Two primary studies have investigated these effects. Van Tuyl *et al.* impacted the Hybrid III lower leg in altered postures at energies representative of an automotive crash (2016). Peak axial force was not affected by ankle flexion, and TI_{Adj} was lowest in plantarflexion. Both peak axial force and TI_{Adj} were highest in neutral postures. The inversion and eversion postures had the largest influence on injury metrics, contrary to previous cadaveric studies that have suggested that inversion and eversion do not influence injury risk.

Grigoriadis *et al.* investigated the responses of the HIII and MIL-Lx to under-body blasts in two different seated ankle postures, neutral and 30°-plantarflexion (2019). Anthropomorphic Test Devices were impacted at 8.7 m/s, and the loading was assessed at the tibia and by two force plates at the hind- and forefoot. Traditional means of assessing injury risk, peak axial force and the Revised Tibia Index, were not statistically varied in the lower limbs of the ATDs in the altered posture. This study concluded that ATDs cannot accurately be used with current IRCs to predict the probability of under-body blasts (UBB) injury of the lower limb when they are positioned in non-standard postures.

1.9 A Novel Instrumented Boot

In an effort to improve the translation of PMHS injury criteria to the automotive industry, an instrumented boot was developed (Acharya *et al.*, 2018). This boot acts to address a number of limitations that currently exist with developing injury tolerance levels in cadaveric settings. First, in a typical real-world collision scenario, individuals will be wearing some form of footwear. However, in experimental laboratory testing, cadaveric specimens are rarely equipped with footwear and in ATD testing footwear use is not consistent (Gallenberger *et al.*, 2013). The use of footwear in ATD testing has been shown to reduce axial impact force collected at tibia load cells by up to 72% (Quenneville & Dunning, 2012). Furthermore, in current ATDs employed in automotive collision tests, injury to the foot/ankle complex is grouped and evaluated at the tibia load cells. This neglects to provide information on forces developed in the foot during impact. Finally, traditional injury evaluation metrics do not account for the risk of injury to various regions of the foot. Insight into the regional loading that the plantar surface of the foot experiences during axial impacts may provide an indication as to areas which are at

greatest risk of injury. With this in mind, a custom force-sensing insole was designed (Figure 1.9) and calibrated to convert applied sensor resistance to force (Acharya *et al.*, 2018).

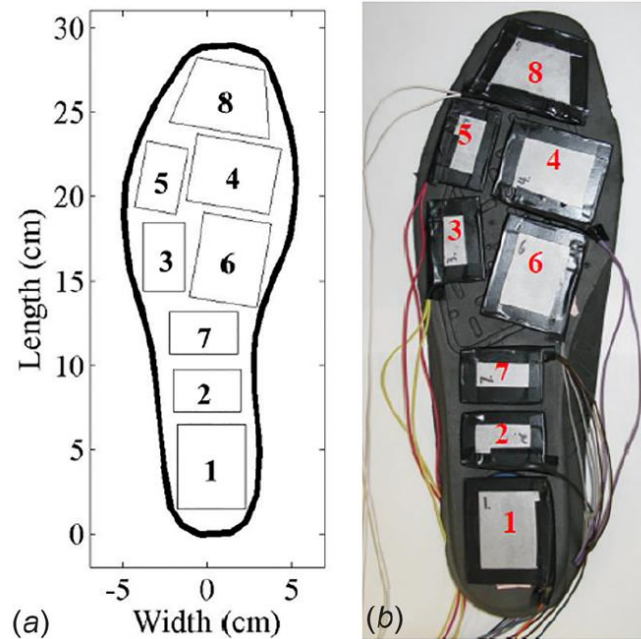


Figure 1.9: Instrumented Boot Insole

Piezoresistive sensors covering the main loading regions of the insole, based on (a) the schematic, and (b) their corresponding locations on the insole of the instrumented boot. Figure adapted from Acharya *et al.*, (2018).

Post mortem human surrogates do not have load cells (except in instances when they are embedded, which alter stiffness and possible stress concentrations of the leg), so a point of comparison between ATDs and PMHS is valuable. Collecting forces at the plantar surface of the foot, rather than at tibia load cells, allows for greater characterization and understanding of axial impact response and the injury risks to different regions of the foot. This is valuable for instances when the foot is oriented in a non-standard posture, allowing for examination of loading patterns and resultant injury outcomes. It also acts as a transferrable device between

PMHS and ATD's to evaluate the discrepancies that exist amongst surrogates and allows for a relationship to be developed *via* an external tool. If the boot is used during ATD testing, reliable injury criteria and tolerance limits of the foot can be recorded. Finally, information gathered from the instrumented boot when conducting axial impact testing on cadaveric specimens may be used for future iterations of ATD feet.

1.10 Study Rationale and Overview

Most cadaveric studies have investigated the fracture tolerance of the lower leg when positioned in a neutral posture, but in order to design suitable protective measures in vehicles, the fracture tolerance of the foot must be well understood in a range of ankle postures. To the author's knowledge, no previous studies have developed injury metrics for the mid- and forefoot and nobody has examined how these metrics may change with altered ankle postures. This is significant because vehicular occupants may assume a range of positions while driving and may not be adequately protected by current methods of assessing foot injury risk at the tibia.

Many previous lower extremity impact studies have also used specimens that include the foot, tibia and fibula and knee. Although this representation is more realistic, disarticulation of the foot at the tibiotalar joint allows for the ability to isolate the foot and assess injury risk to this vulnerable region, while simultaneously collecting data in the tibia that is immediately relevant to the automotive industry. In the current work, PMHS feet were secured to ATD tibias, allowing for force collection at the upper and lower tibia load cells. These tests also enabled the evaluation of the stiffness of the MIL-Lx foot in comparison to cadaveric feet.

In order to accurately collect load data from the instrumented boot, the insole sensors were recalibrated at loading rates representative of automotive impact rates, presented in Chapter

2. This was done primarily to automate the process and remove subjectivity, as well as to provide more accurate force data over the range of impact energies expected in an automotive collision. This boot was then applied to two ATD models, the Hybrid III and MIL-Lx, and regional loading and load cell measures were assessed over a range of initial ankle postures (Chapter 3). Chapter 4 focuses on the development of a novel technique for mounting cadaveric feet to ATD tibia shafts, in order to assess injury risk to the foot while simultaneously collecting industry-relevant loading metrics.

The work presented herein assessed the effect of ankle posture on ATD Injury Assessment Reference Values, using insole sensors calibrated for automotive collision applications in addition to traditional injury assessment sites. Furthermore, the biofidelity of the ATD foot was assessed in a neutral posture as compared to cadaveric feet, providing a valuable technique for assessing foot fractures while simultaneously collecting load data relevant to the automotive industry.

1.11 Objectives and Hypothesis

The objectives of this thesis were:

1. To automate the processing and calibrate the sensors over a wider range of impact energies in order to attain accurate and repeatable data collection of sensor forces.
2. To investigate and compare the effects of ankle posture on the peak axial forces collected from the tibia load cells and from the instrumented boot, as well as analyze the distribution of forces on the plantar surface of the foot in the Hybrid III lower leg and MIL-Lx ATD models under axial dynamic loading.

3. To develop a method to mount PMHS feet onto MIL-Lx tibia shaft, in order to assess foot/ankle injury risk while collecting data relevant to the automotive industry.
4. To compare the force distribution on the plantar surface of the foot and tibia load data of PMHS feet and ATD feet under axial impacts, to assess the biofidelity of the ATD foot.

The corresponding hypotheses were:

1. Both the Hybrid III and MIL-Lx models will be insensitive to ankle postural changes. The Hybrid III model will record loads at the distal tibia load cell that are greater than those recorded in the proximal MIL-Lx load cell in identical impacts. The Hybrid III and the MIL-Lx will have different regional loading responses due to greater compliance in the MIL-Lx foot.
2. Due to the stiffer nature and increased mass of the MIL-Lx foot, the tibia load cells will collect higher forces when equipped with the MIL-Lx foot in comparison to PMHS feet.

Chapter 2 – Instrumented Boot Sensor Calibration

Overview: This chapter introduces the instrumented boot, a novel tool used to quantify force at the plantar surface of the foot. This tool may be applied to both PMHS and ATDs during injury limit generation and safety evaluation tests to primarily evaluate injury risk to this historically ignored region of the body, and furthermore to address the differences in compliance between surrogates. This chapter outlines the procedure that was used to calibrate the insole sensors used throughout the remainder of this research. The procedure used a dynamic calibration method to convert changes in voltage across a piezoresistive polymer to the applied axial force.

2.1 Introduction

As outlined in Chapter 1, the foot-ankle complex is frequently injured in automotive collisions, accounting for approximately 10% of all AIS 2+ injuries (Morgan *et al.*, 1991). Although injuries to this region are rarely life-threatening, they frequently cause long-term impairment and pain and have substantial outpatient costs (Morris *et al.*, 1997; Richter *et al.*, 2001). Previous research in this field has demonstrated that axial force is a good predictor of injury to this region (Klopp *et al.*, 1997).

Anthropomorphic Test Device (ATD) lower extremities are instrumented with 5-axis upper and lower tibia load cells, and current methods of assessing injury risk to the lower leg are typically based upon forces and moments collected in the tibia shaft (Mertz *et al.*, 2003;

Yoganandan *et al.*, 2015). This method of data collection has many limitations. Firstly, it neglects injury risk to the foot, grouping lower extremity injuries together and evaluating for them at the tibia shaft. This location of injury assessment is an inaccurate representation of what may occur to the foot during these scenarios. It neglects injury risk to specific regions to the foot, *i.e.*, toe crushing scenarios that would likely not be detected relying only on tibia load cell forces and moments.

Next, the use of footwear during safety crash testing and developing PMHS injury response corridors is inconsistent. Often during safety tests, ATDs are dressed with some form of footwear (Insurance Institute for Highway Safety, 2004); however, during the development of PMHS injury criteria, the cadaver is often nude (Funk *et al.*, 2002; Yoganandan *et al.*, 1999). Depending on testing conditions, the use of footwear during these scenarios has been shown to reduce axial impact force by 50-65% at the tibia load cells (Bir *et al.*, 2008; Quenneville & Dunning, 2012). Humanetics offers a standard NHTSA shoe, designed to represent a men's Oxford dress shoe, though the use of this shoe is not consistent among industry collision testing as it is not a required test condition (Insurance Institute for Highway Safety, 2004). Adding instrumentation to the plantar surface of the foot, affixed to the insole of a shoe, addressed many of these challenges. The instrumented insole could easily be transferred to other forms of footwear, and the use of a consistent form of footwear eliminates this discrepancy. Furthermore, ATD's are widely accepted as being stiffer than PMHS (Kuppa *et al.*, 1997; Quenneville & Dunning, 2012), so the use of a scaling factor to compare PMHS response and ATD response is often employed.

2.1.1 Instrumented Boot Design

The instrumented boot was designed by Van Tuyl and has eight piezoresistive sensors covering the majority of the plantar surface of the foot (2014). A size 11 Kodiak® Quantum II work boot (Kodiak Group Holdings Co., Cambridge, ON, Canada) was equipped with an array of piezoresistive force sensors. The sensors were designed with three different geometries to cover all major load-bearing surfaces of the foot. Piezoresistive sensors were developed using Lingstat (Caplinq Corporation, Ottawa, ON, Canada), a commercially-available polymer with piezoresistive properties. The polymer was sandwiched between plates of 16-gauge cold-rolled steel to act as electrodes and mechanical support. These sensors were installed on the insole, directly below where the foot would rest.

All eight sensors were connected in a voltage divider configuration, arranged in parallel in order to be excited using a single power source (1.5 V D-cell battery). The applied resistance across each sensor was calculated based on the 102.0- Ω reference resistor, the excitation voltage, and the voltage across the sensor measured by the data acquisition system (NI PXIe-1082 National Instruments Corporation, Austin, TX), sampled at 50,000 Hz.

This boot provides insight into the gap in injury criteria that exists in regard to the foot while undergoing impacts (Acharya *et al.*, 2018). This boot provides investigators with information regarding the complex loading that occurs during a frontal vehicular collision, including the relative location and magnitude of the axial force that is inflicted on the plantar surface of the foot. It has the ability to provide regional load assessment, valuable for instances when the brake pedal and toe pan intrusion affect occupants in motor vehicle collisions. The sensors on the instrumented boot were previously validated and calibrated over a limited range of impact energies (Acharya *et al.*, 2018).

There are many advantages to this boot. Using the boot in both PMHS impact testing to develop fracture thresholds, as well as ATD impact tests to measure the tibia axial force, allows for reliable injury criteria and tolerance limits of the foot to be recorded. It can be easily translated to ATDs during impact testing, removing the need for a scaling factor between surrogates, and providing a relationship for the boot to be used with existing injury limits. When using the instrumented boot, a scaling factor to account for the difference between PMHS and ATD is not necessary, as the forces applied while conducting injury and non-injury testing can be read directly off the boot and provide comparative data.

The boot allows for greater assessment of the tolerance of the human foot under complex loading, like in cases when the ankle is oriented in a non-standard posture. The instrumented boot also is an effective force detection device in all postures, as it has been shown to be relatively insensitive to shear loading (Acharya *et al.*, 2018).

2.1.2 Prior Boot Testing

The sensors were previously calibrated using a process developed by Acharya *et al.* at kinetic energies between 101 and 280 J (2018). Preliminary testing of the boot found the net summation of all boot sensors recorded forces that were consistently 120-130% higher than those collected by the distal tibia load cell in the Hybrid III lower leg ATD (Acharya *et al.*, 2018). This emphasizes the importance of collecting load data at the plantar surface of the foot and quantifies some of the force dissipation that may occur between this location and the tibia load cells. When tested in a neutral posture, it was found that the hindfoot carried 49% of the total load collected by all sensors, due to its orientation directly under the ankle joint, indicating that load is not evenly distributed on the foot during axial impacts (Acharya *et al.*, 2018).

2.1.3 Improved Sensor Calibration

Initial testing of the sensors using the Acharya calibration method indicated that the data collection process was subjective according to the user analyzing the data. This was because the impact profile, determined by the variation of the acquired sensor voltage during impact, was based upon user input. Small changes in identifying the start and end of impact could alter results substantially. Furthermore, the sensor data analysis during booted impact testing was lengthy and labour-intensive.

In order to remove some of the subjectivity from this process, an automated program was designed to detect the start and end of impact using MATLAB (The MathWorks Inc., Natick, MA, USA). The impact was considered to have initiated 1 ms prior to the voltage profile reaching 10% of its minimum value and concluded 1 ms after the voltage profile reached 10% of its minimum value. This is a similar procedure as to what is used for determining the start and end of impact from tibia F_z data (Van Tuyl *et al.*, 2016) allowing the impact duration to be autonomously determined. In order to generate a more efficient process, a relationship directly comparing the sensor voltages and corresponding force was also developed.

The objective of this work was to dynamically calibrate the piezoresistive sensors under conditions representative of those that they would experience during axial impacts representative of automotive collisions. This involved measuring whether the piezoresistive material was a consistent and repeatable device to measure the application of axial force, and developing a protocol that was more efficient and objective than the previous method. In order to ensure the sensors were adequate in sensing force at fracture-producing thresholds, they were recalibrated in a similar manner to the protocol developed by Acharya *et al.*

2.2 Methods

In an effort to attain an appreciation of the magnitude of impact that each sensor would experience during testing, ATD tests were conducted while wearing the instrumented boot and the change in sensor voltage was recorded. The boot was impacted over a range of energies to assess the magnitude of voltage variation for each of the sensors, in order to develop new calibration targets for the sensors. The booted impacts were conducted on both the Military Lower Extremity (MIL-Lx) and the Hybrid III (Humanetics Innovative Solutions, Plymouth, MI, USA) lower leg ATDs.

All testing was completed using a pneumatic impacting apparatus, which has previously been used in many impact studies (Acharya *et al.*, 2018; Martinez *et al.*, 2018; Chakravarty *et al.*, 2017). A steel projectile was propelled down an acceleration tube by compressed air towards the testing chamber. Impulse was transmitted to the plantar surface of the foot *via* an ankle positioner, which was mounted on low-friction linear bearings. A block of rubber foam was placed on the surface of the ankle positioning device being struck in order to control pulse duration. This foam was replaced every four impacts to mitigate any potential accumulated damage.

The testing procedure was controlled, and data were collected, using a custom-written LabVIEW (National Instruments, Austin, TX, USA) program. A uniaxial accelerometer (MMA1200, Freescale Semiconductor, Austin, TX, USA) was mounted on the ankle positioner to collect footplate accelerations. Two optical sensors (PZ-V31P, Keyence Corporation, Osaka, Japan) were mounted over the projectile exit from the acceleration tube to collect impact velocity, which had 0.05 m/s sensitivity at 6 m/s velocity. All data, including that collected from

the insole sensors and load cells, were recorded at 50 kHz, well above the proposed minimum sampling rate of 10 kHz detailed in ATD specifications (Society of Automotive Engineers, 2003).

The Hybrid III and MIL-Lx lower leg models were each in turn fitted with the instrumented boot and fixed to a proximal bracket at the knee that was suspended on a linear rail and bearing system (Figure 2.1). This allowed free translation and rotation of the surrogate after impact. The boot laces were tightened by hand. Impacts were targeted at a velocity of 5 m/s, with a target impulse duration of 20 to 50 ms to simulate motor vehicle conditions (McKay & Bir, 2009). In order to increase the impact energy and resulting force that each sensor would endure during the calibration impacts, impacting mass was increased while impact duration and velocity remained consistent. Projectile masses ranging from 5.6 to 9.6 kg were used in order to be in the expected range of impact conditions conducted herein. The ATDs were tested at neutral posture, 15°-dorsiflexion, and 15°-plantarflexion, to ensure sensor voltage drops in altered ankle postures were also captured. One unrecorded settling impact was applied to ensure the ATD foot rested against the insole sensors, followed by five impacts to ascertain the sensor readings. Impacts were delivered to the plantar surface of the foot, which rested on an angled plate in order to distribute the load across the entirety of the foot.

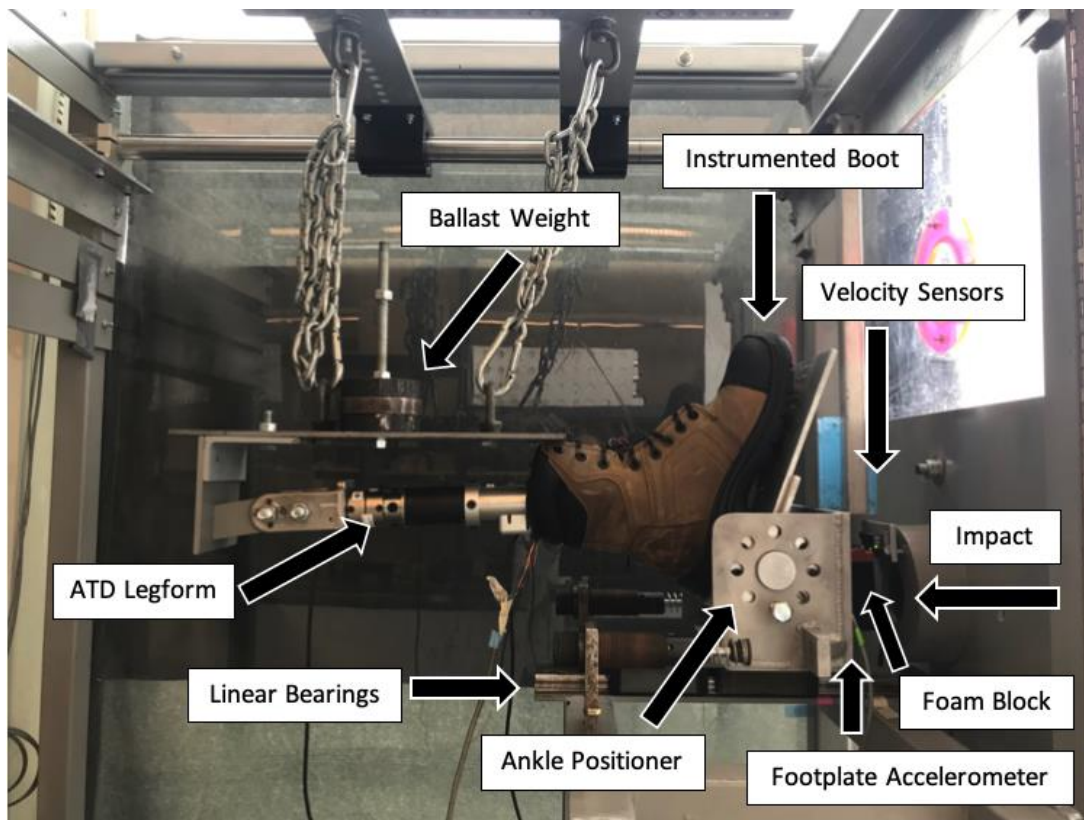


Figure 2.1: MIL-Lx in the Pneumatic Impacting Apparatus

Important components of the system are labelled, with the ATD positioned in a plantarflexed ankle posture.

The changes in each sensor voltage during the impact events were recorded, and impacting parameters were developed in order to be in the expected range of voltage variation. The sensor voltage response during impact typically ranged between 0.48 and 0.92 V of variation among all impacts, depending on the location of the sensor, ATD ankle posture, and impact mass. Detailed voltage data of these impacts can be found in Appendix B.

A 5-point dynamic calibration method was developed by Acharaya *et al.*, as sensor voltage variations have been previously demonstrated to be dependent on the load rate (Van Tuyl, 2014). A similar 5-point calibration protocol was adapted from this process. Impacts were

then conducted on isolated sensors, using variable impact mass, to target voltage drops that were observed in the ATD testing process.

2.1.4 Dynamic Sensor Calibration Impact Procedure

The sensors were sandwiched between layers of foam, that was secured to a six-axis load cell (IF-625, Humanetics Innovative Solutions), to measure the axially applied force during impact, F_z (Figure 2.2). The purpose of foam was to control the impact duration, while also attempting to calibrate the sensors under conditions in which they would be placed in the boot. The load cell was secured to the impact plate by a specially-designed jig machined out of high strength steel (Appendix C). Impact energy was increased by increasing the impacting mass while keeping the desired impact velocity at 5 m/s, representative of an automotive collision loading rate.

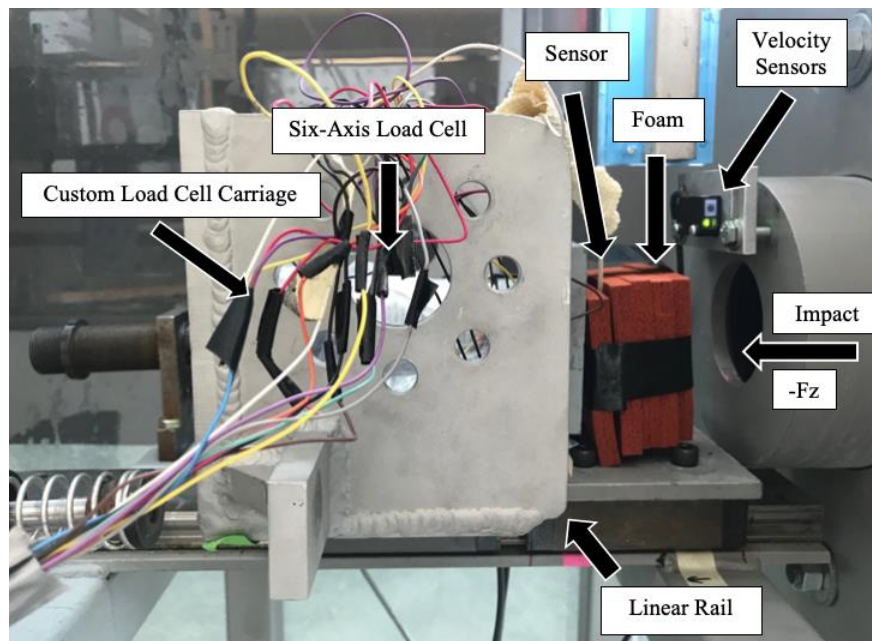


Figure 2.2: Sensor Calibration Impact Setup

A depiction of the impacting protocol for calibration of all eight piezoresistive sensors, with important elements of the setup outlined. The load cell appears behind the foam, from the direction of impact.

Each of the eight insole sensors was impacted at five different impact masses, ranging from 0.75 to 3.6 kg (Table 2.1). Each impact condition was conducted four times, with the first impact being a “settling” impact, to allow the sensor to be well settled in the foam before recording impacts. This was conducted to address changes in sensor responses that were observed in repeated impacts as a result of increased stiffness (Van Tuyl, 2014) and details of repeated impacts are found in Appendix D. The average of impacts two, three and four were used for the development of the calibration curves. In total, 160 impacts were conducted across all eight sensors. The impact masses required to generate the appropriate change in sensor voltages (ranging from 0.48 and 0.92 V) were found using an iterative approach (Table 2.1).

Table 2.1: Impact Parameters for Sensor Calibration

Projectile impact mass required to achieve the change in sensor voltages that were found during booted ATD testing. Impact masses were varied until the approximate targeted change in voltage was achieved. This was the basis of the sensor calibration matrix.

Impact Mass (kg)	Targeted Impact Energy (J)	Targeted Change in Voltage (V)
0.75	13.5	0.45
1.5	27	0.72
1.9	34.2	0.77
2.6	46.8	0.84
3.6	64.8	0.96

2.2.1 Data Analysis

The instantaneous impact velocity, load cell force, time, and sensor voltage were all recorded by a custom-designed LabVIEW (National Instruments Corporation, Austin, TX, USA) program (Appendix E), and read in by a data acquisition unit (NI PXIe-1082, National Instruments Corporation, Austin, TX), sampled at a rate of 50 kHz. The data were then analyzed using a MATLAB (The MathWorks Inc., Natick, MA) program (Appendix F) to automate the process, in an effort to remove user influence.

From each test, the minimum sensor voltage during impact and maximum force (measured using the in-line load cell) were determined and averaged, in an effort to increase repeatability of the sensors. These average values were used as one data point on an array. These points were then plotted for each sensor, and a polynomial line of best fit was generated ($y=ax^b+c$) using the EzFit Toolbox on MATLAB, the basis of the calibration procedure. Each sensor had six data points, five of which represented each of the impact masses, and an additional data point to represent the unloaded condition of the sensor. Each sensor has a distinct calibration curve, in which the minimum voltage during any impact may be entered, and the force during impact can be calculated.

2.3 Results

The average instantaneous impact velocity was 5.95 ± 0.5 m/s for all tests. Repeated impacts showed good consistency (Table 2.2). The minimum voltage and force were graphed and displayed to the user, in an effort to ensure the data entries selected by the program were

correct (Figure 2.3). All repeated trials averaged coefficients of variation (CoV) of 9.5% (Appendix G).

Table 2.2: Repeated Trials of Sensor Impacts

Each sensor was impacted three times, and the results were averaged. The table shows voltage and force results from sensor 1 impacts, with a 2.5 kg impact mass.

Trial	Minimum Voltage (V)	Maximum Force (N)
1	-1.0259	-3268.2
2	-1.081	-3269.5
3	-1.1004	-3194.7
Average	-1.0691	-3244.2

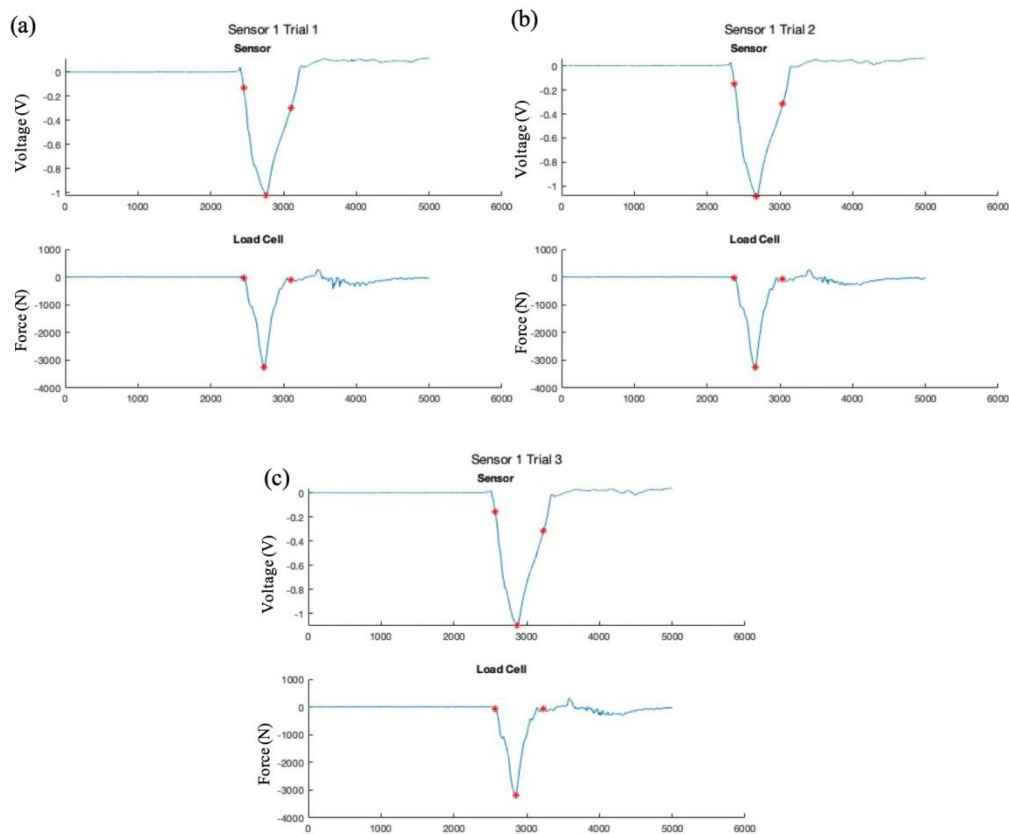


Figure 2.3: Repeated Trials of Sensor 1 Impacts

Impacts using a 2.5 kg impact mass of (a) Trial 1, (b) Trial 2, and (c) Trial 3 identical impacts. An example of what the user processing the data would see, confirming the start of impact, peak sensor voltage and load cell force, and end of impact (shown in red).

Each sensor had a calibration equation of the form

$$F = a * v^b + c,$$

where F is the force, a , b , and c are variables dependent on the calibration curves generated during the calibration process, and v is the minimum voltage read off the sensors during the impact event (Table 2.3).

Table 2.3: Calibration Curve Coefficients

Sensors 1 through 8 each had a unique calibration equation for converting voltage (v) to force (F), presented in the form $F = a * v^b + c$.

Sensor	a	b	c	R ²
1	3077.0	2.1600	70.635	0.823
2	4411.1	1.1505	-72.915	0.918
3	3492.3	1.1657	3.1832	0.839
4	1977.9	2.0756	14.917	0.958
5	4507.8	2.0082	8.4085	0.998
6	4041.0	1.0683	2.4178	0.949
7	4650.9	3.3741	195.13	0.951
8	2166.5	3.7715	373.25	0.949

Each calibration curve can be found in Appendix H. An example of Sensor 1 curve is shown in Figure 2.4.

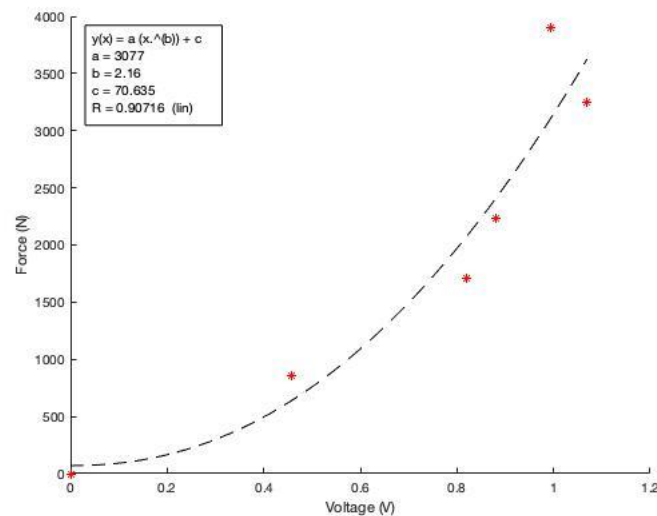


Figure 2.4: Sensor 1 Calibration Curve

Calibration points fitted with a polynomial line of best fit for all Sensor 1 impacts.

2.4 Discussion

Foot and lower leg injury as a result of motor vehicle collisions can be painful and costly. The incidence of these injuries may be reduced by adequately capturing the amount of force applied to the foot during impact. The instrumented boot was previously developed to address these limitations, and the present work was conducted to calibrate at an expanded range and automate this process. The improved calibration of the instrumented boot provides an accurate and repeatable method of assessing force on the plantar surface of the foot. This device will allow injuries generated in a controlled laboratory environment to be correlated to the applied load and easily translated into automotive collision testing using ATDs. It also provides the potential to develop regional injury metrics.

The use of the piezoresistive polymers as force sensors allowed for an inexpensive and repeatable assessment of force at the plantar surface of the foot. These sensors have previously shown a high correlation to toe and ankle load cell measurements over a range of impact parameters (Acharya *et al.*, 2018), and were developed specifically for this purpose. The array of insole sensors also has the ability to provide regional loading information at discrete locations, with excellent resolution. Commercial sensors do not typically allow for load ranges necessary for injury generation (*i.e.* greater than 8 kN) at acquisition rates necessary for impact testing (greater than 20 kHz). Those that do come in predetermined sizes, an array of which would leave approximately 25% of the surface area uncovered. The unique geometry of these sensors allows for the majority of the plantar surface to be covered, allowing for the assumption that the summation of the insole sensors provides the absolute force that the plantar surface of the foot experiences during impact.

The repeated tests during these impacts indicated that the insole sensors were a reliable tool for assessing force. The three repeated impacts after the settling impact provided very consistent results, in terms of impact duration, peak load cell force and sensor voltage. A polynomial fit was used to produce the calibration equations as this showed a good representation of the data while keeping the calibration process as simple as possible. It is possible that this fit was not the optimal mathematical representation for the voltage-force graph. However, the calibration process yielded R^2 results between 0.823 and 0.998, indicating a very good mathematical representation of the force-voltage data.

Difficulties with the piezoresistive polymer resulted in Sensor 4 impacts only produced three usable calibration points. This was because some of the voltage-force graphs produced during impacts had very erratic voltage readings. This may have been caused by the electrodes

touching during impacts, causing the circuit to momentarily short, and the voltage to fall to zero during impact. Upon inspection, this may have occurred because the polymer shifted slightly during impacts, causing the steel plates to come in contact with one another. This did not happen for all calibration tests, only the last two: impact masses of 1.9 kg and 3.5 kg. A similar reaction happened during one of the Sensor 7 tests. This polymer was secured more tightly for future tests so the plates would not shift during impact on ATD and PMHS tests. Electrical tape was used to secure the polymer between the steel plates, which may have caused shifting during impact. Some of the calibration curves exhibited a linear response. This may have been due to variations in how tight the sensors were wrapped. Furthermore, it is unknown what the effects of aging may have on the piezoresistive properties of the polymer.

This calibration process was developed in order to mimic the intended impact parameters as closely as possible. This was done through using the exact velocity and duration (and therefore load rate) of the expected impacts for the boot's purpose, based on preliminary full booted ATD impacts. However, when the sensors are in the boot insole, the stiffness of the boot is unknown, which may cause the sensors to experience different loading rates. Now that the tool has been robustly calibrated, it will be useful for future foot and ankle injury studies, by providing force readings on the plantar surface of the foot.

Chapter 3 - ATD Impact Testing in Altered Ankle Postures

Overview: This chapter explores the axial impact responses of two commonly used ATDs, the Hybrid III and Military Lower Extremity, under five different ankle postures. The instrumented boot (Chapter 2) was employed during impacts to assess the load distribution variations among postures and between ATD models. Both posture and ATD model affected the load distribution on the foot, highlighting the need to establish regional injury limits, as well as limits for non-neutral postures. The increase in forefoot loading during plantarflexion was not reflected in the standard industry metrics, suggesting that increased fracture risk to the forefoot would not be detected. The differences in load distribution between the models also demonstrated that these ATDs are not equivalent models, as they are currently treated, highlighting the importance of selecting the appropriate surrogate for the intended loading conditions.²

3.1 Introduction

Anthropomorphic Test Devices (ATDs) are commonly used to assess injury risk to the foot-ankle complex, where the lower leg is typically instrumented solely with an upper and lower tibia load cell. Although ankle and toe load cells exist for the Hybrid III foot, they are not often employed in industry testing. Injury risk to this region is typically grouped with the rest of the

² A version of this work was presented at the International Research Council on Biomechanics of Injury (IRCOBI) Meeting, Florence, Italy, September 2019, and was published in the conference proceedings: de Lange, J., Quenneville, C.E. (2019). Influence of Ankle Posture and ATD Model on the Distribution of Forces on the Foot Under Impact Loading. *IRCOBI Conference Proceedings* (No. IRC-19-100).

lower leg and evaluated based on tibia peak axial force (F_z) or the Tibia Index (TI) measured by the tibia load cells, and sometimes foot acceleration (Insurance Institute for Highway Safety, 2014). The premise of the TI is to combine the axial load and bending moment in the lower leg into a single value related to injury potential. A TI score less than one indicates a passing test, whereas a TI score greater than one indicates a failing test, and therefore a poor safety rating.

There are many limitations to the current methods of developing and applying injury risk curves to lower extremities. Injury risk curves, which relate the probability of injury to metrics obtained from the aforementioned instrumentation, are developed using post-mortem human subjects (PMHS). Research efforts have historically focused on the ankle positioned in a 90° tibia-to-foot (neutral) posture (Yoganandan *et al.*, 2014; Yoganandan *et al.*, 2015), though vehicular occupants may assume a range of ankle postures while driving (Behr *et al.*, 2010). A limited number of PMHS studies have investigated the effect of ankle posture on injury mechanism, severity, and type, and results have suggested that dorsiflexed ankle postures are more resistant to injury (Crandall *et al.*, 1998) and that plantarflexed ankle postures are more likely to result in distal tibial fractures (Grigoriadis *et al.*, 2019; Smolen & Quenneville, 2016). Ankle posture and its effect on injury risk have not been reflected in current injury risk curves.

The Hybrid III 50th Male (Humanetics Innovative Solutions, Plymouth, MI, USA) is the most widely used ATD in automotive impact testing, approximating the height and weight of the 50th percentile adult male. However, this model has been shown to be relatively insensitive to ankle posture changes (Grigoriadis *et al.*, 2019; Van Tuyl *et al.*, 2016). The shaft of the Hybrid III leg is angled, attached anteriorly at the knee. This causes the Hybrid III leg shaft to be angled when positioned in a neutral position, defined as the line between the center of both the knee clevis and ankle joint. The Hybrid III has a steel shaft, with little to no compliance, making it

much stiffer than natural bone. Concerns over the Hybrid III's response to underbody blasts, particularly its overly stiff structure, led to the development of the MIL-Lx (Military Lower Extremity, Humanetics Innovative Solutions, Plymouth, MI, USA), which is commonly used for analyzing anti-vehicular land mine protective systems. The MIL-Lx leg incorporates a straight knee clevis, tibia shaft, and ankle, as well as a compliant element. Studies have demonstrated the effect of ATD selection on injury risk assessment, indicating that the Hybrid III and MIL-Lx legs generate considerably different force-time and peak force measurements (Grigoriadis *et al.*, 2019; Pandelani *et al.*, 2010; Quenneville & Dunning, 2012; Quenneville *et al.*, 2017). This is partly due to the Hybrid III foot lacking cushioning elements, whereas the MIL-Lx has compression-absorbing elements in the tibial shaft and heel (Pandelani *et al.*, 2010). Differences between the surrogate ankle design elements may alter the post-impact kinematics (*i.e.* by rotating the foot about the tibia differently), which may alter the load transmission through the lower leg. While the MIL-Lx is accepted as having a more biofidelic tibia, neither ATD model currently provides any indication of regional loading the foot may encounter during impacts. The differences in load distribution between the two ATD models, and how that is transmitted to the tibia load cells, could alter injury risk assessment in frontal collisions.

The purpose of this study was to assess the force distribution across the plantar surface of the foot using two common ATD surrogates: the Hybrid III and the MIL-Lx 50th percentile male leg forms. Five different degrees of ankle flexion were investigated to evaluate how ankle posture affects the axial load and bending moment collected in the tibia load cell, and corresponding injury risk. The instrumented boot was also used on both models to assess plantar surface load distribution.

3.2 Methodology

3.2.1 Experimental Testing Protocol

Impacts were conducted at a kinetic energy of approximately 280 J in the pneumatic impacting apparatus described in Chapter 2 (Figure 2.1). Ankle posture was controlled by the ankle positioner, and care was taken to ensure each ATD was axially aligned in the direction of impact, and only the foot was rotated about the ankle joint. The stiffness of the ankle joint is controlled by a screw at the heel of the ATD, and effort was taken to ensure this remained consistent among trials. The flesh analogs of both ATD models were removed to facilitate proper alignment of the ATDs, and neutral posture of the leg was defined as the long axis (defined as the line connecting the knee clevis to the center of rotation of the ankle joint) at a 90° angle to the plantar surface of the boot. Ballast weight was secured to the suspension jig to bring the total mass of each leg form to 12.9 kg, to compensate for the total mass of a 50th percentile male leg, simulating linear inertial properties of the remainder of the leg (Bull *et al.*, 2016). All impacts were delivered at a velocity of approximately 5.8 m/s and a duration of approximately 20 ms, intended to be in the range of realistic impact conditions resulting from a frontal collision (Crandall *et al.*, 1998; McKay & Bir, 2009). Each ATD was axially impacted in five ankle postures: neutral, 10°-plantarflexion, 20°-plantarflexion, 10°-dorsiflexion and 20°-dorsiflexion, with five repeated impacts conducted at each posture. Two unrecorded settling impacts were performed at the start of each ATD testing sequence to ensure the boot was worn in.

The testing procedure was controlled, and data were collected, using a custom-written LabVIEW (National Instruments, Austin, TX, USA) program. A uniaxial accelerometer (MMA1200, Freescale Semiconductor, Austin, TX, USA) was mounted on the ankle positioner to collect footplate accelerations. Two optical sensors (PZ-V31P, Keyence Corporation, Osaka,

Japan) were mounted over the projectile exit from the acceleration tube to collect instantaneous impact velocity. All data, including the two 5-axis load cells (F_x , F_y , F_z , M_x and M_y) in the upper and lower tibia and the eight boot insole sensors, were recorded at 50 kHz.

3.2.2 Data Analysis

For data presentation and interpretation, Sensors 4, 5, and 8 were grouped together to form the “forefoot” loading region, Sensors 3, 6, and 7 were grouped to form the “midfoot” loading region, and Sensors 1 and 2 formed the “hindfoot” region (Figure 3.1). The net plantar surface force was also analyzed using the instrumented boot. Tibia load cell data were dual-pass filtered using a second-order Butterworth low-pass filter with a cutoff frequency of 1,250 Hz (North Atlantic Treaty Organization, 2007). Metrics were assessed at the distal tibia load cell for the Hybrid III leg and the proximal tibia load cell for the MIL-Lx, in accordance with industry standards (Bull *et al.*, 2016). Impact duration was considered to have begun 1 ms before the distal F_z data increased to 10% of the peak F_z and concluded 1 ms after the distal F_z fell below 10% of the peak F_z . The five repeated trials were averaged, and the standard deviation was determined. The primary outcomes from the ATD were the peak axial forces in the upper and lower load cells, as well as the Tibia Indices (TI).



Figure 3.1: Regional Sensor Groupings

The sensors were grouped into three regions for data presentation and interpretation, where the blue region represents the forefoot, the orange the midfoot and the yellow the hindfoot.

The Tibia Index is a widely accepted injury criterion for the lower leg. The Adjusted Tibia Index (TI_{Adj}) was developed to account for the geometry of the Hybrid III leg (Welbourne & Shewchenko, 1987; Zuby *et al.*, 2001). Tibia Indices were calculated according to the following equations:

$$TI = \frac{F}{F_c} + \frac{\sqrt{M_x^2 + M_y^2}}{M_c} \quad \text{Equation 3.1}$$

$$TI_{Adj} = \frac{F}{F_c} + \frac{\sqrt{M_x^2 + (M_{y, distal} - 0.006398 F_z)^2}}{M_c} \quad \text{Equation 3.2}$$

In these equations, TI corresponds to injury risk (where values greater than 1 indicate failure), F is the applied axial force and M_x and M_y are measured tibia moments. F_c and M_c are the critical values previously determined using cadaveric testing, 35.9 kN and 225 Nm, respectively (Kuppa *et al.*, 2001). Equation 3.1 was used to calculate the proximal TI for MIL-Lx impacts, while Equation 3.2 was used for Hybrid III distal tibia load cell analysis (Bull *et al.*, 2016).

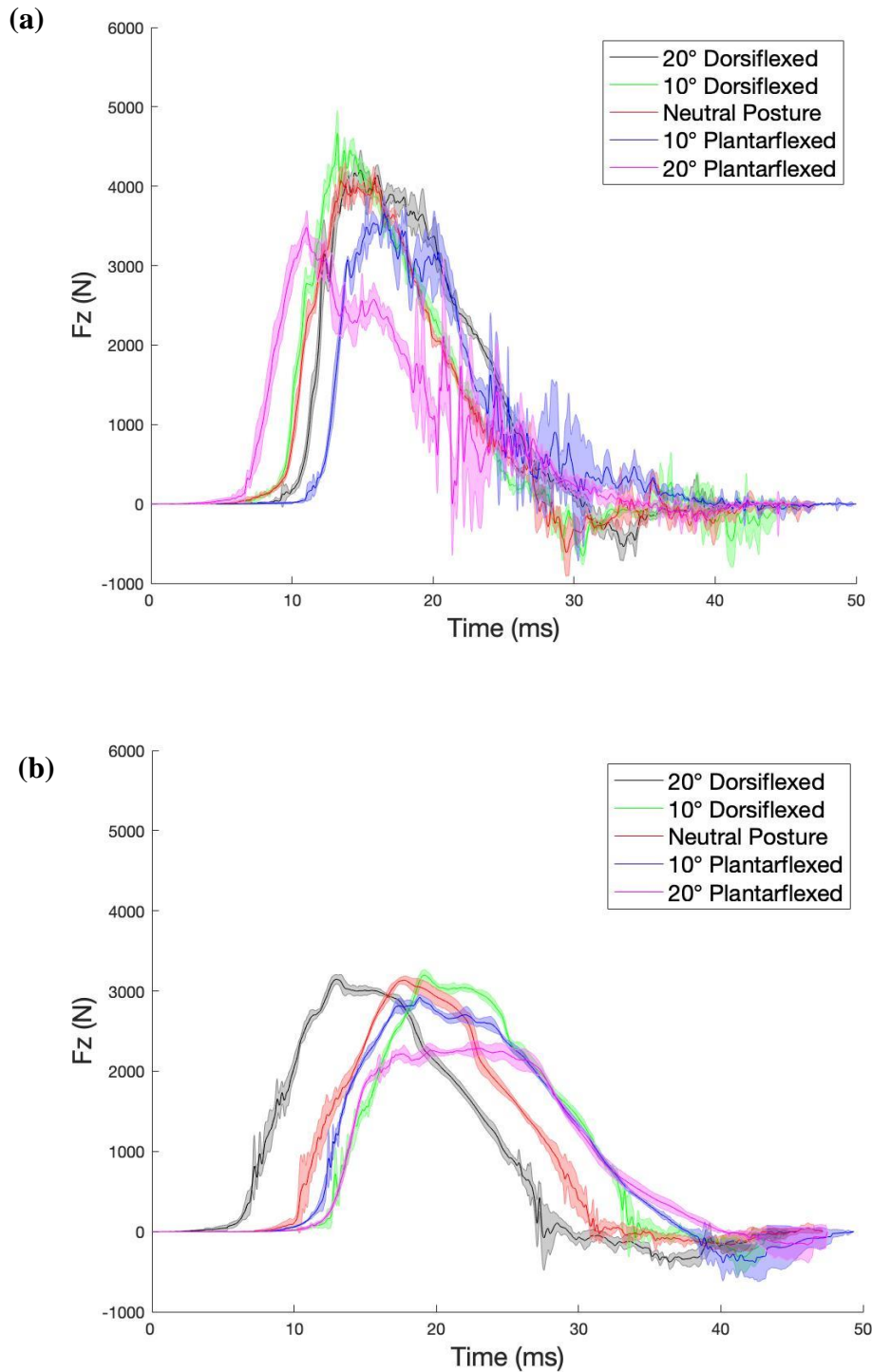
An unpaired t -test was conducted to compare the net boot forces between ATDs at each posture. A one-way ANOVA with a post hoc Tukey test was also conducted to compare the net boot forces among postures, with a significance threshold of $\alpha=0.05$.

3.3 Results

A total of 50 axial impacts were conducted for the purposes of this study, with an average instantaneous impact velocity of 5.86 ± 0.11 m/s. The footplate acceleration was 125 ± 10 g for the Hybrid III and 127 ± 8 g for the MIL-Lx, showing no significant difference between ATD models ($p=0.43$). The impact duration differed for the two ATD models ($p=0.03$) and was an

average of 16.4 ± 1.2 ms for the Hybrid III and 22.1 ± 2.5 ms for the MIL-Lx. Five force-time curves were produced for each ATD, one for each posture, with the mean trace graphed, and shaded regions bounding it representing the standard deviation range (Figure 3.2). Within each posture, impacts were aligned by their peak force. All five repeated tests had very similar time durations, indicating the methodology of producing these curves was repeatable. The Hybrid III force traces were generally noisier and had a larger standard deviation range than the MIL-Lx model. The MIL-Lx also reached a lower peak force over generally longer impact durations. The axial force measurements (F_z , Figure 3.3) and Tibia Indices were plotted for each ATD in each posture (Figure 3.4).

The sums of each sensor's peak axial force collected from the instrumented boot were compared to the tibial load data collected in the ATDs for each posture (Figure 3.5). Each sensor's voltage was converted to force per the calibration process developed in Chapter 2. The boot read forces greater than the tibia load cell across all postures, for both ATDs. In the Hybrid III model, the boot collected forces 24-26% higher than forces collected at the distal tibia load cell, and in the MIL-Lx, the boot collected forces 46-58% higher than forces collected at the proximal tibia load cell (depending on posture). The tibia load cells and boot sensors followed the same trend with posture in both ATDs, with an offset scaling magnitude.

**Figure 3.2: Average Force-Time Traces**

For the (a) Hybrid III distal tibia load cell and (b) MIL-Lx proximal tibia load cell, presented for the five tested postures. Standard deviation regions are indicated with shading.

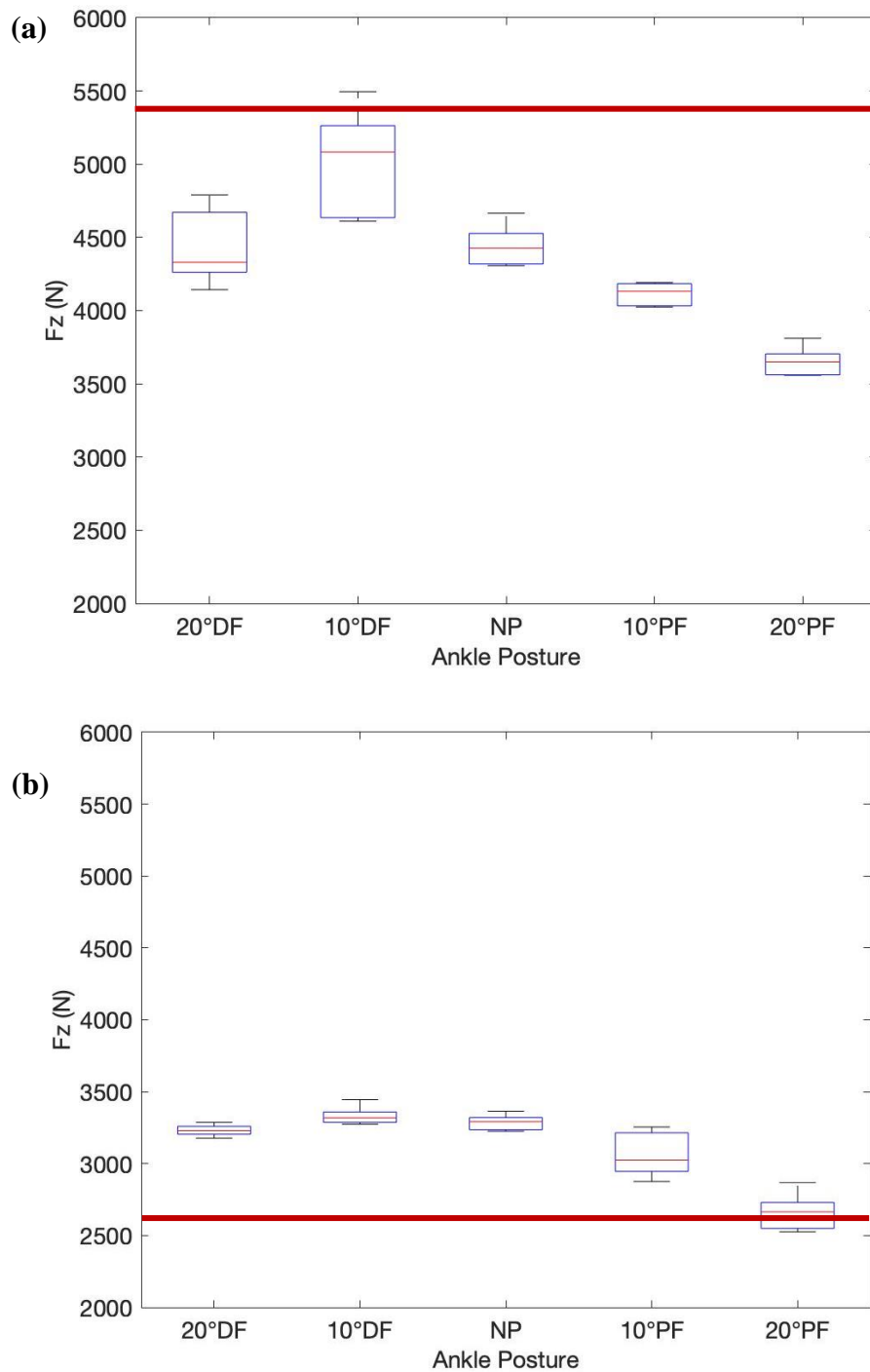


Figure 3.3: Peak Axial Forces

Results from the (a) Hybrid III distal tibia load cell and (b) the MIL-Lx proximal tibia load cell, presented at the five tested postures, with 10% injury risk indicated by the red line.

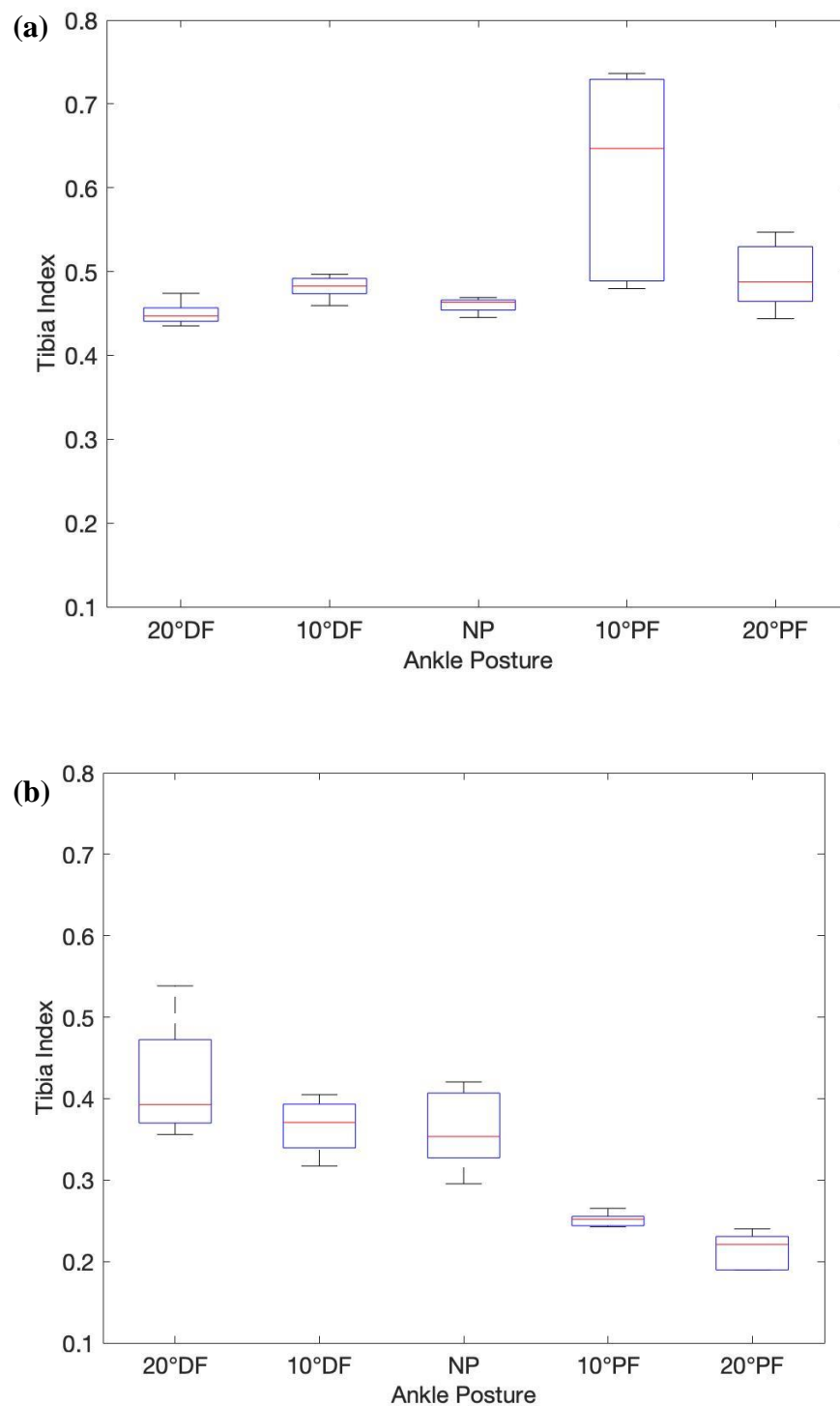


Figure 3.4: Tibia Indices

(a) TI_{Adj} , collected from the Hybrid III distal tibia load cell and (b) TI , collected from the MIL-Lx proximal tibia load cell, at the five tested postures.

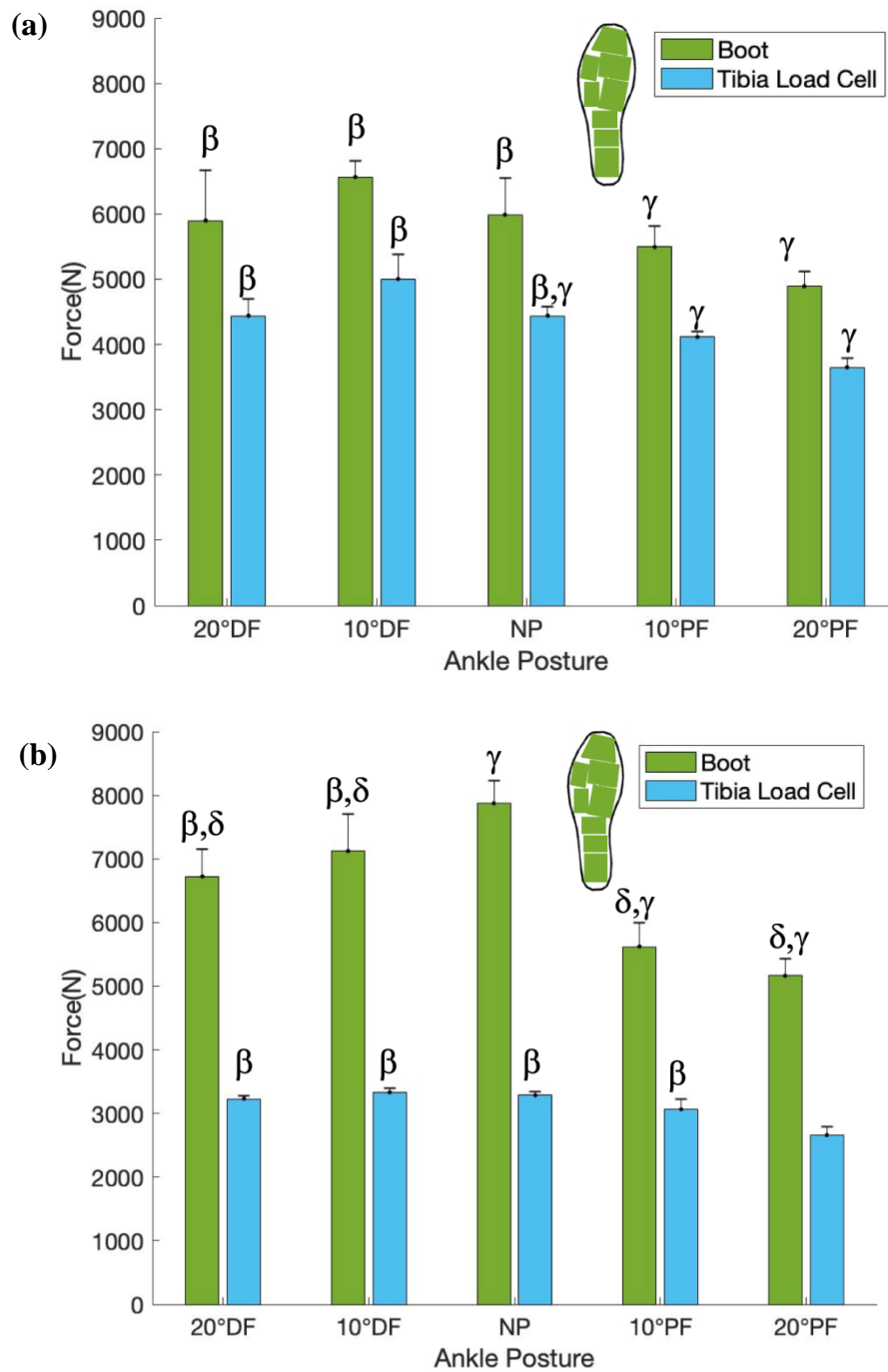


Figure 3.5: Peak ATD Tibia Forces in Comparison to Net Insole Sensor Forces

(a) The Hybrid III distal tibia load cells were examined and (b) the MIL-Lx proximal load cells, measured at varying degrees of flexion. β indicates a significant difference from the 20°-plantarflexed posture, γ indicates a difference from the 20°-dorsiflexed posture, and δ indicates a significant difference from the neutral posture.

The effect of posture was more pronounced in the boot on the MIL-Lx. The tibia load cells collected a larger portion of the net boot forces when the ankle was in the plantarflexed posture. The boot collected the highest loads in the 10°-dorsiflexed posture for the Hybrid III. The 20°-plantarflexed posture was significantly different from the dorsiflexed and neutral postures in the Hybrid III, and both plantarflexed postures were significantly different from the 20°-dorsiflexed posture. In the MIL-Lx, the boot collected the highest loads when the ankle was positioned in neutral. The dorsiflexed postures were significantly different from the neutral posture, and the 20°-plantarflexed postures and the plantarflexed postures were significantly different from the neutral posture and the 20°-dorsiflexed posture. Results from the *t*-test indicated that when ATDs were in the same posture, all net boot forces were statistically different from one another, with the exception of the 20°-dorsiflexed posture.

When examining the distribution of load across the plantar surface of the foot in varied postures, two primary trends were observed in both ATD leg forms (Figure 3.6). Firstly, in all impacts, the hindfoot carried the majority of the load, which was followed by midfoot and then forefoot (except for the MIL-Lx at 20°-plantarflexion, where this was reversed). Secondly, as the ankle moved from dorsiflexion through neutral and into plantarflexion, a portion of the hindfoot load was transferred to the other regions, primarily the forefoot. This effect was most pronounced in the MIL-Lx.

At neutral (NP), the hindfoot recorded 71% of the load in the Hybrid III model and 80% of the total load in the MIL-Lx model. The forefoot recorded 14% of the loads in the Hybrid III and 5% of the loads in the MIL-Lx. When the ankle was positioned in the plantarflexed (PF) postures, the sensors in the hindfoot region decreased substantially in both ATD models. The Hybrid III model recorded hindfoot forces of 49% and 51% in 10°- and 20°-plantarflexion,

respectively, while the MIL-Lx hindfoot loading decreased to 67% in the 10°-plantarflexion and 52% in the 20°-plantarflexed posture. This load was mostly transferred to the forefoot, which increased from 18% to 25% in the Hybrid III model (but demonstrated no trend with increasing angle) and for the MIL-Lx increased from 5% to 12% and 32% in the 10°-plantarflexed postures and the 20°-plantarflexed postures, respectively.

In dorsiflexion (DF), the hindfoot sensor loads reduced slightly from 75% in the 10°-plantarflexed posture to 70% in the 20°-plantarflexed postures in the MIL-Lx. The forefoot region collected 9% of the total load at the 10°-dorsiflexed posture and 12% at the 20°-dorsiflexed posture in the Hybrid III model. In contrast, in the MIL-Lx the forefoot loading in this posture increased from 6% in the 10°-dorsiflexed posture, and 11% in the 20°-dorsiflexed posture. In general, for both surrogates, the dorsiflexed postures exhibited lower loads in the forefoot as compared to plantarflexed postures.

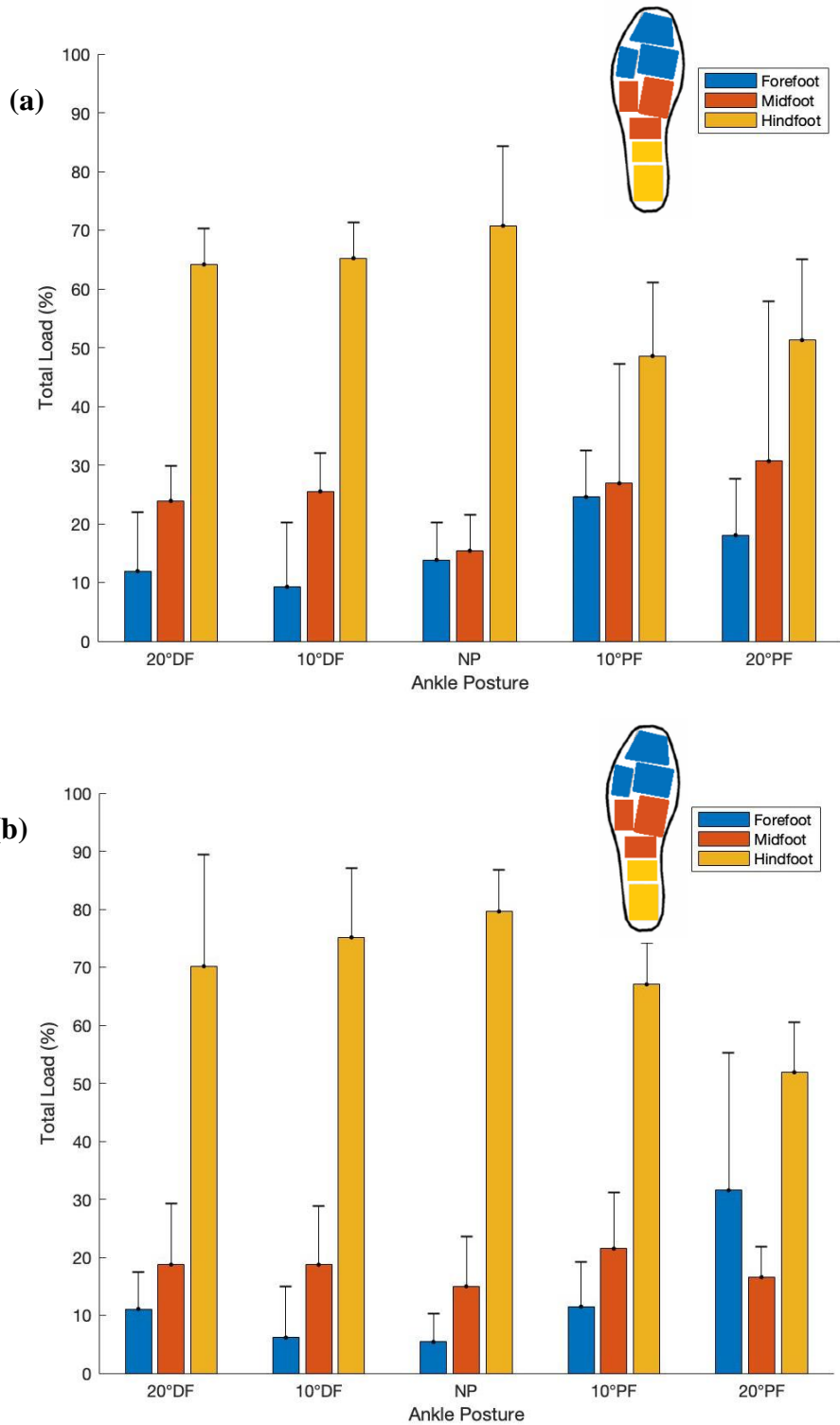


Figure 3.6: Regional Boot Loading

The insole sensors were divided into three regions, presented in (a) the Hybrid III and (b) the MIL-Lx in the five tested postures.

3.4 Discussion

It has been demonstrated by multiple researchers that injury risk to the lower leg may be altered when the foot is positioned in a non-neutral posture (Crandall *et al.*, 1998; Dong *et al.*, 2013; Ed, 2005; Grigoriadis *et al.*, 2019; Smolen & Quenneville, 2016). However limited studies have examined the effect of initial posture on the response of ATD model lower legs (Grigoriadis *et al.*, 2019; Van Tuyl *et al.*, 2016), which must have a biofidelic response in order to be considered an appropriate model for predicting injury to this region. Of these previous studies, none has conducted as extensive an evaluation of ankle posture and foot/ankle injury as the present study. The effect of ankle posture on both the traditional injury metrics of axial load and Tibia Index, as well as the new location of measurement of the plantar surface of the foot, were collected under conditions representative of frontal motor vehicle collisions. Impacts were delivered in the range of the results of a frontal crash simulation by Crandall *et al.*, (1998) that reported a floor velocity of 5 m/s. Similarly, impact duration was in the range of 15 to 45 ms, representative of a frontal automotive impact (McKay & Bir, 2009). Impacts were conducted using both the Hybrid III and the MIL-Lx ATD models, and both surrogates proved to be consistent models with the MIL-Lx showing slightly better repeatability results in comparison with the Hybrid III, which is consistent with a previous study (Pandelani *et al.*, 2010).

The peak axial force (as measured by the industry-standard load cell in each surrogate) showed a decreasing trend as the ankle was moved from dorsiflexion through neutral and into plantarflexion. The Hybrid III force values were consistently higher than the MIL-Lx, which is unsurprising given the acknowledged stiffer nature of this surrogate. As the MIL-Lx is more compliant, it has a correspondingly lower injury criterion, at 2.6 kN, versus the 5.4 kN threshold

typically used for the Hybrid III (North Atlantic Treaty Organization, 2007). Interestingly, the Hybrid III would have ‘passed’ all of the tests conducted herein, as all peak axial forces were below the 5.4 kN threshold. This is in contrast to the MIL-Lx which would have ‘failed’ four of five postures, in which the peak axial force was greater than the 2.6 kN injury criterion, which suggests that the two surrogates and their respective injury criteria are not entirely equivalent. This is in contrast with a previous study (Quenneville *et al.*, 2017) that found that the Hybrid III lower leg exceeded its criterion at lower impact conditions than the MIL-Lx. However, the impact durations in the present study were greater than that previous one (which was simulating anti-vehicular mine blasts, with impact durations in the 10-15 ms range). The same previous study noted that the relative performance shifted when energy attenuating mats were included, which in effect extended the impact durations, and may be more in agreement with the impact conditions applied in the present study. The 2.6 kN load limit on the MIL-Lx was developed for blast loading rates, while the 5.4 kN limit was developed for automotive loading rates, which may be why the load limits and their respective injury criteria did not agree in this assessment (North Atlantic Treaty Organization, 2007).

When comparing the summation of peak boot sensor forces to tibia load cells, the sensors consistently collected forces that were higher than the tibial load cells. This is unsurprising due to the force dissipation that occurs between the plantar surface of the foot and the tibia, and these results align well with a previous study conducted by Acharya (2018), who found ankle and toe load cell forces to be consistently 120-130% higher than tibia forces under axial impacts. The statistical analyses that were conducted on the data demonstrated that postural effects were significant among postures when analyzing net boot forces.

The increased forefoot loads in plantarflexed postures that were observed in this study are similar to those observed in a previous study conducted by Grigoriadis *et al.* (2019), in which force sensors collected load data at the forefoot and midfoot. A notable difference in the present study was an increase in hindfoot loading in the plantarflexed posture as compared to the neutral posture in the Hybrid III ATD. This recent study displayed similar force-time traces to the current study, where the MIL-Lx measured force values consistently lower and with a longer impact duration than that of the Hybrid III. In neutral postures, the surrogate tibia shaft was most aligned with the direction of impact, and therefore most stiff. This resulted in higher peak forces and shorter impact durations, a trend also observed in a previous study (Van Tuyl *et al.*, 2016). The TI_{Adj} and peak F_z values reported in that study also showed very similar trends in varying degrees of flexion when compared to the current study.

In all impact scenarios, for each posture and for each model, the hindfoot sensors carried most of the load. This is unsurprising as the hindfoot lies directly under the ankle joint. Furthermore, ATDs do not mimic muscle loading in the ankle, so forces acting on the forefoot cause the ankle to rotate with minimal resistance. Measuring the force distribution in PMHS under similar impact conditions and recording injuries in specimens with the distribution of forces in the ATDs would be a useful step in developing regional injury criteria for the foot.

While the axial force measures did not show much variation in either model with altered postures, the same cannot be said about the Tibia Index measures. In the Hybrid III, moving from dorsiflexion to plantarflexion increased Tibia Index. As this move decreased axial force, this means that the bending moment was substantially increased with altered posture, which may be a function of the irregular geometry of the Hybrid III lower leg. Because the ‘neutral’ lower leg posture for a Hybrid III has the tibia already at an angle, this likely led to the development of

artificial bending moments under axial loading, which has been previously observed (Quenneville & Dunning, 2012). Conversely, the MIL-Lx decreased in Tibia Index when moving from dorsiflexion to plantarflexion. This trend is in contrast to PMHS studies, which suggest the dorsiflexed posture is more resistant to injury in comparison to other postures (Crandall *et al.*, 1998), indicating that *TI* may not be a reliable assessment of injury risk as it relates to posture. These data also suggest that the *TI* and *TI_{adj}* are sensitive to different factors, making them difficult to comparatively assess, showing only similar values in the 20° dorsiflexion posture. This also highlights the interdependence of axial force and Tibia Index as assessment metrics.

This study found that both posture and ATD model affected the load distribution across the insole of the boot. As the ankle was moved from dorsiflexion to plantarflexion, loads in the hindfoot tended to decrease and get redistributed to the mid- and forefoot regions. The hindfoot loading trend paralleled the tibia axial force trend, suggesting these two were highly correlated, but while the Hybrid III had higher axial forces, the MIL-Lx had higher hindfoot percentages. This may have been the result of ankle rotations during impact, or load being converted into bending and highlights the complex kinematics associated with these impacts. In plantarflexion, the forefoot proved to be particularly vulnerable, carrying a large percentage of the total load, and thus injuries to this region may require separate injury criteria and evaluation of risk for more complete assessments of safety. Interestingly, none of the metrics evaluated herein showed the dorsiflexion posture as being more resistant to injury, as was noted in a previous cadaveric study (Crandall *et al.*, 1998), which may be a function of the simpler joint representation in an ATD when compared to PMHS (with ligamentous structures and numerous irregular bones that may alter the load path).

Both the Hybrid III and the MIL-Lx showed the greatest boot loading in the hindfoot when positioned in a neutral posture, a trend that was not observed in the F_z and TI data. This suggests that there may be important information to be gained by examining plantar surface force distribution. This lack of correlation with existing metrics may be a reason why the mid- and forefoot regions have not been previously studied in impact testing, although they would be particularly vulnerable in scenarios of impingement. However, the boot sensors had large coefficients of variation (CoV). This was particularly problematic for the forefoot and midfoot regions, due to the smaller magnitudes of values at these locations; however, for the hindfoot region, CoV values ranged between 0.07 and 0.23. These values highlight that more work needs to be done to improve the repeatability of the insole as a tool. The CoV values for axial force in the ATDs were all acceptable (<8%), as were most of the Tibia Index CoV (but not all, with values exceeding 10% for one Hybrid III posture, and three MIL-Lx postures). The large standard deviations of the regional boot sensor loading (Figure 3.6) are a compound effect of test variability and ATD variability (similar to the standard deviation bars in Figure 3.3), as well as boot sensor and ankle kinematic variabilities. Due to these factors, the boot forces have larger errors associated with the presented results.

Analysis of the data suggests that ankle posture was a good indicator for peak F_z , hindfoot loading, and forefoot loading, as these data showed correlating results. Interestingly, there was not a correlation of TI as it relates to ankle posture, the basis upon which many current injury limits are set. This further emphasizes the need for greater load characterization in this region of the body. The significant differences between impact duration in the models, 16.3 ms and 22.1 ms for the Hybrid III and MIL-Lx models, respectively, were not surprising due to the increased compliance of the MIL-Lx model. The footplate accelerations were not significantly

different between models (125 ± 10 g for the Hybrid III and 127 ± 8 g for the MIL-Lx), which is also unsurprising as this metric is a direct result of the applied kinetic energy.

3.4.1 Study Limitations

There were a few limitations to the current study. The five trials conducted in each posture were done consecutively and were not randomized, due to time constraints of altering the ankle positioner between tests. It is possible that there was some accumulated damage or relaxation to the surrogate (or instrumented boot) with the repeated impacts. However, the number of impacts was similar to the number of impacts applied during the calibration process, and therefore any insole compression and relaxation should have been conducted prior to data collection.

There may have also been small differences in the lacing of the boot on the two ATDs, but this was minimized as best as possible by having the same researcher tighten the boot on each surrogate. There were some inconsistencies in trends with the altered postures (*e.g.* the Hybrid III forefoot load percent increasing for 10° of plantarflexion, then decreasing at 20°). Testing a greater number of ankle postures may make trends in the data more evident. Ballast weight was affixed at a single location on the supporting bracket within the impacting apparatus, and as such did not realistically represent the distribution of mass that would occur in the natural lower limb. This may not have provided natural rotational inertia and could have altered post-impact kinematics. However, given the axial impact scenario, and the relatively modest percent of ballast weight as compared to the total weight of the lower leg, overall kinematics were likely similar, and minimal rotation was observed upon examination of high-speed video. Furthermore, this was consistent among all tests.

Next, the flesh analog of both ATDs was missing during impacts. Pandelani *et al.* found that while the MIL-Lx showed almost no difference when the skin was fitted, the Hybrid III lower leg recorded forces up to 10% higher when fitted with the flesh analog (2010). This may have affected the peak axial forces that were recorded during impacts. Also, while the data collected at the mid- and forefoot regions are of interest herein, there are no established injury criteria for these regions, making it difficult to evaluate the potential importance of this loading. Finally, tests were conducted only at a single impact speed, and always with the impact aligned with the lower leg axis. Further investigation on the implications of impact velocity, duration and acceleration may affect the force distribution on the foot. Any out-of-posture of the lower limb (not just ankle) would require separate and further investigation.

3.5 Conclusions

This study emphasized the importance of selecting the correct surrogate as well as considering initial ankle posture when developing injury criteria for the lower extremity. This study also outlined the importance of developing regional injury criteria for the foot and moving beyond the gross measures indicating global mechanics. Increased loading to regions of the foot in different postures would go undetected without the use of instrumentation on the plantar surface of the foot. Finally, it is evident from these findings that ankle posture plays a large role in the force distribution on the plantar surface of the foot (as well as in tibia load cell measures, as previously noted). Since injury criteria are typically developed when the ankle is in a neutral posture, care must be taken when aligning the ATD foot according to the tibia shaft during collision testing to provide an accurate representation of injury risk. Finally, posture-specific injury risk curves should be developed to account for the different varying load transmission

pathways, and these data may guide future developments of more biofidelic foot/ankle models. To the author's knowledge, this is the first study to assess the load distribution at the plantar surface of the foot under impact loading. It is also the first application of the novel instrumented insole and will form the baseline for comparison with future post-mortem human subjects to develop regional injury metrics.

Chapter 4 – A Technique to Assess the Impact Response of the Human Foot/Ankle Using an ATD Tibia

Overview: This chapter explores the axial impact responses of three representations of the lower leg: the intact post mortem human subject (PMHS) lower leg, the Military Lower Extremity (MIL-Lx), and an adapted lower leg that combines the MIL-Lx tibia shaft and cadaveric foot. Impact testing was conducted with lower leg representations in a neutral posture to assess the load transmission through each and to determine whether mounting the natural foot to the MIL-Lx tibia gave a realistic impact response. Load data were collected at the plantar surface through the use of the instrumented boot, as well as at the tibia load cells in the MIL-Lx shaft.

4.1 Introduction

The foot/ankle complex accounts for up to 10% of all non-minor injuries (AIS 2+) in automobile crashes (Crandall *et al.*, 1996). Although there has been a decrease in the overall frequency of injuries related to car crashes, foot and ankle injuries continue to increase in both severity and frequency (Richter *et al.*, 2001). These injuries are typically very painful and can lead to long-term impairment (Richter *et al.*, 2001).

In the automotive industry, typical methods of injury assessment use Anthropomorphic Test Device (ATDs), with injury risk to the foot and ankle usually grouped and evaluated using load cells in the tibia. Two main lower leg ATD models exist, the Hybrid III 50th Male and the

Military Lower Extremity (MIL-Lx, Humanetics Innovative Solutions, Plymouth, MI, USA). The response of the MIL-Lx has been investigated both at the whole body level (McKay, 2010) and at the tibia level (Quenneville & Dunning, 2012), and is generally accepted as having a more biofidelic response.

While the biofidelity of the MIL-Lx tibia has been evaluated and compared to other surrogates, this has only been investigated as a whole or on the isolated tibia, and with no known studies investigating the foot/ankle response. Load is transmitted through the foot/ankle to the tibia, where injury risk is assessed. If the foot/ankle doesn't transmit the load correctly, then tibia assessments may be incorrect. As such, it is important to examine the biofidelity of the MIL-Lx foot to either validate the current ATD model or provide data for an improved design.

While ATDs are valuable tools with load cells to collect forces and can act in a repeatable manner, they do not undergo injuries. Cadaveric testing is advantageous as it allows for the identification of fracture limits, locations, and mechanisms. However, it is also very expensive, requires a lot of preparation, and generates fracture sites that are extremely variable, due to the variation that exists among specimens. Additionally, this type of testing does not collect internal load data. Researchers have attempted to measure fracture forces in cadaveric testing by implanting load cells proximal to the tibia (*e.g.* Yoganandan *et al.*, 1996) or in the tibia itself (*e.g.* Funk, 2002). This makes it extremely challenging to assess fracture risk and compare it to ATD measurements.

Foot/ankle injuries are impactful, as they involve many articular surfaces to disrupt, often leading to post-traumatic osteoarthritis and have poor vascularization for healing (Dischinger *et al.*, 2004). The foot/ankle region is often neglected when assessing injury risk, by evaluating all injury risk to the lower extremity at ATD load cells in the tibia. The exact fracture force

required to fracture a cadaveric foot, collected while simultaneously reading the forces collected in the tibial shaft, would allow for direct translation into industry how much force is required to generate a foot fracture, and the type of fracture endured (*e.g.* Figure 4.1). To the author's knowledge, no previous studies exist that examine the axial impact response of the isolated cadaveric foot while simultaneously collecting tibia load cell measures.

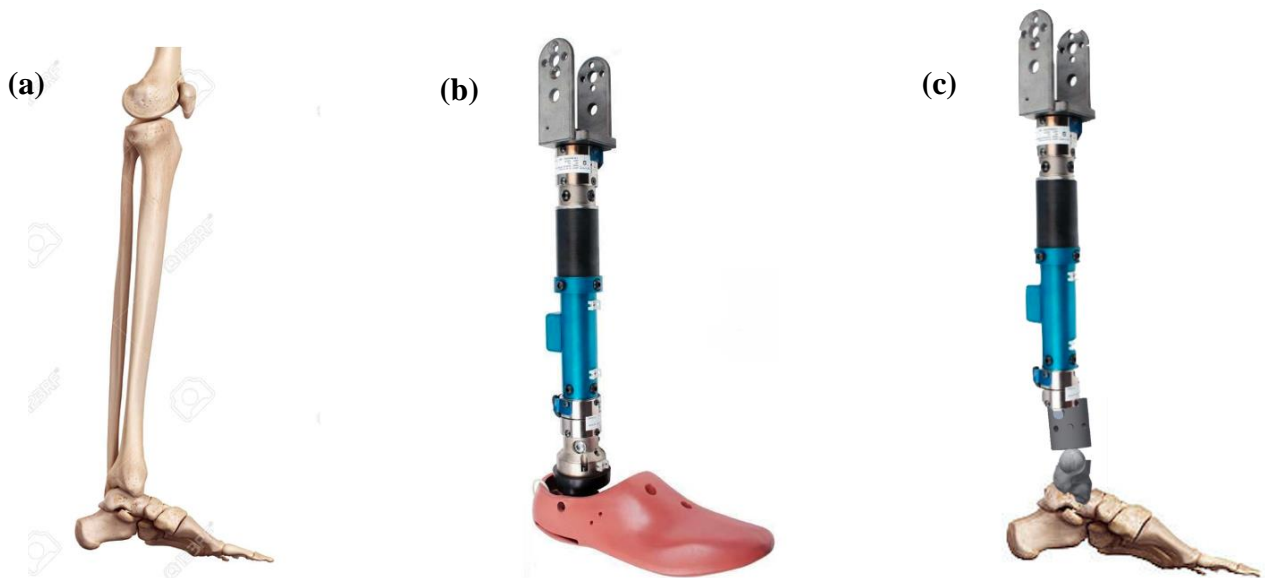


Figure 4.1: Three Lower Leg Representations Tested

The goal of this study was to combine (a) the cadaveric lower leg with (b) the MIL-Lx to form (c) an adapted leg form to assess injury risk and mechanism in the foot while collecting load data that is relevant to industry testing from the tibia shaft.

The purpose of this study was to first compare the axial impact response of intact PMHS lower legs to the MIL-Lx at energies similar to those experienced in vehicular collisions and secondly, to develop a method to mount PMHS feet onto the MIL-Lx tibia shaft. This was done to facilitate the investigation of foot fractures while collecting industry-relevant metrics. The

axial impact responses of all lower leg representations were compared based on force data collected on the plantar surface of the foot by using the instrumented boot, in order to assess whether regional load distribution varied among specimen representations. Where applicable, load data collected in the MIL-Lx were also compared. The objective was to quantify the differences between these leg form representations to investigate whether this technique was appropriate for axial impact tests.

4.2 Methodology

4.2.1 General Testing Approach

All impact testing was completed using the pneumatic impacting apparatus outlined in Chapter 2. Briefly, impact masses were propelled down an acceleration tube by a pneumatic system. Each specimen (Table 4.1) was wearing the instrumented boot while tested, and impacts struck the plantar surface of the foot *via* an ankle positioner. Each ankle was oriented in a neutral position when impacted, defined as when the plantar surface of the instrumented boot was at a 90° angle to the MIL-Lx tibia shaft or PMHS tibial ridge. Ballast weight was secured to the suspension jig to bring the total mass of each specimen to 12.9 kg, the total mass of a 50th percentile male leg, to simulate natural linear inertial properties (Bull *et al.*, 2016). A block of rubber foam (2” thick) was placed on the surface of the ankle positioning device being struck in order to control pulse duration. This foam was replaced after each specimen to mitigate any potential accumulated damage.

Table 4.1: Lower Leg Characteristics

Characteristics of the lower leg representations tested.

Test	Age	Sex	Foot Length (cm)
MIL-Lx	N/A	N/A	26.1
Specimen 1	69	Female	22.2
Specimen 2	69	Male	27.3
Specimen 3	95	Male	27.3

Forces developed during impacts are dependent on stiffness, and as this varies among specimens it is, therefore, challenging to target. However, the kinetic energy of the impact is controllable, so this was used as the target impact parameter in this study. All impacts were delivered at a velocity of approximately 5 m/s and a duration of approximately 50 ms, intended to be in the range of realistic impact conditions resulting from a frontal collision (Crandall *et al.*, 1998; McKay & Bir, 2009). One low-energy unrecorded impact was performed at the start of each specimen in an effort to seat the foot within the boot (kinetic energy of 20-25 J). In order to increase impact energy while duration and velocity remained constant, the projectile mass was then increased, so the impact energy of 80 J was used for all comparative impacts. This was considered a low-energy impact and was designed to be a sub-failure level.

The testing procedure was controlled, and data were collected, using a custom-written LabVIEW (National Instruments, Austin, TX, USA) program, similar to that of Chapter 3. All data, including the two 5-axis load cells (Fx, Fy, Fz, Mx and My) in the upper and lower tibia and the eight boot insole sensors, were recorded at 50 kHz. The data collected from the sensors on the instrumented boot were assessed for peak force and distribution of force along the plantar surface of the foot. Sensors were grouped into three regions: the forefoot, midfoot and hindfoot.

4.1.2 MIL-Lx Testing

The Military Lower Extremity (MIL-Lx) was fitted with the instrumented boot and tested three times. It was suspended in the pneumatic impacting apparatus and supported at the knee clevis. One unrecorded impact was conducted at the start of the testing sequence.

4.1.3 Intact PMHS Testing

Three fully intact specimens sectioned distal to the tibial plateau (aged 78 ± 15 years) were tested. The specimens were x-rayed in the anterior-posterior and lateral views prior to impacting (Appendix I) in order to check for any history of trauma in the specimens. An orthopaedic surgeon evaluated the x-rays and declared there were no pre-existing injuries in the specimens.

Specimens were dissected 2” down from the tibial plateau. They were potted using dental cement in a section of 4”-diameter circular PVC piping, to provide a consistent method to support the specimens while testing and ensure proper axial alignment. The consistent alignment was ensured through the use of a laser level projected along the tibial ridge, and the bone was embedded to the full depth of the PVC pipe (2”). All specimens were thawed for a minimum of 12 hours before testing. The leg form was mounted in the impacting chamber in a neutral ankle posture (Figure 4.2).

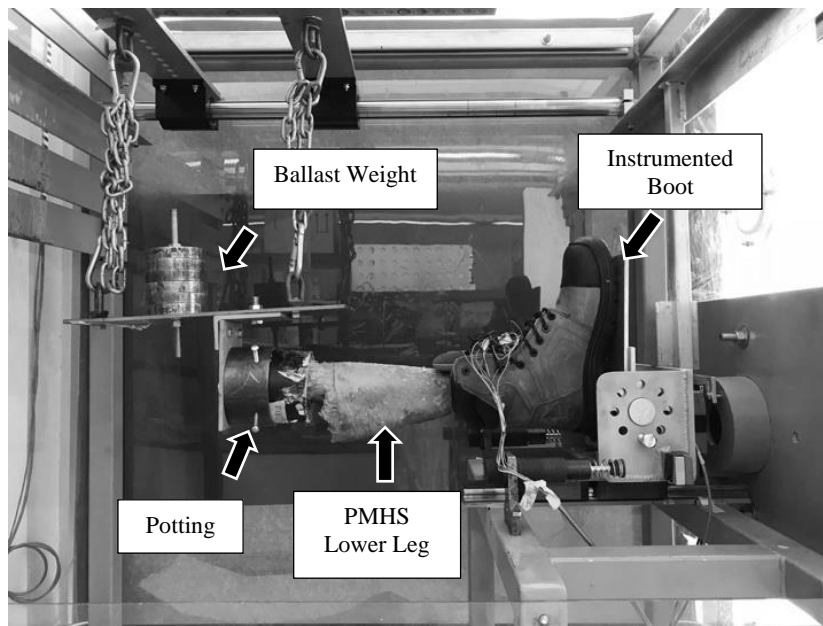


Figure 4.2: Test Setup with Cadaveric Leg in Place

One of the three specimens used for testing inserted into the impacting apparatus and ready for testing.

4.1.4 Adapted Legform Testing

The specimens were disarticulated at the tibiotalar joint and x-rayed in the anterior-posterior and lateral views after disarticulation (Appendix I) in order to verify no damage to the bone occurred. An orthopaedic surgeon again evaluated the x-rays and declared there were no pre-existing injuries in the specimens.

In order to develop injury tolerance thresholds specific to the foot that are directly translatable to the MIL-Lx, isolated cadaveric feet were tested. The MIL-Lx was chosen as the ATD tibia shaft due to its superior biofidelic properties in comparison to other ATDs (McKay, 2010; Quenneville *et al.*, 2017). There were several challenges associated with mounting a cadaveric foot to an ATD tibia. First, soft tissue support was necessary to facilitate proper alignment of the foot with respect to the artificial tibial shaft, in an effort to replicate natural joint

motion during initial positioning. Secondly, natural load transmission between the talus and the ATD shaft was important so that no abnormal stress concentrations on the bone surface could affect the fracture force or location. Finally, the correct alignment and attachment of the MIL-Lx tibia shaft itself to the foot was challenging.

In order to facilitate proper alignment of the foot with respect to the tibia shaft, all soft tissue distal to and surrounding the talus was preserved. The deltoid ligaments and lateral ligaments (posterior tibiofibular, posterior talofibular, and superior fibular), were sutured with a Krakow stitch, using a 2.0 FiberWire suture (Arthrex, Inc., Naples, Florida, USA, Figure 4.3). A Krakow stitch was chosen as the suturing mechanism to reduce the likelihood of shredding or tearing of the tissue. As force is applied, the mechanism tightens around a bundle of fibres and prevents the sutures from pulling through the fibres, providing a secure attachment of the suture to the tendon or ligament (Krackow *et al.*, 1986). These sutures were chosen specifically for this application due to their superior strength, allowing for a tight loop to be secured to the ligament groups. The flexor digitorum longus medial tendon, extensor hallucis longus medial tendon, tibialis posterior medial tendon and tibialis anterior medial tendon were also secured with a Krakow stitch, using Coated VICRYL® Plus Antibacterial (polyglactin 910) sutures (Ethicon Inc., Somerville, NJ, USA). These tendons and ligaments have been reported to all play an important role in ankle joint stability (Campbell *et al.*, 2014; Golanó *et al.*, 2016).

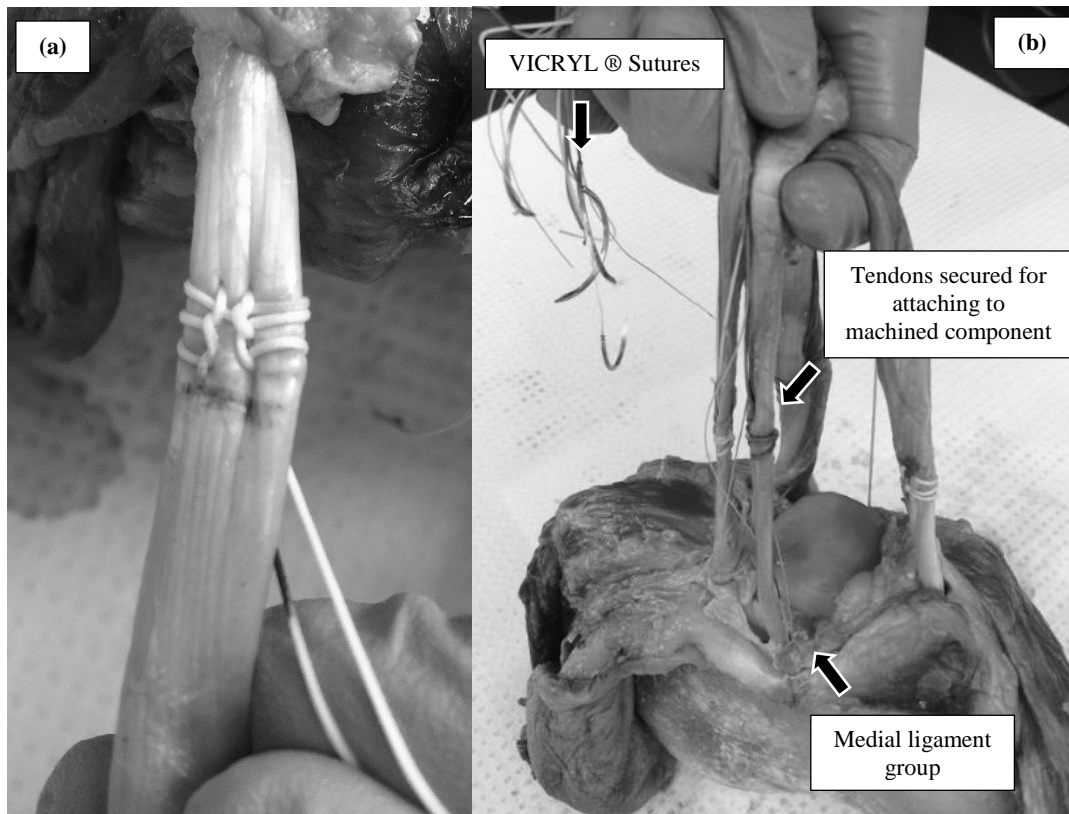


Figure 4.3: Suturing Technique

(a) The Krakow stitch used for suturing each tendon and ligament and (b) the four tendons and the medial and lateral ligament groups surrounding the ankle joint were sutured using a Krakow stitch, in order to facilitate securing the cadaveric foot to the MIL-Lx tibial shaft.

A secondary challenge with attaching a cadaveric foot to the ATD shaft was attempting to keep load transmission natural. In an effort to do so, the distal tibia and fibula of each specimen were optically scanned, and 3D printed to replicate natural bone geometry. The distal end of the specimen's tibia and fibula were scanned using a handheld optical scanner (Artec Eva, Artec 3D, Hamm, Luxembourg). These scans were processed using Artec Studio 3D and converted to a model as a stereolithography (STL) file using Autodesk Meshmixer (Autodesk, San Rafael, CA, USA). Two channels were added through the medial and lateral malleoli, to facilitate attaching medial and lateral ligament suture wires, in an effort to control the line of

action. The model was designed to replicate the natural articular surface specific to each specimen, and 3D printed in ABS plastic, to support the union of the MIL-Lx ATD shaft and the PMHS foot (Figure 4.4).

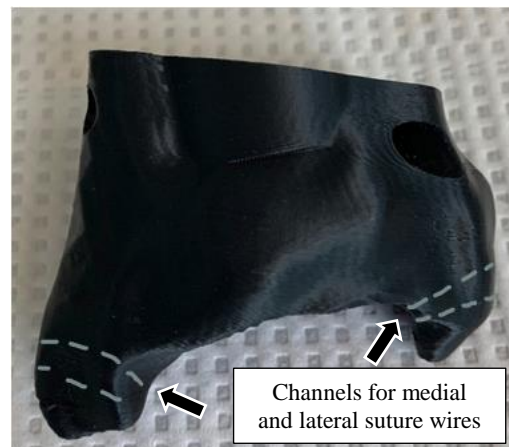


Figure 4.4: 3D Printed Distal Tibia and Fibula

A 3D printed component based on the natural mating geometry of the tibia/fibula was made from ABS and designed with channels added on the medial and lateral malleoli for threading of the ligament sutures.

Finally, to address the challenge of aligning the MIL-Lx tibial shaft at a 90° angle to the plantar surface of the foot (neutral posture), a custom steel component was designed and machined that was used to secure the 3D printed component to the MIL-Lx ATD shaft. A ball joint was created in the ankle to allow the MIL-Lx to rest at a 90° angle to the plantar surface of the foot. This alignment was confirmed by resting the 3D printed component in its natural setting on top of the talus and placing the machined component on top of this. A bull's eye level rested proximal to the machined component, and once levelled polymethylmethacrylate (PMMA, Simplex P Bone Cement, Stryker, MI, United States) was used to fill the gap between the 3D

printed component and the steel attachment in an effort to prevent the fixture from rotating upon impact (Figure 4.5).

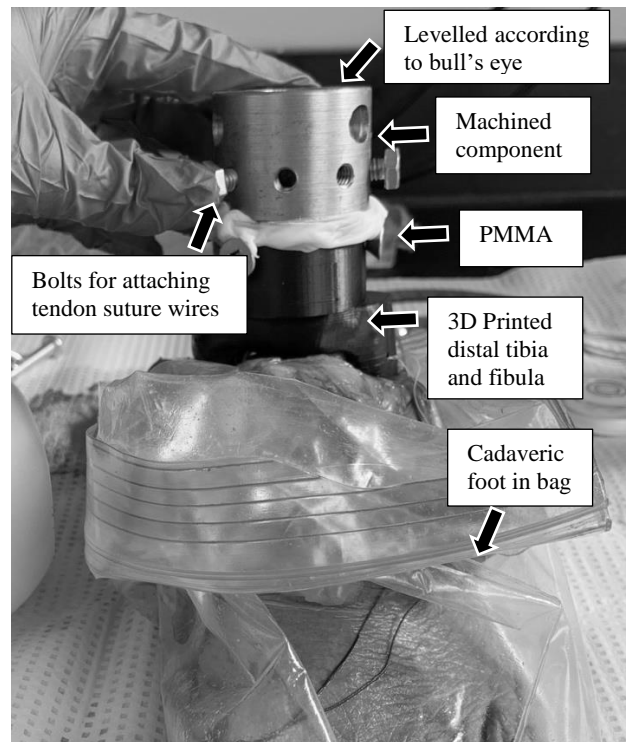


Figure 4.5: Newly Formed Ankle Joint

Components of the attachment apparatus between the cadaveric foot and MIL-Lx tibial shaft.

This piece had a series of eight threaded holes around the circumference of the part to allow for tendons to be attached. Detailed drawings of these components can be found in Appendix C. The entire specimen was then inserted into a sealable plastic bag, to facilitate ease of insertion into the instrumented boot, and maintain the cleanliness of the boot.

The sutures were secured tightly such that there was visible tension in each of the suture wires, as recommended by an orthopaedic surgeon. The sutured tendons on each specimen were

secured to the same bolt in the machined component in an effort to keep consistency among specimens.

4.1.5 Data Analysis

Data collected from the boot for all three lower leg representations were comparatively assessed. In the adapted leg form and MIL-Lx, tibia load cell data were dual-pass filtered using a second-order Butterworth low-pass filter with a cut-off frequency of 1,250 Hz, in accordance with industry impact testing standards (North Atlantic Treaty Organization, 2007). Impact duration was considered to have begun 1 ms before sensor 1 (hindfoot sensor) decreased to 10% of the peak voltage and concluded 1 ms after the voltage fell below 10% of the peak voltage. Changes in voltage were converted to force readings in accordance with the calibration protocol that was developed in Chapter 2.

A one-way Analysis of Variance (ANOVA) with post hoc Tukey test was conducted on both the net boot forces and regional forces for all three leg representations. An unpaired *t*-test was conducted to compare the load cell peak axial forces between the adapted leg form and the MIL-Lx, for both the proximal and distal load cells. Each of these tests had a significance threshold of $\alpha=0.05$.

4.3 Results

Impact velocities ranged from 4.7 to 5.4 m/s (Table 4.2). X-rays pre- and post-impact confirmed there was no damage in the specimens at any stage of the process. The average kinetic energy of these impacts was 79 ± 13 J.

Table 4.2: Specimen Impact Information

Impact results from the intact specimens, adjusted specimens (cadaveric feet with MIL-Lx shaft) and failure impact.

Specimen	Velocity (m/s)	Kinetic Energy (J)
Intact Specimens	4.7 ± 0.3	76.7 ± 16
Adjusted Specimens	5.0 ± 0.5	80.7 ± 16
MIL-Lx	5.4 ± 0.1	93 ± 2

Results from the instrumented boot showed the intact lower limbs caused an average peak boot force of 4578 ± 753 N (Figure 4.6). Based on the ANOVA, no statistical differences were found among lower leg representations when comparing net boot forces, suggesting that stiffness is comparable at the plantar surface of the foot ($p=0.35$). This is despite the MIL-Lx having higher average peak insole forces (4348 N) than the adapted leg forms (3493 N). The hindfoot region carried the bulk of the load for all impacts, ranging from 46-70% depending on the leg type, with the MIL-Lx consistently recording the largest hindfoot forces (Figure 4.7). Based on the ANOVA, no statistical differences were found for forefoot readings ($p=0.24$) and midfoot readings ($p=0.08$), although hindfoot readings were statistically different ($p=0.0007$) among lower leg representations.

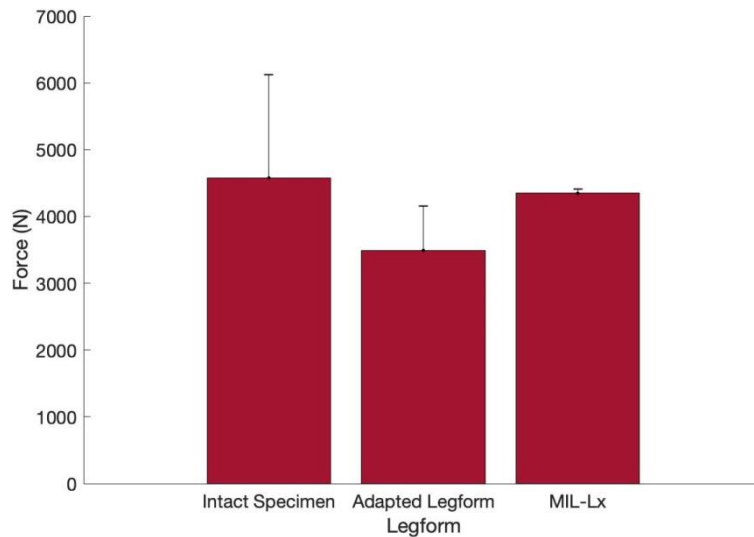


Figure 4.6: Net Insole Sensor Forces

Comparison of the total insole force collected from the plantar surface of the foot for all leg forms.

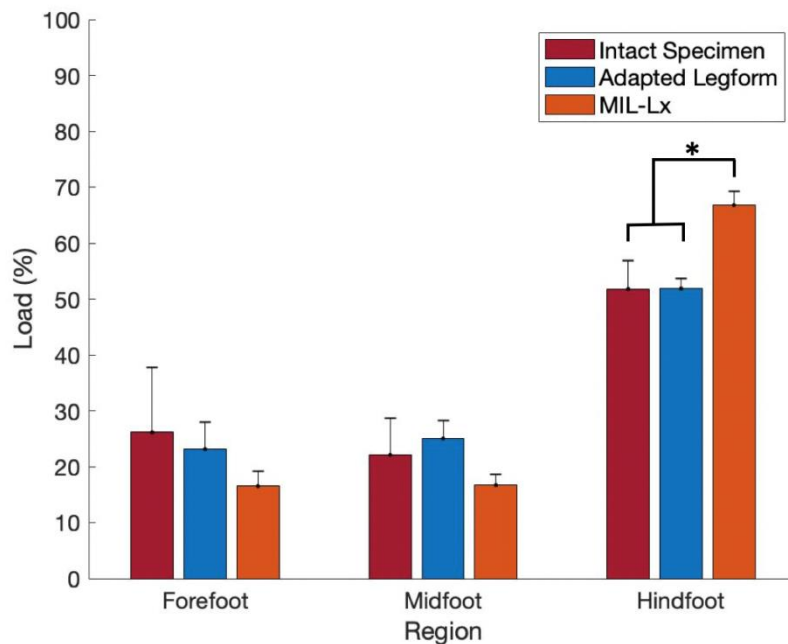


Figure 4.7: Comparison of Regional Loading Responses

Regional loading comparisons of all lower leg representations, where the forefoot loads were collected from sensors 4, 5, and 8, the midfoot loads were collected from sensors 3, 6, and 7 and the hindfoot loads were collected from sensors 1 and 2 (* = $p < 0.05$).

The adapted lower legs, with the MIL-Lx tibial shaft and PMHS foot, caused an average peak boot force of 3493 ± 575 N, and an average peak proximal tibia force of 1516 ± 295 N (Figure 4.8). Results between the proximal load cells collected for both the adapted surrogates and the MIL-Lx were significantly higher ($p=0.03$), as were they for the distal load cells ($p=0.03$).

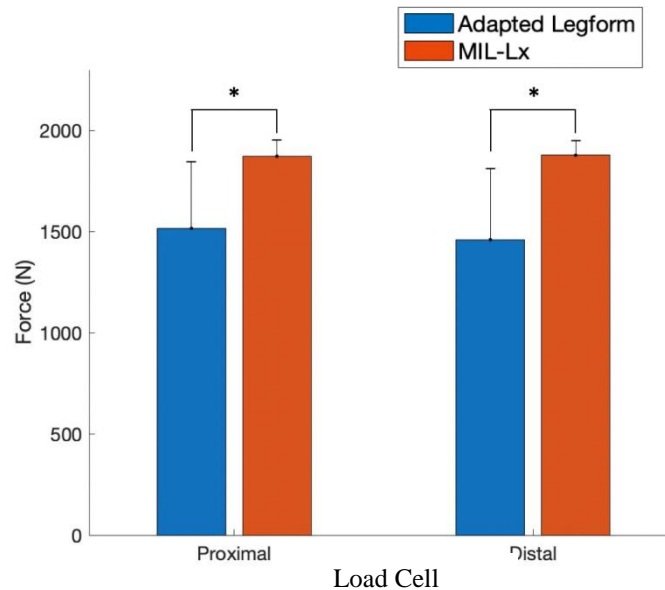


Figure 4.8: Comparison of Proximal and Distal Load Cell Forces

Proximal and distal tibia load cell forces of adapted specimens one, two and three, compared to the intact MIL-Lx surrogate (* = $p < 0.05$).

4.4 Discussion

This study subjected three lower leg representations (intact cadaveric lower legs, the MIL-Lx, and adapted lower legs with the MIL-Lx tibia shaft and cadaveric feet) to low-energy axial impacts for the purpose of evaluating the differences in impact response among surrogates. This study is the first of its kind to investigate the isolated cadaveric foot. Impact time durations

and velocities were consistent with those measured during vehicular collision scenarios (McKay & Bir, 2009). The plantar surface force distribution remained consistent among the intact lower legs and adapted lower legs, suggesting this was a feasible method for combining testing subjects. Through the development of a novel technique to evaluate fracture force while collecting ATD metrics, more accurate injury criteria may be proposed in the future. This adapted surrogate technique will be used for evaluating the fracture tolerance of isolated cadaveric feet.

No significant differences in net boot forces were found among lower leg representations, despite the fact that impact velocity was 15% higher in the MIL-Lx impacts as compared to the intact specimens. Although the MIL-Lx was impacted at a velocity 8% higher than the adapted specimens, net boot insole sensor forces read forces 25% higher than those measured by the insole sensors for the adapted lower leg representation. This means that the effects were likely not all related to variations in velocity, and were related to changes in stiffness. This translation of force into the proximal tibia load cell remained 23% higher in the MIL-Lx in comparison to the adapted lower leg representation. The differences in force dissipation that the MIL-Lx exhibited in comparison to the cadaveric foot suggest the MIL-Lx foot may be overly stiff. This is unsurprising, given its material composition, and emphasizes the importance of developing an ATD foot that has similar characteristics of cadaveric feet, as the foot transmits the load to the tibia, where injury risk is assessed.

In contrast, net boot forces between the MIL-Lx and intact lower legs were comparable. This may suggest that perhaps the MIL-Lx tibia is too compliant, or having many compliant elements in series (like the boot) alters the response, as suggested by Quenneville *et al.* (2017).

This emphasizes the importance of understanding the relative stiffness in series and creating transfer functions that account for the various compliant elements.

The significantly higher hindfoot forces in the MIL-Lx may have been a result of the stiffer ankle in the MIL-Lx in comparison to the intact and adapted leg forms, which allow for more ankle joint motion. Interestingly, the forefoot and midfoot forces were not significantly different between all lower leg representations, despite variations in foot size. The cadaveric feet varied in size, which caused the forefoot readings to be slightly reduced in specimen one. These results may suggest that the MIL-Lx foot does not distribute forces along the plantar surface of the foot in the same mechanism as cadaveric feet.

Previous studies have developed injury criteria for the entire lower leg. By focusing on isolated cadaveric feet, while also collecting tibia load data, this study assessed the impact characteristics of feet specifically.

4.1.6 Study Limitations

There were a few limitations to the current study. Firstly, this study was completed with a small sample size (N=3). The specimens were from an older population (average age of 78 years) and varied in foot length, which may have had implications when comparing to the MIL-Lx foot, considering its larger size. However, evaluation of the adapted leg form was compared to the original same specimens, which is advantageous. Furthermore, testing a greater number of specimens with the proposed protocol will enable an analysis of current injury standards.

Next, although the optical scanning procedure was intended to replicate natural human anatomy as closely as possible, the lack of cartilage and the artificial fixation of tendons and ligaments could have altered the responses of the feet. Every effort was made to replicate the

natural ankle; however, this model was not verified. As impacts were delivered in a neutral ankle posture, and in compression, this likely was not a substantial issue and although it may have affected post-impact joint motion, that was not the focus of this work.

The technique developed herein does not include the cadaveric tibia or fibula. If this approach is used in future injury tests, this technique would not evaluate injury risk to the tibia and fibula, which can be injured in these types of events. Findings from Funk *et al.* indicated that the primary location of fracture in axial impact tests is the calcaneus (2001). Furthermore, in tests that involved both calcaneal fractures and pilon fractures, acoustic emission results indicated the calcaneus fractured before the tibia. It is likely that fractures of the foot would occur prior to fractures of the tibia and fibula, so testing isolated cadaveric feet is acceptable to determine the exact force at which fracture may occur, but should be used with the understanding that tibia and fibula risk is not captured.

Often times when vehicular occupants see an impending collision, they will start to panic brake, activating muscles in the calf through tensioning the Achilles tendon. No Achilles tensioning was applied for any testing. The exact amount of tension actually activated through the Achilles is relatively unclear. Funk *et al.* based their 1.5-2 kN of Achilles tension on pedal forces measured during braking from volunteer driving simulations (2002). It is also uncertain how tensile forces through the Achilles differ for different specimen populations, though it may be possible to apply a scaling factor based on Funk's study. Funk *et al.* derived injury risk corridors as a function of Achilles tension, indicating a lack of Achilles tension decreases fracture risk by up to 40% (Funk *et al.*, 2002). Furthermore, the effects of muscle tension may be better investigated using numerical models (*e.g.* Chang *et al.*, 2008). Although Achilles tensioning is thought to compressively load the tibia, perhaps affecting fracture location, it is

challenging to apply this amount of tension. Furthermore, this would also introduce a plantarflexing moment about the ankle joint, shifting the reaction force away from the calcaneus. Next, current ATD models used in automotive collision testing do not incorporate Achilles tension, although it has been proposed for the THOR-Lx. In order to provide the best comparison, muscle activation was neglected herein.

4.5 Conclusions

This study presented a method to assess injury risk to the isolated foot while collecting data that is immediately relevant to the automotive industry. The similar force readings collected at the plantar surface of the foot showed that doing this did not affect the load response to the foot. Results suggest that the MIL-Lx foot could be improved in stiffness characteristics, and this study will provide data that can be used for this design. It is the first study of its kind to propose an adapted lower leg in order to gather axial force data that may be directly applied to assessment methods used in the automotive industry.

Chapter 5 – General Discussion and Conclusions

Overview: This chapter reviews the study rationale, objectives, and hypotheses for this work established in Chapter 1. It summarizes the main outcomes established in this work and their relevance to the research field. The overall strengths and limitations of the thesis are presented, and future research directions are proposed.

5.1 Summary

Axial loading of the plantar surface of the foot is an important lower extremity injury mechanism due to the frequency and severity of injuries this causes in frontal automotive collisions. During these collisions, occupant ankle posture may vary dramatically among individuals, but it is unknown how these effects translate to injury mechanism, and Injury Reference Values collected through Anthropomorphic Test Devices (ATDs). The majority of experimental testing in the development of injury criteria for the lower leg has been conducted with the foot oriented in a neutral posture, creating a 90° angle between the tibial ridge and plantar surface of the foot. Less work has been conducted to assess the postural effects on ATDs, and how this may relate to cadaveric injury metrics. Commonly used ATDs such as the Hybrid III 50th Male and the Military Lower Extremity (MIL-Lx, Humanetics Innovative Solutions, Plymouth, MI, USA) do not have injury limits that account for postural effects. No known studies have conducted injury development testing for automotive collision applications specifically looking at load applied to the plantar surface. A tool that could be applied to both

PMHS and ATDs focusing on foot/ankle injury risk provided greater loading information to this vulnerable anatomical region. The distribution of forces concentrated on the plantar surface of the foot during impact is also valuable insight to attain, as it may be an indication as to where fracture may occur and capture injurious scenarios such as foot entrapment that wouldn't be noticed with current tibia metrics.

The overall purpose of this work was to assess the impact response of PMHS and ATDs in a range of postures using a novel instrumented boot. This was achieved through directly studying the effect of ankle posture on ATD Injury Assessment Reference Values, using insole sensors that were calibrated for automotive collision applications in addition to traditional injury assessment sites. Furthermore, the MIL-Lx foot was studied to assess the biofidelity in a neutral posture as compared to cadaveric feet, providing a valuable technique to assess foot fractures while simultaneously collecting load data relevant to the automotive industry.

The first phase of this work was to calibrate insole sensors over a range of impact energies representative of those experienced on the plantar surface of the foot as a result of a frontal automotive collision (*i.e.*, Objective 1, Chapter 2 – Instrumented Boot Sensor Calibration). The eight insole sensors were constructed from piezoresistive material between steel backing plates and connected in a voltage divider configuration. The sensor impact parameters were developed based on voltage changes collected during ATD testing, and a new calibration method was developed and completed to provide a robust calibration method that is automated and covers a wide range of impact conditions.

The instrumented insole was then applied to the Hybrid III 50th Male lower leg and the MIL-Lx to comparatively assess the effects of ankle posture on injury criteria (*i.e.*, Objective 2, Chapter 3 - ATD Impact Testing in Altered Ankle Postures). Automotive collision impacts were

simulated using the pneumatic impacting apparatus based on velocity and impact duration values collected from the literature for these loading incidents. The MIL-Lx recorded lower peak axial forces and longer impact durations, as well as showed greater repeatability in comparison to the Hybrid III. The insole sensors consistently collected forces greater than those collected in the tibia shaft of both surrogates, and that ankle posture was found to play a large role in the force distribution on the plantar surface of the foot. The Hybrid III was more sensitive to postural changes than the MIL-Lx under these impact conditions. Furthermore, it was found that the two surrogates and their corresponding injury criteria are not equivalent (*i.e.*, Hypothesis 1 accepted).

A novel technique of attaching PMHS feet to the MIL-Lx ATD tibia shaft was developed in order to assess the biofidelity of the MIL-Lx foot as well as conduct impact tests while collecting tibia data relevant to the industry (Objective 3, Chapter 4 – A Technique to Assess the Impact Response of the Human Foot/Ankle Using an ATD Tibia). Three cadaveric specimens were tested at low-energy axial impacts using the pneumatic impacting apparatus and the response was compared to both the cadaveric foot and MIL-Lx tibia, and the fully intact MIL-Lx. When comparing intact PMHS to feet with the MIL-Lx shaft, this new technique did not alter the foot response, making it a viable method for evaluating impact response to this region. Furthermore, results suggest the MIL-Lx foot is stiffer than cadaveric feet, by measuring greater peak axial forces in the tibia shaft during MIL-Lx tests (*i.e.*, Hypothesis 2 accepted).

5.2 Limitations and Strengths

Limitations and strengths specific to each phase of the research were discussed in detail in each chapter; however, there are general strengths and limitations applicable to the entirety of this work.

Delivering impacts to an isolated anatomical region does not accurately replicate the conditions experienced in an intact body and could have an effect on the post-kinematic response of the lower leg. However, using isolated specimens allowed for a clear understanding of the differences in load transmission between ATD feet and cadaveric feet. Furthermore, reducing the cadaveric material required for this study was advantageous, as PMHS are expensive and limited and can now be used in other studies.

Additionally, impacts along a linear path do not necessarily recreate conditions of a frontal collision, in which structural components of the vehicle may play a role in loading of the lower leg, or the leg itself could be in a different posture (*i.e.*, out-of-position loading of the tibia). Only ankle posture was investigated in this study, while the tibia remained in line with the direction of loading. A work boot is not typical footwear employed of car occupants, and this may have affected the ATD responses, as work boots are generally heavier and stiffer in comparison to typical footwear occupants may wear in a collision. The test setup allowed for loading distributed along the plantar surface of the foot. However, a pedal may concentrate forces in one region, which may lead to higher loading in that region. Cadaveric testing of this nature also does not take into account muscle tension that is likely to occur in a vehicular occupant that is aware of an impending collision. Muscle tension in the foot may affect the stiffness of the foot. However, it is currently unknown how much muscle tension is generated in these types of scenarios and how that relates to dynamic properties of the foot, so attempting to mimic that in impact testing would have required many assumptions and challenges.

Another limitation of this study is not testing the THOR-Lx to comparatively assess the impact responses with the Hybrid III and MIL-Lx ATDs. Although this is a newer ATD, the New Car Assessment Program does not currently employ this ATD during crash testing due to

the expensive nature and the lead time required to attain the THOR-Lx, nor have federal standards been set (Rosekind, 2019). Additionally, this study used a work boot to collect impact data while most vehicular occupants will be wearing shoes. Although the piezoresistive sensors were designed to cover most of the insole surface, the sensor resolution was not high, with only eight sensors, and the grouping of sensors into the three regions may not have been anatomically relevant for different sized feet. The calibration process identified some error in sensor readings, which would have propagated through the results of subsequent chapters. Furthermore, although efforts were taken to attempt to keep the work boot tied consistently (*i.e.*, lacing through the same hole during every impact), this may not have been entirely consistent with how the foot was placed within the boot or how tight the laces were tightened.

This work was a systemic investigation of postural effects using two currently very widely used ATDs. To the author's knowledge, this study was the first of its kind to look at plantar surface loading and distribution under real-world automotive loading conditions. Furthermore, this study quantified load dissipation through the foot during axial impacts. A valuable contribution to the field was the development of a new technique to blend PMHS and ATDs for injury limit development.

5.3 Future Directions

Now that a technique has been developed for mounting cadaveric feet to the ATD tibia, a valuable contribution to this field would be employing the instrumented boot on cadaveric feet and impacting them to failure. Doing so while collecting tibia load data will enable the development of injury risk curves specific to foot/ankle injuries. It would also be interesting to use this new technique to examine how ankle posture affects loads collected at the tibia and the

foot and compare these data to the ATD data collected in this study. Furthermore, the use of the piezoresistive sensors and the data collected in this thesis can aid in the design of an improved ATD foot design. The sensors provide an effective method of collecting force data at discrete locations and may be applied to other regions of the body.

5.4 Significance

This work outlined the importance of selecting the correct surrogate as well as considering initial ankle posture when developing injury criteria for the lower extremity. To the author's knowledge, no previous studies have examined load distribution on the plantar surface of the foot during dynamic axial loading representative of automotive collisions. Most cadaveric studies have investigated the fracture tolerance of the lower leg when positioned in a neutral posture, and automotive impact testing is conducted with ATDs positioned in a neutral ankle posture. However, in order to design suitable protective measures in vehicles, ATDs must be sensitive to changes affecting injury risk. This is significant because injuries to this anatomical region are frequent and debilitating and may not be adequately protected by current methods of assessing foot injury risk at the tibia.

Furthermore, this research is the first of its kind to investigate the isolated cadaveric foot and its response to dynamic impact loads for automotive collision applications. Many previous lower extremity impact studies have also used specimens that include the foot, tibia and fibula and knee. Although this representation is more realistic, the disarticulation of the foot at the tibiotalar joint allows for the ability to assess only foot injuries. The proposed configuration allows for force collection at the load cells in the ATD tibia shaft that can be used to directly

compare to data collected in the automotive industry during crash testing. This work will assist the automotive industry in recognizing the shortcomings of current injury assessment techniques.

References

- Acharya, I., Van Tuyl, J. T., de Lange, J., & Quenneville, C. E. (2018). A Force-Sensing Insole to Quantify Impact Loading to the Foot. *Journal of Biomechanical Engineering*, *141*(2), 024501. <https://doi.org/10.1115/1.4041902>
- Behr, M., Poumarat, G., Serre, T., Arnoux, P. J., Thollon, L., & Brunet, C. (2010). Posture and muscular behaviour in emergency braking: An experimental approach. *Accident Analysis and Prevention*, *42*(3), 797–801. <https://doi.org/10.1016/j.aap.2009.04.010>
- Bir, C., Barbir, A., Dosquet, F., Wilhelm, M., van der Horst, M., & Wolfe, G. (2008). Validation of lower limb surrogates as injury assessment tools in floor impacts due to anti-vehicular land mines. *Military Medicine*, *173*(12), 1180–1184. Retrieved from <http://www.ncbi.nlm.nih.gov/pubmed/19149335>
- Bull, A. M. J., Clasper, J., & Mahoney, P. F. (Eds.). (2016). *Blast Injury Science and Engineering*. Switzerland: Springer International Publishing.
- Campbell, K. J., Michalski, M. P., Wilson, K. J., Goldsmith, M. T., Wijdicks, C. A., LaPrade, R. F., & Clanton, T. O. (2014). The ligament anatomy of the deltoid complex of the ankle: A qualitative and quantitative anatomical study. *Journal of Bone and Joint Surgery - American Volume*, *96*(8), 1–10. <https://doi.org/10.2106/JBJS.M.00870>
- Carpanen, D., Masouros, S., & Newell, N. (2016). Surrogates of Human Injury. In A. M. J. Bull, J. Clasper, & P. Mahoney (Eds.), *Blast Injury Science and Engineering* (pp. 189–198). Springer.
- Chakravarty, A. B., Martinez, A. A., & Quenneville, C. E. (2017). The Injury Tolerance of the

Tibia Under Off-Axis Impact Loading. *Biomedical Engineering Society*, 45(6), 1534–1542.

<https://doi.org/10.1007/s10439-017-1824-6>

Chang, C., Rupp, J., & Kikuchi, N. (2008). Development of a finite element model to study the effects of muscle forces on knee-thigh-hip injuries in frontal crashes. *Stapp Car Crash Journal*, 52(November), 475–504.

Crandall, J. R., Kuppa, S. M., Klopp, G. S., Hall, G. W., Pilkey, W. D., & Hurwitz, S. R. (1998). Injury mechanisms and criteria for the human foot and ankle under axial impacts to the foot. *International Journal of Crashworthiness*, 3(2), 147–162.

<https://doi.org/10.1533/cras.1998.0068>

Crandall, Jeff R., Martin, P. G., Sieveka, E. M., Pilkey, W. D., Dischinger, P. C., Burgess, A. R., O'Quinn, T. D., Schmidhauser, C. B. (1998). Lower Limb Response and Injury in Frontal Crashes. *Accident Analysis and Prevention*, 30(5), 667–677.

Crandall, Jeff R., Portier, L., Petit, P., Hall, G. W., Bass, C. R., Klopp, G. S., Hurwitz, S., Pilkey, W. D., Trosseille, X., Tarrière, C., Lassau, J.-P., Eppinger, R. H. (1996). Biomechanical Response and Physical Properties of the Leg, Foot, and Ankle. *SAE Technical Paper Series*, 1. <https://doi.org/10.4271/962424>

Dischinger, P. C., Read, K. M., Kufera, J. A., Kerns, T. J., Burch, C. A., Jawed, N., Burgess, A. R. (2004). Consequences and costs of lower extremity injuries. *Annual Proceedings. Association for the Advancement of Automotive Medicine*, 48, 339–353. Retrieved from <http://www.ncbi.nlm.nih.gov/pubmed/15319134><http://www.pubmedcentral.nih.gov/articlerender.fcgi?artid=PMC3217424>

Dong, L., Zhu, F., Jin, X., Suresh, M., Jiang, B., Sevagan, G., Cai, Y., Li, G., Yang, K. H. (2013). Blast effect on the lower extremities and its mitigation: A computational study.

Journal of the Mechanical Behavior of Biomedical Materials, 28, 111–124.

<https://doi.org/10.1016/j.jmbbm.2013.07.010>

Gilchrist, M. D. (Ed.) (2005). *IUTAM Symposium on Impact Biomechanics: From Fundamental Insights to Applications* (Vol. 124). <https://doi.org/10.1007/1-4020-3796-1>

Forman, J. L., Lopez-Valdes, F. J., Duprey, S., Bose, D., Del Pozo De Dios, E., Subit, D.,

Gillispie, T., Crandall, J.R., Segui-Gomez, M. (2015). The tolerance of the human body to automobile collision impact - A systematic review of injury biomechanics research, 1990-2009. *Accident Analysis and Prevention*, 80(2015), 7–17.

<https://doi.org/10.1016/j.aap.2015.03.004>

Funk, J. R. (2002). The Axial Injury Tolerance of the Human Foot/Ankle Complex and the Effect of Achilles Tension. *Journal of Biomechanical Engineering*, 124(6), 750.

<https://doi.org/10.1115/1.1514675>

Funk, J. R. (2011). Ankle injury mechanisms: Lessons learned from cadaveric studies. *Clinical Anatomy*, 24(3), 350–361. <https://doi.org/10.1002/ca.21112>

Funk, J. R., Srinivasan, S. C. M., Crandall, J. R., Khaewpong, N., Eppinger, R. H., Jaffredo, A.

S., Potier, P., Petit, P. Y. (2002). The Effects of Axial Preload and Dorsiflexion on the Tolerance of the Ankle/Subtalar Joint to Dynamic Inversion and Eversion. *SAE Technical Paper Series*, Vol. 46, pp. 245–265. <https://doi.org/10.4271/2002-22-0013>

Funk, J. R., Tournet, L. J., George, S. E., & Crandall, J. R. (2010). The Role of Axial Loading in Malleolar Fractures. *SAE Technical Paper Series*, Vol. 1. <https://doi.org/10.4271/2000-01-0155>

Gallenberger, K., Yoganandan, N., & Pintar, F. (2013). Biomechanics of foot/ankle trauma with variable energy impacts. *Annals of Advances in Automotive Medicine*, 57(2013), 123–132.

- Golanó, P., Vega, J., de Leeuw, P. A. J., Malagelada, F., Manzanares, M. C., Götzens, V., & van Dijk, C. N. (2016). Anatomy of the ankle ligaments: a pictorial essay. *Knee Surgery, Sports Traumatology, Arthroscopy*, 24(4), 944–956. <https://doi.org/10.1007/s00167-016-4059-4>
- Gore, A. I., & Spencer, J. P. (2004). The Newborn Foot. *American Family Physician*, 69(4), 865–872.
- Grigoriadis, G., Carpanen, D., Webster, C. E., Ramasamy, A., Newell, N., & Masouros, S. D. (2019). Lower Limb Posture Affects the Mechanism of Injury in Under-Body Blast. *Annals of Biomedical Engineering*, 47(1), 306–316. <https://doi.org/10.1007/s10439-018-02138-4>
- Humanetics Innovative Solutions. (n.d.). Hybrid III 50th Male. Retrieved December 28, 2018, from <https://www.humaneticsatd.com/crash-test-dummies/frontal-impact/hiii-50m>
- Humanetics Innovative Solutions. (2013). Military Lower Extremity (50th Male) Legs. Retrieved December 28, 2018, from <https://www.humaneticsatd.com/crash-test-dummies/aerospace-military/mil-lx-legform>
- Humanetics Innovative Solutions. (2015). *Hybrid-III 50th Male Dummy Brand Harmonized Parts Catalog*. Retrieved from <http://www.humaneticsatd.com/crash-test-dummies/frontal-impact/hiii-5f>
- Insurance Institute for Highway Safety. (2004). *Guidelines for Using the UMTRI ATD Positioning Procedure for ATD and Seat Positioning*. (December).
- Insurance Institute for Highway Safety. (2014). *Moderate Overlap Frontal Crashworthiness Evaluation - Guidelines for Rating Injury Measures*.
- Iyo, T., Maki, Y., Sasaki, N., & Nakata, M. (2004). Anisotropic viscoelastic properties of cortical bone. *Journal of Biomechanics*, 37(9), 1433–1437. <https://doi.org/10.1016/j.jbiomech.2003.12.023>

- King, A. I. (2018). The Biomechanics of Impact Injury. In *Medicine & Science in Sports & Exercise* (Vol. 50). <https://doi.org/10.1249/01.mss.0000544407.69747.7a>
- Kinsky, T., & Buenger, B. (2004). The Flexible Pedestrian Legform Impactor and Its Impact on Vehicle Design. *International Technical Conference on the Enhanced Safety of Vehicles*, 1–7.
- Kitagawa, Y., Ichikawa, H., King, A. I., & Levine, R. S. (1998). A Severe Ankle and Foot Injury in Frontal Crashes and Its Mechanism. *SAE Technical Paper Series*, 1(724).
<https://doi.org/10.4271/983145>
- Klopp, G. S., Crandall, J., Hall, G. W., Pilkey, W. D., Hutwitz, S. R., & Kuppa, S. M. (1997). Mechanisms of injury and injury criteria for the human foot and ankle in dynamic axial impacts to the foot. *IRCOBI Conference -Hannover*. Retrieved from
http://www.ircobi.org/wordpress/downloads/irc1997/pdf_files/1997_4.pdf
- Krackow, K. A., Thomas, S. C., & Jones, L. C. (1986). A new stitch for Ligament-Tendon Fixation. *The Journal of Bone and Joint Surgery*, 68(5), 764–766.
- Kuppa, S; Haffner, M; Eppinger, R; Saunders, J. (1998). Lower extremity response and trauma assessment using the THOR-Lx and Denton leg in frontal offset vehicle crashes. *SAE Technical Paper*, (456), 1–12.
- Kuppa, S., Wang, J., Haffner, M., & Eppinger, R. (2001). Lower Extremity Injuries and Associated Injury Criteria. *SAE Technical Paper*, 4.
- Kuppa, Shashi M, Klopp, G. S., Crandall, J. R., & Kleinberger, M. (1997). Axial Impact Characteristics of Dummy and Cadaver Lower Limbs. *National Highway Traffic Safety Administration*, 1608–1617.
- Longhitano, D., & Turley, J. E. (2001). Lower Extremity Response of the Thor-Lx Compared tot

he Hybrid III Lower Leg in Frontal Barrier Crash Tests. *SAE Technical Paper*, (Figure 1), 1–21.

Manning, P., Wallace, A., Owen, C., Roberts, A., Oakley, C., & Lowne, R. (1993). Dynamic Response and Injury Mechanism in the Human Foot and Ankle and an Analysis of Dummy Biofidelity. *Proc. of the 16th International Technical Conference on the Enhanced Safety of Vehicles*, 1960–1998.

Manning, P., Wallace, W. A., Roberts, A. K., Owen, C. J., & Lowne, R. W. (2010). The Position and Movement of the Foot in Emergency Manoeuvres and the Influence of Tension in the Achilles Tendon. *SAE Technical Paper Series*, 1. <https://doi.org/10.4271/973329>

Martinez, A. A., Chakravarty, A. B., & Quenneville, C. E. (2018). The effect of impact duration on the axial fracture tolerance of the isolated tibia during automotive and military impacts. *Journal of the Mechanical Behavior of Biomedical Materials*, 78(June 2017), 315–320. <https://doi.org/10.1016/j.jmbbm.2017.11.013>

McKay, B. J. (2010). Development of lower extremity injury criteria and biomechanical surrogate to evaluate military vehicle occupant injury during an explosive blast event. Retrieved from https://search.proquest.com/docview/807668028?accountid=26642%0Ahttp://link.periodicos.capes.gov.br/sfxlcl41?url_ver=Z39.88-2004&rft_val_fmt=info:ofi/fmt:kev:mtx:dissertation&genre=dissertations+%26+theses&sid=ProQ:ProQuest+Dissertations+%26+Theses+Global

McKay, B. J., & Bir, C. A. (2009). Lower Extremity Injury Criteria for Evaluating Military Vehicle Occupant Injury in Underbelly Blast Events. *Stapp Car Crash Journal*, 53(November), 229–249.

- Mertz, H. J., Irwin, A. L., & Prasad, P. (2003). Biomechanical and scaling bases for frontal and side impact injury assessment reference values. *Stapp Car Crash Journal*, 47(October), 155–188. <https://doi.org/2003-22-0009> [pii]
- Morgan, R. M., Eppinger, R. H., & Hennessey, B. C. (1991). Ankle Joint Injury Mechanism for Adults in Frontal Automotive Impact. *SAE Technical Paper Series*, 100, 1959–1968. <https://doi.org/10.4271/912902>
- Morris, A., Thomas, P., Taylor, A. M., & Wallace, W. A. (1997). Mechanisms of fractures in ankle and hind-foot injuries to front seat car occupants - an in-depth accident data analysis. Loughborough University.
- North Atlantic Treaty Organization. (2007). Test Methodology for Protection of Vehicle Occupants against Anti-Vehicular Landmine Effects. *RTO Technical Report*, 323(April).
- Owen, C., Roberts, A., Manning, P., & Lowne, R. (1998). Positioning and Bracing of the Lower Leg During Emergency Braking - A Volunteer Study. *1998 IRCOBI Conference Proceedings*, (September), 1996–1998.
- Palmertz, C., Jakobsson, L., & Karlsson, A.-S. (1998). Pedal Use and Foot Positioning During Emergency Braking. *1998 IRCOBI Conference Proceedings*.
- Pandelani, T., Reinecke, D., & Beetge, F. (2010). In pursuit of vehicle landmine occupant protection : Evaluating the dynamic response characteristic of the military lower extremity leg (MiL-Lx) compared to the Hybrid III (HIII) lower leg. *Council for Scientific and Industrial Research (CSIR) 3rd Biennial Conference*, Paper DS04-PA-F.
- Quenneville, C. E., & Dunning, C. E. (2012). Evaluation of the Biofidelity of the HIII and MIL-Lx Lower Leg Surrogates Under Axial Impact Loading. *Traffic Injury Prevention*, 13(1), 81–85. <https://doi.org/10.1080/15389588.2011.623251>

- Quenneville, C. E., Fournier, E., & Shewchenko, N. (2017). The Effect of Anthropomorphic Test Device Lower Leg Surrogate Selection on Impact Mitigating System Evaluation in Low- and High-Rate Loading Conditions. *Military Medicine*, *182*(9), e1981–e1986. <https://doi.org/10.7205/milmed-d-16-00358>
- Quenneville, C. E., McLachlin, S. D., Greeley, G. S., & Dunning, C. E. (2011). Injury tolerance criteria for short-duration axial impulse loading of the isolated tibia. *The Journal of Trauma*, *70*(1), E13–E18. <https://doi.org/10.1097/TA.0b013e3181f6bb0e>
- Richter, M., Thermann, H., Wippermann, B., Otte, D., Schrott, H. E., & Tscherne, H. (2001). Foot fractures in restrained front seat car occupants: A long-term study over twenty-three years. *Journal of Orthopaedic Trauma*, *15*(4), 287–293. <https://doi.org/10.1097/00005131-200105000-00009>
- Rosekind, M. (2019). *Detailed Comments on Proposed NCAP Modifications*.
- Rudd, R. W. (2009). Updated Analysis of Lower Extremity Injury Risk in Frontal Crashes in the United States. *21st ESV Conference*, (March), no. 09-0556.
- Salzar, R. S., Livers, W. B., Bailey, A. M., & Crandall, J. R. (2015). Leg, Foot and Ankle Injury Biomechanics. In N. Yoganandan, A. M. Nahum, & J. W. Melvin (Eds.), *Accidental Injury: Biomechanics and Prevention* (Third). <https://doi.org/10.1007/978-1-4939-1732-7>
- Schmitt, K.-U., Niederer, P., Muser, M., & Walz, F. (Eds.). (2010). *Trauma Biomechanics: Accidental injury in traffic and sports* (Third). Springer.
- Seipel, R. C., Pintar, F. A., Yoganandan, N., & Boynton, M. D. (2001). Biomechanics of Calcaneal Fractures: A Model for the Motor Vehicle. *Clinical Orthopaedics and Related Research*, (388), 218–224.
- Shin, J., & Untaroiu, C. D. (2013). Biomechanical and Injury Response of Human Foot and

- Ankle under Complex Loading. *Journal of Biomechanical Engineering*, 135(October 2013), 1–8. <https://doi.org/10.1115/1.4025108>
- Smolen, C., & Quenneville, C. E. (2016). The effect of ankle posture on the load pathway through the hindfoot. *Proceedings of the Institution of Mechanical Engineers, Part H: Journal of Engineering in Medicine*, 230(11), 1024–1035. <https://doi.org/10.1177/0954411916670423>
- Society of Automotive Engineers (2003). Surface Vehicle Recommended Practice, (R) Instrumentation for Impact Test - Part 1 - Electronic Instrumentation. *SAE J211/1*.
- Taylor, A., Morris, A., Thomas, P., & Wallace, A. (1997). Mechanisms of lower extremity injuries to front seat car occupants - An in-depth accident analysis. *1997 IRCOBI Conference*, pp. 53–72.
- Van Tuyl, J. (2014). *Development of a Force Sensing Insole To Quantify Impact Loading To the Foot* (MAsc Thesis). McMaster University, Canada.
- Van Tuyl, J., Burkhart, T. A., & Quenneville, C. E. (2016). Effect of posture on forces and moments measured in a Hybrid III ATD lower leg. *Traffic Injury Prevention*, 17(4), 381–385. <https://doi.org/10.1080/15389588.2015.1089356>
- Welbourne, E. R., & Shewchenko, N. (1987). Improved Measures of Foot and Ankle Injury Risk from the Hybrid III Tibia. *Proceedings of the 16th International Technical Conference on the Enhanced Safety of Vehicles*, 1618–1627.
- Yoganandan, N., Arun, M. W. J., Pintar, F. A., & Banerjee, A. (2015). Lower Leg Injury Reference Values and Risk Curves from Survival Analysis for Male and Female Dummies: Meta-analysis of Postmortem Human Subject Tests. *Traffic Injury Prevention*, 16, 100–107. <https://doi.org/10.1080/15389588.2015.1015118>

- Yoganandan, N., Arun, M. W. J., Pintar, F. A., Szabo, A. (2014). Optimized Lower Leg Injury Probability Curves From Postmortem Human Subject Tests Under Axial Impacts. *Traffic Injury Prevention*, 9588(15), S151–S156. <https://doi.org/10.1080/15389588.2014.935357>
- Yoganandan, N., Banerjee, A., Hsu, F. C., Bass, C. R., Voo, L., Pintar, F. A., & Gayzik, F. S. (2016). Deriving injury risk curves using survival analysis from biomechanical experiments. *Journal of Biomechanics*, 49(14), 3260–3267. <https://doi.org/10.1016/j.jbiomech.2016.08.002>
- Yoganandan, N., Pintar, F. A., Boynton, M., Begeman, P., Prasad, P., Kuppa, S. M., Morgan, R. M., Eppinger, R. H. (1996). Dynamic Axial Tolerance of the Human Foot-Ankle Complex. *SAE Technical Paper Series*, 1(1996), 1887–1898. <https://doi.org/10.4271/962426>
- Yoganandan, N., Pintar, F. A., Gennarelli, T. A., Seipel, R., & Marks, R. (1999). Biomechanical Tolerance of Calcaneal Fractures. *Association for the Advancement of Automotive Medicine*, 345–356.
- Yoganandan, N., Pintar, F., Banerjee, A., Schlick, M., Chirvi, S., Uppal, H., Merkle, A., Voo, L., Kleinberger, M. (2015). Hybrid III Lower Leg Injury Assessment Reference Curves Under Axial Impacts Using Matched-Pair Tests. *Biomedical Sciences Instrumentation*, (51), 230–237.
- Zeidler, F. (1984). The significance of lower limb injuries of belted drivers. *Journal of Orthopaedics*.
- Zuby, D. S., Nolan, J. M., Sherwood, C. P. (2001). Effect of Hybrid III Leg Geometry on Upper Tibia Bending Moments. Insurance Institute for Highway Safety. *SAE International*, 110(2001), 177–189.

Appendix A – Glossary of Anatomical Terms

Achilles tendon	Fibrous tissue connecting muscles of the leg to the calcaneus.
Anterior	Situated towards the front of the body from the midline.
Anthropomorphic	Made to resemble human form.
Articulation	Area where two bones are attached for the purposes of facilitating motion.
Axial lower leg loading	In line with the long axis of the tibia.
Biofidelity	Ability of model accurately represent the biological system it is based upon.
Cadaveric	Of, or pertaining to, a human body.
Calcaneus	Heel bone; situated in the back of the foot.
Distal	Further away from the middle of the body.
Dorsiflexion	Motion of the ankle caused by raising the foot upwards.
Eversion	Motion of the ankle caused by moving the sole of the foot away from the midline.
Fibula	Small bone of the lower leg extending between the knee and ankle.
Inversion	Motion of the ankle caused by moving the sole of the foot towards the midline.
Joint	Location of contact between two bones that permits bone movement.
Lateral	Further away from the midline.
Ligament	Connective tissue attaching bone to another bone.
Malleolus	Bony prominence on each side of ankle, part of tibia and fibula.

Medial	Closer to the midline.
Plafond	Distal articular surface of the tibia.
Plantar	Towards the bottom of the foot.
Plantarflexion	Motion of the ankle caused by lowering the foot downwards.
Plateau	Proximal articular surface of the tibia.
Posterior	Situated towards the back of the body from the midline, synonymous with dorsal.
Proximal	Closer to the middle of the body.
Talus	Bone in the ankle articulating with tibia and calcaneus.
Tarsal	Group of bones of the foot.
Tendon	Connective tissue attaching muscles to bone.
Tibia	Large bone of the lower leg extending between the knee and ankle.
Tibiotalar	Joint between the tibia and talus.
Subtalar	Joint between the talus and calcaneus. Synonymous with talocalcaneal joint.
Vascularization	Supply of blood vessels.

Appendix B – Variations in Sensor Voltage Responses

Table B.1: Detailed ATD Impact Data for Sensor Recalibration

Detailed impact data is recorded for both a) the Hybrid III and b) the MIL-Lx ATDs to determine the range of voltages to calibrate the sensors over. Data were collected for impact masses ranging from 5.9 to 9.6 kg, and postures ranging from 15°-plantarflexion to 15°-dorsiflexion. All values are in volts (V).

a)

Hybrid III															
15°-Dorsiflexion						Neutral Posture					15°-Plantarflexion				
Sensor	Trial 1	Trial 2	Trial 3	Trial 4	Trial 5	Trial 1	Trial 2	Trial 3	Trial 4	Trial 5	Trial 1	Trial 2	Trial 3	Trial 4	Trial 5
1	0.95835	0.92067	0.82107	0.81076	0.73766	0.7754	0.83232	0.80895	0.82838	0.82482	0.66949	0.6998	0.657	0.69405	0.72773
2	0.53625	0.51338	0.4634	0.50757	0.38305	0.49533	0.48752	0.46503	0.46977	0.49795	0.33213	0.31489	0.34019	0.31651	0.3242
3	0.07935	0.09061	0.00981	0.02181	0.01069	0.04906	0.03612	0.03831	0.04137	0.05199	0.02862	0.05143	0.05643	0.05087	0.04362
4	0.05815	0.05473	0.19181	0.17944	0.16088	0.17819	0.21555	0.21905	0.21993	0.22136	0.19912	0.14926	0.17257	0.187	0.16951
5	0.03121	0.02062	0.01512	0.01425	0.0125	0.0493	0.03937	0.04393	0.05449	0.0738	0.15297	0.08842	0.12023	0.13173	0.13997
6	0.11886	0.12946	0.10434	0.10847	0.09691	0.18788	0.13427	0.11484	0.13052	0.14164	0.0303	0.02431	0.03493	0.02399	0.04267
7	0.17319	0.15249	0.10839	0.23039	0.13643	0.17898	0.16861	0.136	0.13256	0.16992	0.06066	0.0556	0.06903	0.05922	0.08046
8	0.0094	0.01012	0.00706	0.00925	0.01	0.01219	0.01012	0.01331	0.01256	0.01269	0.06536	0.05949	0.0503	0.07249	0.05674

b)

MIL-Lx															
15°-Dorsiflexion						Neutral Posture					15°-Plantarflexion				
Sensor	Trial 1	Trial 2	Trial 3	Trial 4	Trial 5	Trial 1	Trial 2	Trial 3	Trial 4	Trial 5	Trial 1	Trial 2	Trial 3	Trial 4	Trial 5
1	0.91973	0.9058	0.8172	0.8988	0.71767	0.81739	0.83469	0.83707	0.81114	0.79658	0.74984	0.78096	0.7614	0.80039	0.83794
2	0.37831	0.3848	0.37368	0.39443	0.37881	0.40092	0.41167	0.32795	0.33345	0.33432	0.32845	0.33332	0.33694	0.33944	0.33026
3	0.11305	0.16142	0.11999	0.1008	0.11624	0.1098	0.10111	0.10436	0.09799	0.11611	0.10218	0.10786	0.10136	0.10061	0.10792
4	0.04848	0.04249	0.03424	0.04573	0.02924	0.19993	0.18406	0.16026	0.18425	0.14626	0.40936	0.40473	0.38668	0.35869	0.41723
5	0.03006	0.17128	0.02931	0.12523	0.04031	0.16559	0.15703	0.13841	0.16909	0.14991	0.41186	0.4083	0.40655	0.39118	0.37456
6	0.11584	0.10897	0.14464	0.11534	0.14683	0.12427	0.14008	0.17426	0.15089	0.13271	0.09335	0.11115	0.12771	0.12377	0.12384
7	0.08715	0.0874	0.08646	0.08508	0.08983	0.07977	0.0799	0.08102	0.08383	0.07584	0.04748	0.04923	0.05354	0.04966	0.05566
8	0.00731	0.01506	0.00887	0.01425	0.0065	0.00894	0.00825	0.00781	0.01343	0.01006	0.10917	0.10086	0.0863	0.0893	0.06949

Appendix C – Technical Drawings

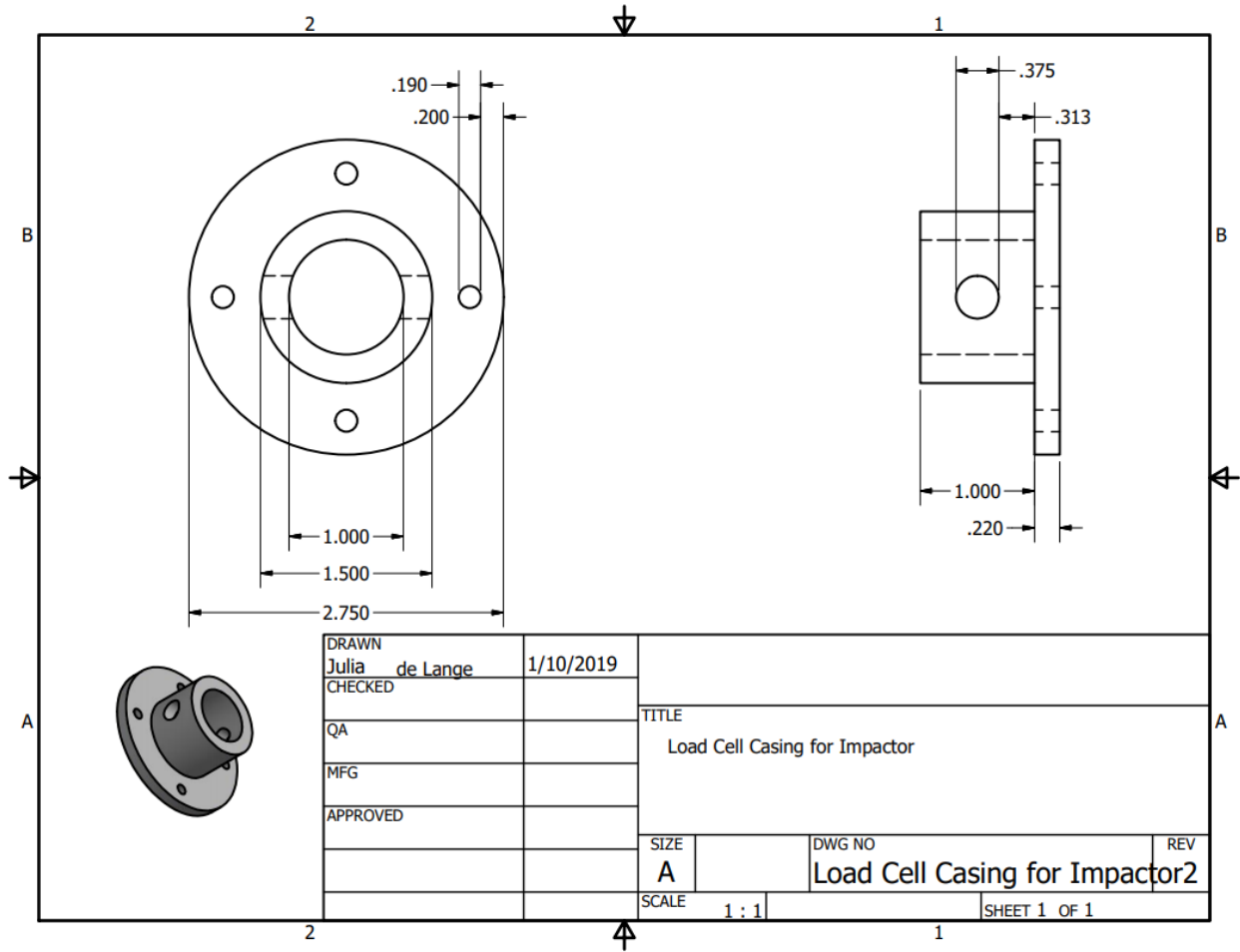


Figure C.1: Fixture for Securing Load Cell to Impact Plate
 All dimensions in inches and the part was machined of low carbon steel.

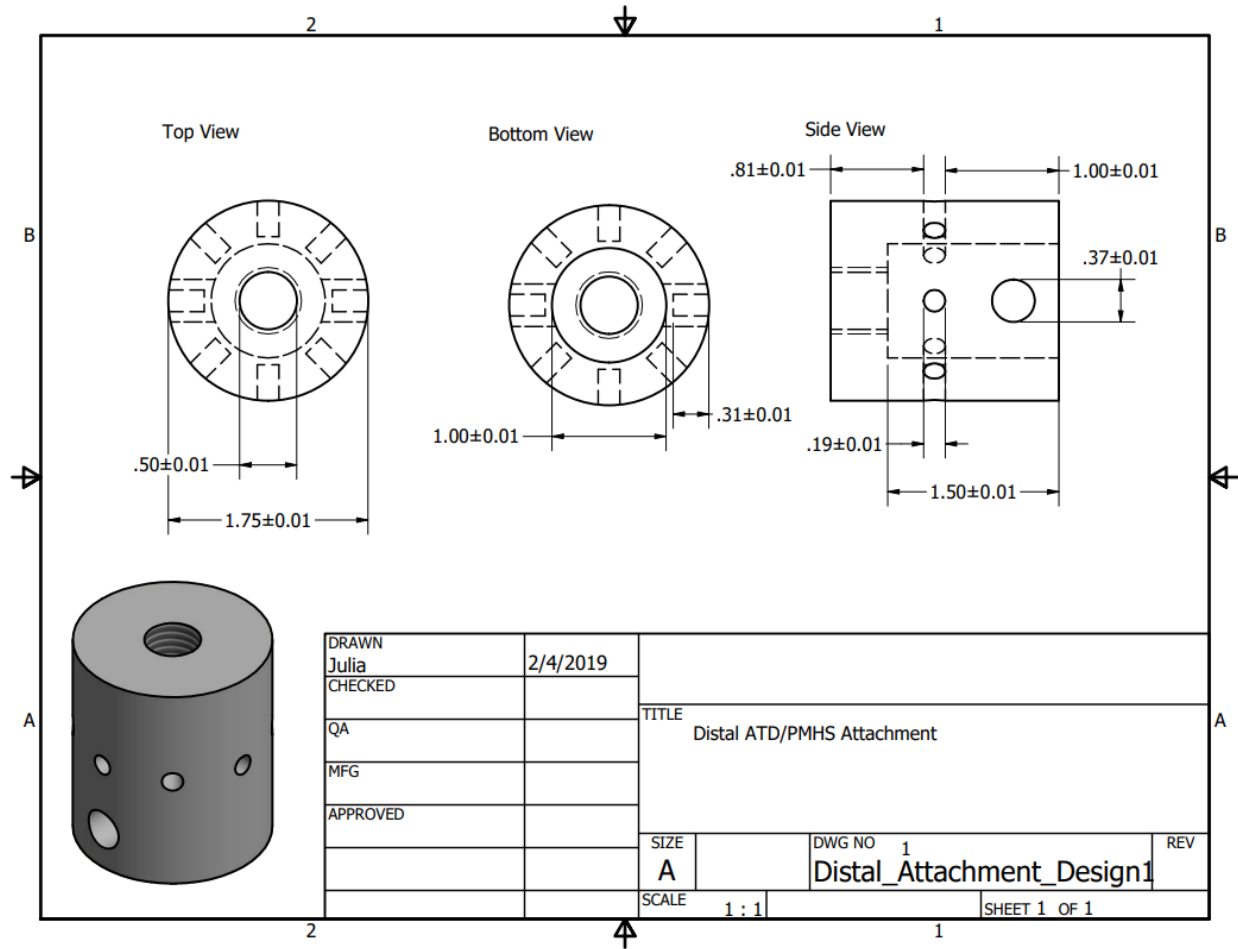


Figure C.2: Component to Facilitate Attaching ATD to PMHS
 All dimensions are in inches and part was machined of low carbon steel.

Appendix D – Settling Impact Effects

Repeated testing of Sensor 8 conducted by Acharya *et al.* displayed a small change in the line of best fit from the first impact to second impacts, due to the sensors settling into position. After the small initial change, the sensors exhibited a repeatable response, which is why throughout this study a “settling” impact was conducted for the first impact of all sensors.

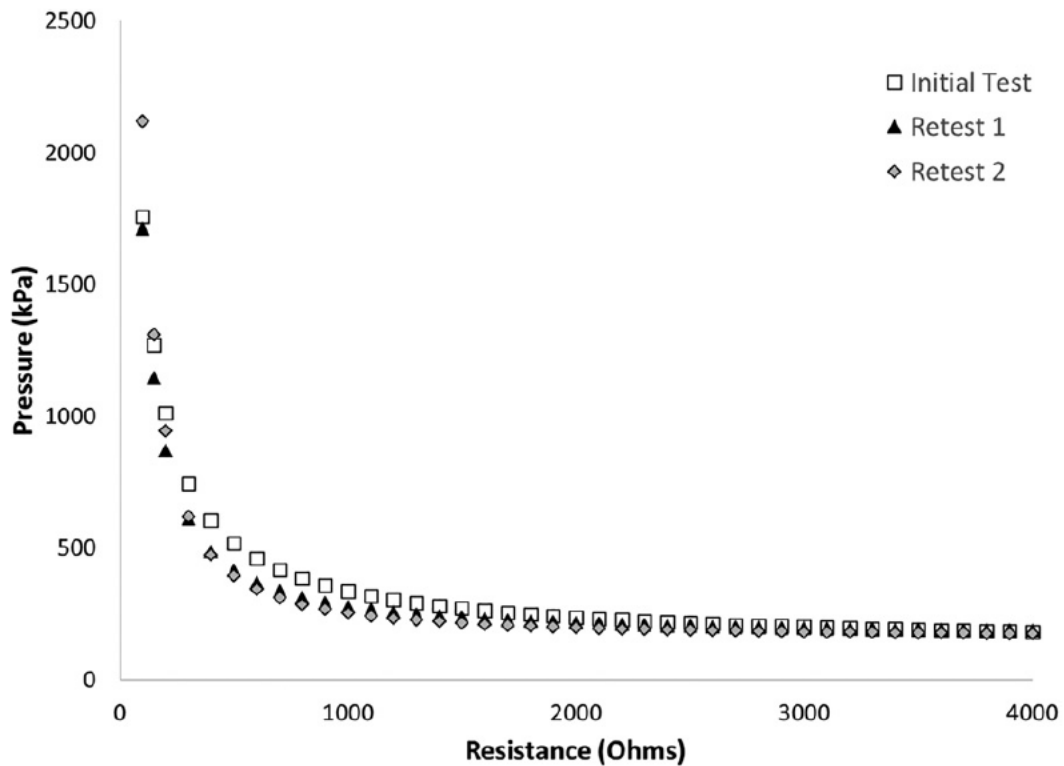


Figure D.1: Repeatability Testing

Impact response of the first test as compared to repeated testing of one of the sensors of the instrumented boot (sensor 8), conducted by Acharya *et al.* (2018).

Appendix E – LabVIEW® Program

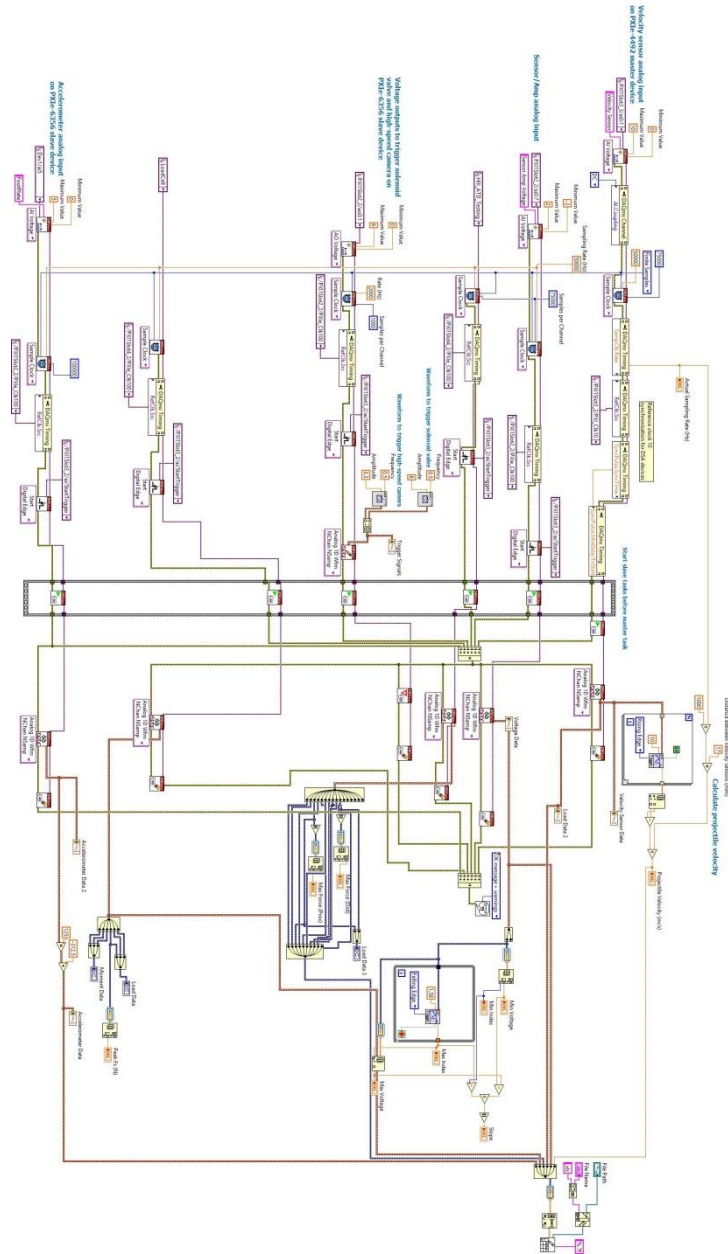


Figure E.1: Sensor Calibration Back Panel

This includes an input for the velocity sensors, footplate accelerometers, load cell and all sensor voltage and excitation voltage. It also included triggering signals for the pneumatic valve to open. All data was saved to Excel documents to be processed by MATLAB®.

Appendix F – Matlab® Sensor Calibration Program

```
clc;
clear all;
close all;
profile on;

impact_mass = 'M26'; %insert impact mass and sensor for whatever you are
analyzing
sens_num = 'S1';
files = dir(fullfile('cropped_data', sens_num, impact_mass, '*.mat'));
curve_vars = cell(1, 3);
r = cell(1, 3);
Slope_Avg_Res = cell(1, 3);
j=1;

% go through each of the same impacts to collect calibration curve variable
coefficients
for file = files'
    a = 2E6; %baseline values for the program to start from
    b = -0.3;
    c = -2E5;
    disp(strcat('Opened: ', file.name));
    data = load(fullfile('cropped_data', sens_num, impact_mass, file.name));
    data = data.croppedData; %retrieve data and assign variables
    ext_volt = data(:,3);
    sens_volt = data(:,4);
    sens_res = abs(102./((ext_volt./sens_volt) - 1));
    pressure = (data(:,12)*(-1));

    deriv = (abs(diff(sens_volt-1.4)));
    threshold = 0.01;
    impact = 0;
    impact_detect = zeros(length(deriv), 1);
    count = 0;

    %% detect impact duration by 10% of the minimum sensor value
    sens = (sens_volt*(-1)+1.5);
    impact = abs(sens)>(0.3*abs(max(sens)));

    counter=0;
    t=1;
    for j=1:length(sens)-1
```

```

        if impact(j+1,1)~=impact(j,1)
            counter(t)=j;
            t=t+1;
        end
    end
    impact_start = counter(1)-50;
    impact_fin   = counter(2)+50;

    impact_dur = (impact_fin - impact_start)/50; %calculate length of impact
%%
    [min_voltage, impact_min_idx] = min(sens_volt);
    [min_pressure, min_pressure_idx] = max(pressure);

    Slope_AvgRes      =      [Slope_Avg_Res,      (abs((sens_res(impact_min_idx))-
(sens_res(impact_start))))/(impact_min_idx-impact_start)];
    Slope_Avg_Res = [Slope_Avg_Res, Slope_AvgRes];

    figure %plot sensor voltage with start, end, and minimum voltage
highlighted
    subplot(2,1,1);
    hold on
    plot(sens_volt);
    plot(sens_volt, 'r*', 'MarkerIndices', [impact_start impact_fin
min_pressure_idx]);
    hold off
    title('Sensor');

    subplot(2,1,2); %plot load cell force with start, end, and minimum force
highlighted
    hold on
    plot(pressure);
    plot(pressure, 'r*', 'MarkerIndices', [impact_start impact_fin
min_pressure_idx]);
    hold off
    title('Load Cell');

    x=sens_res(impact_start:(min_pressure_idx-100));
    y=pressure(impact_start:(min_pressure_idx-100));

    figure; %plot force versus voltage
    s=plot(x,y,'linewidth' , 1 , 'color' , 'r ');
    xlim([0 16000]);
    ylim([0 1000000]);
    xlabel('Voltage (V)');
    ylabel ('Force (N)');
    f=ezfit(x,y,'((a*x^b)+c)', [a b c]); %(a+(a*x))*exp(-b*x); a=1200')');

```

```

    showfit(f, 'dispeqboxmode' , 'off' , 'boxlocation' , [0.60 0.81 0.1 0.1],
'fitlinestyle' , '--' , 'fitcolor' , 'k' , 'fitlinewidth' , 3);

    curve_vars = [curve_vars, f.m(1) f.m(2) f.m(3)]; %collect variables for
each iteration
    r = [r, f.r];
    j=j+1;

end

%take average of variables collected
aav=((curve_vars{4}+curve_vars{7}+curve_vars{10})/3);
bav=((curve_vars{5}+curve_vars{8}+curve_vars{11})/3);
cav=((curve_vars{6}+curve_vars{9}+curve_vars{12})/3);
AR_avg=abs((Slope_Avg_Res{4}+Slope_Avg_Res{5}+Slope_Avg_Res{6})/3);
r_avg=abs((r{4}+r{5}+r{6})/3);
R=linspace(10,65000,2000000);

% store data
a = [curve_vars{4};curve_vars{7};curve_vars{10};aav];
b = [curve_vars{5};curve_vars{8};curve_vars{11};bav];
c = [curve_vars{6};curve_vars{9};curve_vars{12};cav];
Slope_AR = [Slope_Avg_Res{4};Slope_Avg_Res{5};Slope_Avg_Res{6};AR_avg];
r = [r{4};r{5};r{6};r_avg];

T = table(a, b, c, r, Slope_AR, 'VariableNames',{'a', 'b', 'c', 'r', 'AR'},
'RowNames',{'Trial 1', 'Trial 2', 'Trial 3', 'Average'})

[filepath,name,ext] = fileparts(file.name);
outputFileName = strcat(sens_num, impact_mass, '_calibcurves');
saved = fullfile('calibration_curves', sens_num, outputFileName);
writetable(T, saved, 'WriteRowNames',true)

```

Appendix G – Sensor Calibration Repeated Impacts

Table G.1: Detailed Sensor Calibration Results

All sensor minimum voltages and maximum forces were extracted during the calibrations and presented here. Coefficients of Variation were also recorded.

Sensor	Trial	Impact Mass (kg)									
		0.75		1.5		2		2.5		3.5	
		Voltage (V)	Force (N)	Voltage (V)	Force (N)	Voltage (V)	Force (N)	Voltage (V)	Force (N)	Voltage (V)	Force (N)
1	2	-0.44734	-815.6	-0.81589	-1700.8	-0.85884	-2190.5	-1.02585	-3269.2	-0.94507	-3547.1
	3	-0.44385	-834.1	-0.81793	-1683.3	-0.8909	-2297.9	-1.08102	-3269.5	-1.01591	-4021.5
	4	-0.48524	-911.3	-0.82834	-1750.1	-0.89232	-2199.3	-1.10039	-3194.7	-1.02077	-4117.4
	Coefficients of Variation:		-0.0500326	-0.05946	-0.0081361	-0.02024	-0.0214981	-0.02675	-0.036177	-0.01328	-0.0426315
2	2	-0.32988	-693.9	-0.45818	-1858.6	-0.62951	-2333.9	-0.90421	-3713.4	-0.83506	-4000.2
	3	-0.19982	-668.2	-0.49417	-2274.5	-0.62799	-2357.2	-0.94126	-3632.9	-0.8536	-3995.1
	4	-0.32977	-755.7	-0.51964	-2202.3	-0.57541	-2237	-0.96102	-3495.4	-0.87328	-4242.8
	Coefficients of Variation:		-0.2619932	-0.06371	-0.0629346	-0.10523	-0.0504202	-0.0276	-0.0308287	-0.0305	-0.0223809
3	2	-0.21301	-661.2	-0.83258	-1988.6	-0.53323	-2260.9	-0.86589	-3176.7	-1.08383	-4151.1
	3	-0.34917	-659.2	-0.83746	-2149.6	-0.56047	-2369.8	-0.87052	-3169.1	-1.07686	-4037.9
	4	-0.35591	-800.7	-0.85667	-2209.9	-0.57695	-2347.6	-0.90276	-3094.6	-1.12513	-4159.6
	Coefficients of Variation:		-0.2634648	-0.11474	-0.0151211	-0.05407	-0.0396485	-0.02474	-0.0228301	-0.01442	-0.0238209
4	2	-0.60484	-761.5	-1.11668	-2288.7	-1.36823	-2205.9	-1.13758	-2808.1	-1.02326	-4053.3
	3	-0.62921	-862.9	-1.12045	-2330.9	-1.13511	-167.5	-1.16822	-2841.5	-0.99438	-4040.7
	4	-0.6118	-709.5	-1.12606	-2189.4	-1.01301	-179.9	-1.15601	-3735.5	-0.90933	-3972.4
	Coefficients of Variation:		-0.0204018	-0.10028	-0.0042103	-0.03201	-0.1539764	-1.37858	-0.0133672	-0.16816	-0.0607056
5	2	-0.47988	-1137.5	-0.67689	-1969.4	-0.72704	-2377.3	-0.86944	-3378.4	-0.55287	-1347.8
	3	-0.46412	-908.4	-0.67396	-2010.5	-0.72002	-2329.8	-0.91826	-3582.2	-0.86258	-3333.9
	4	-0.4351	-925.4	-0.66242	-1970.2	-0.7339	-2353.4	-0.5514	-1407.9	-0.53706	-1070.7
	Coefficients of Variation:		-0.0494123	-0.10523	-0.0113994	-0.00967	-0.0095465	-0.00824	-0.2555018	-0.35149	-0.2820146
6	2	-0.19171	-817.9	-0.95253	-2380	-0.60606	-2055.6	-0.8645	-3234.4	-1.09294	-4204.8
	3	-0.22167	-885.9	-1.52369	-112.9	-0.64776	-2217	-0.90847	-4082.9	-1.06163	-4267.4
	4	-0.24292	-839.4	-1.52272	-1352.8	-0.66342	-2232.3	-0.71291	-3342.2	-1.05689	-4117.1
	Coefficients of Variation:		-0.1176055	-0.041	-0.2471753	-0.88557	-0.0463929	-0.04515	-0.1238155	-0.13	-0.0182992
7	2	-0.46613	-852.3	-0.83723	-2075.1			-0.86466	-3329.4	-0.96204	-4131.1
	3	-0.4824	-957	-0.79094	-2030.1			-0.87526	-3436.3	-0.95759	-4357.9
	4	-0.45506	-831.8	-0.8022	-2289.1			-0.90217	-3496.7	-0.95869	-4294.1
	Coefficients of Variation:		-0.0293936	-0.07628	-0.0297988	-0.06493			-0.0219564	-0.02477	-0.0024159
8	2	-0.30696	-725.3	-0.86972	-1663.7	-0.93581	-1999.6	-1.02019	-2729.2	-1.19902	-4270.8
	3	-0.29408	-746.8	-0.87197	-1666.5	-0.91865	-1981.6	-1.02425	-2695.3	-1.17783	-4577.3
	4	-0.37221	-938.3	-0.8928	-1727.9	-0.91792	-1958.9	-1.02409	-2714.9	-1.13745	-4138.1
	Coefficients of Variation:		-0.1291187	-0.14595	-0.0144911	-0.02152	-0.0109559	-0.0103	-0.0022479	-0.00627	-0.0267019

Appendix H – Sensor Calibration Curves

Each sensor had its own individual calibration curve, presented here.

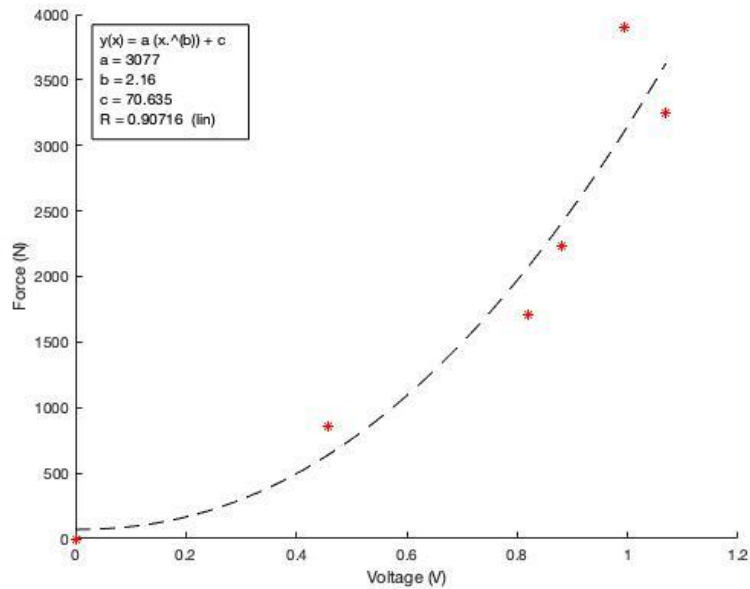


Figure H.1: Sensor 1 Calibration Curve

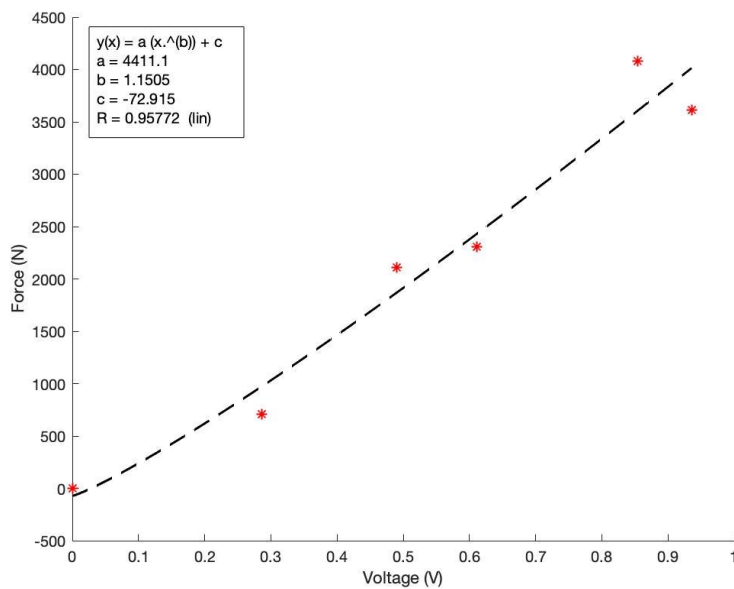


Figure H.2: Sensor 2 Calibration Curve

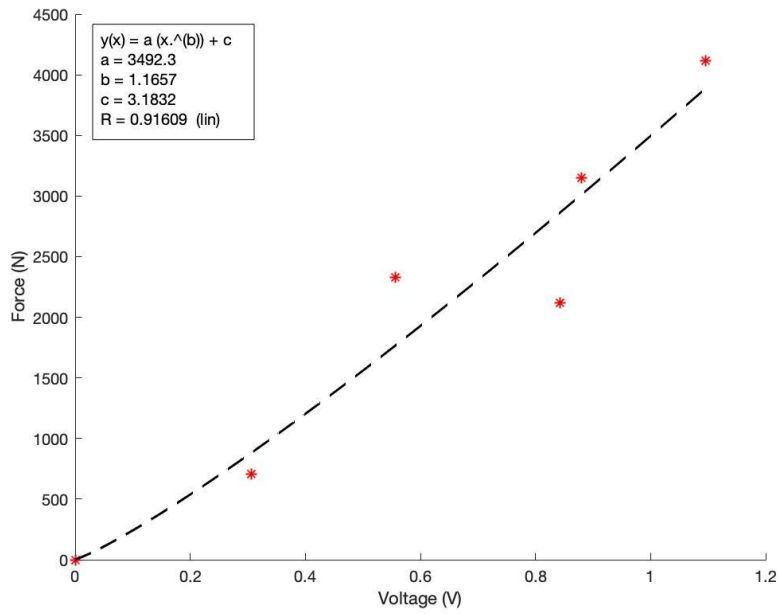


Figure H.3: Sensor 3 Calibration Curve

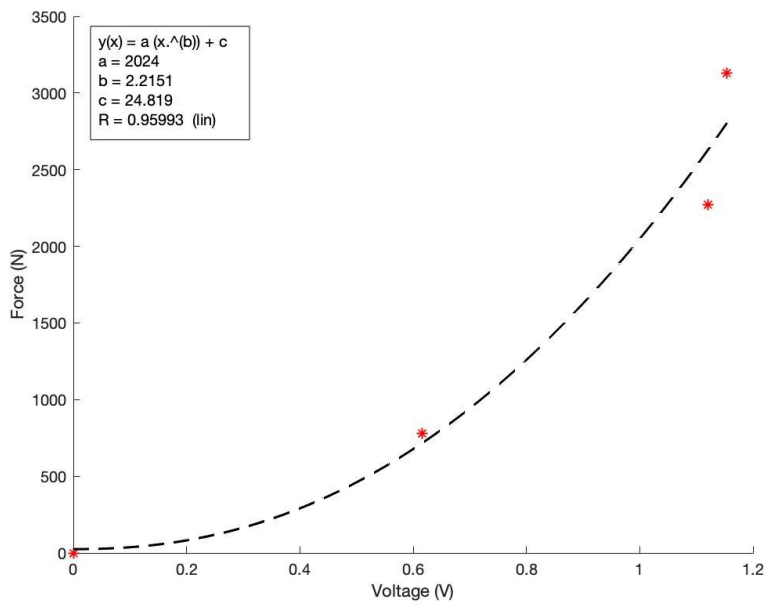


Figure H.4: Sensor 4 Calibration Curve

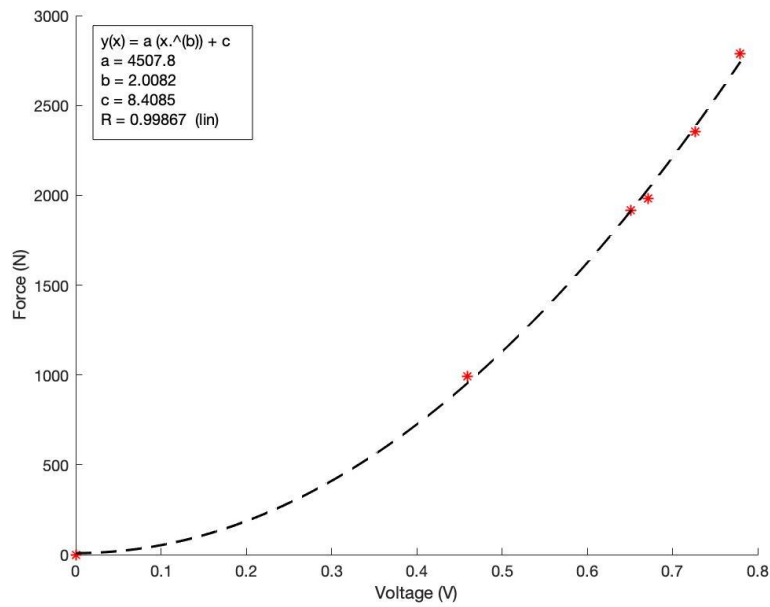


Figure H.5: Sensor 5 Calibration Curve

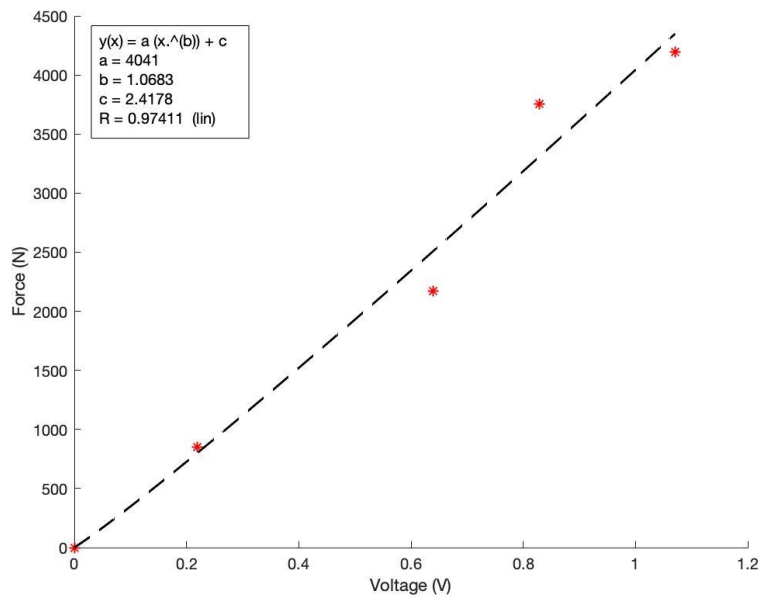


Figure H.6: Sensor 6 Calibration Curve

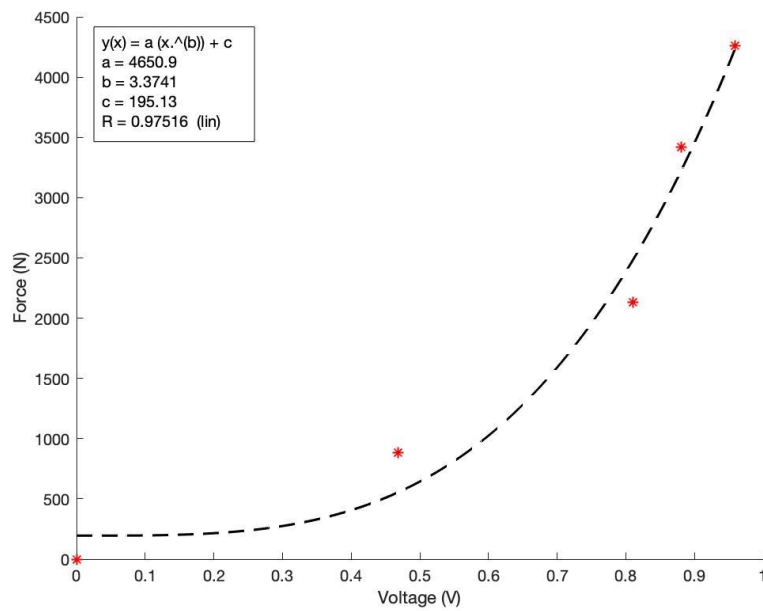


Figure H.7: Sensor 7 Calibration Curve

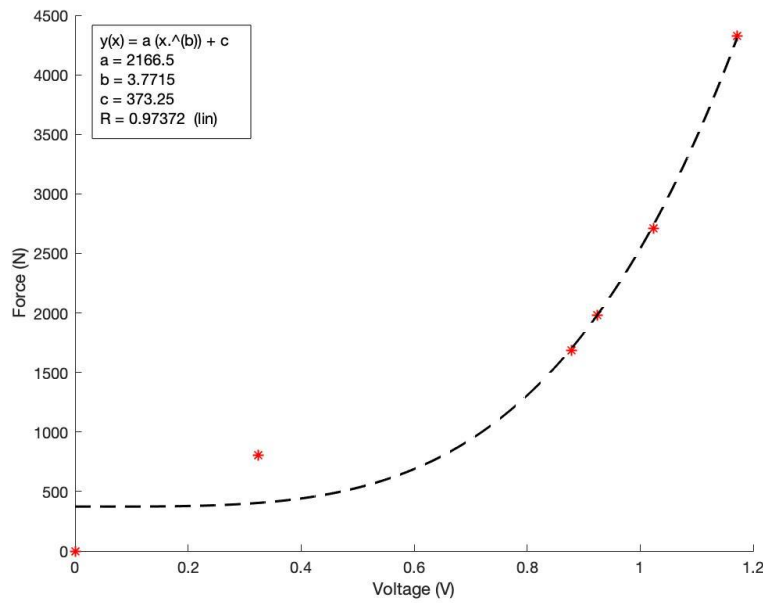


Figure H.8: Sensor 8 Calibration Curve

Appendix I – X-ray Images

Each of the cadaveric specimens referenced in Chapter 4 was x-rayed prior to dissections, after dissection had occurred, and after the axial impacts to check whether damage was incurred. All specimens were x-rayed in the anterior-posterior and lateral views.



Figure I.1: Specimen C171338-L (Specimen 1) Before Dissection

Specimen 1 x-rays in (a) the anterior-posterior and (b) the lateral views prior to dissection to check for a history of damage to the bone.



Figure I.2: Specimen C171338-L (Specimen 1) X-rays After Impact
Specimen 1 x-rays in (a) the anterior-posterior and (b) the lateral views to check whether damage had occurred after impact.



Figure I.3: Specimen F171528-L (Specimen 2) Before Dissection
Specimen 2 x-rays in (a) the anterior-posterior and (b) the lateral views prior to dissection to check for a history of damage to the bone.



Figure I.4: Specimen F171528-L (Specimen 2) X-rays After Impact
Specimen 2 x-rays in (a) the anterior-posterior and (b) the lateral views to check whether damage had occurred after impact.



Figure I.5: Specimen F180193-L (Specimen 3) Before Dissecting
Specimen 3 x-rays in (a) the anterior-posterior and (b) the lateral views prior to dissection to check for a history of damage to the bone.



Figure I.6: Specimen F1890193-L (Specimen 3) X-rays After Impact
Specimen 3 x-rays in (a) the anterior-posterior and (b) the lateral views to check whether damage had occurred after impact.